A Role for the Planar Cell Polarity Pathway in Neuronal Positioning Along the AP Axis of *C. elegans*.

Raymond Tanner

This thesis is submitted as a partial fulfillment of the M.Sc. program in Neuroscience, Faculty of Medicine

Neuroscience Department, Faculty of Medicine

University of Ottawa

Ottawa, Ontario, Canada

2014

Abstract

We sought to investigate the role of the Planar Cell Polarity (PCP) pathway in neuronal positioning along the Anterior-Posterior (AP) axis of *C. elegans*, and chose the worm's DD-type motor neurons as a model. The six DD neurons (DD1-DD6) are evenly spaced in the ventral nerve cord of wild type animals. Here we showed that mutations in core PCP genes caused DD neuron spacing and positioning defects. *prkl-1* double mutant combinations with *vang-1* and *fmi-1* showed a suppression of the more severe *prkl-1* single mutant defects, which was evidence of genetic interactions between these PCP components. We also conducted a candidate screen *of Frizzled, Dishevelled, Wnt*, and *ROCK* genes, and found that *dsh-1/Dishevelled, mom-2/Wnt* and *let-502/ROCK* also played roles in DD neuronal positioning. Both *vang-1* and *prkl-1* were found to function within the nervous system to guide DD neuronal positioning, and *prkl-1* was further identified as playing a cell autonomous role. The origins of observed DD neuron anterior positioning defects were investigated during embryogenesis, in which 1.5 fold stage *prkl-1(ok3182)* embryos displayed delayed intercalation of the DD neurons. This represents a novel role for the PCP pathway in mediating DD neuronal intercalation.

Table of Contents

List of Tables

List of Figures

List of Abbreviations

AP	Anterior-Posterior
CE	Convergence and extension (or convergent extension)
C. elegans	*Caenorhabditis elegans*
CRD	Cystein Rich Domain
PKC	Protein Kinase C
DSH	Dishevelled
EMS	Ethyl Methanesulfonate
FMI	Flamingo
Gα	Heterotrimeric G-Protein alpha subunit
GPCR	G-Protein Coupled Receptor
GSK3	Glycogen synthase kinase 3
JNK	c-Jun N-terminal kinase
PCP	Planar Cell Polarity
PRKL	Prickle
ROCK	Rho associated kinase
ROR	Receptor tyrosine kinase-like orphan receptor
RYK	Receptor-like Tyrosine kinase
tagRFP	Red Fluorescence Protein variant
TM	Transmembrane
VANG	Van Gogh
WT	Wild Type

Acknowledgements

Firstly, I would like to acknowledge and thank my supervisor Dr. Antonio Colavita for bringing me in to his lab and teaching me a great deal about *C. elegans* and genetics. His guidance and support while finishing my project and writing this thesis was greatly appreciated. I would also like to thank my thesis advisory committee, Dr. Diane Lagace and Dr. Mario Tiberi, for their excellent encouragement and feedback during my TAC meetings. Without them, this thesis would not be possible.

I would also like to thank all of my peers in the Colavita lab with whom I had the pleasure of working: Cristina Slatculescu, David Carr, Zhao-ha Ding, Nasrin Habibi-Babadi, Jiravat Visanuvimol, Billy Huang, Ali Ghadban, Aysha Rankin, and Carolin Sachgau. Their friendship both in and out of the lab was instrumental in my success as a student, and helped make our lab a truly enjoyable environment. I would also like to thank all of our summer students and volunteers who helped contribute to our success.

Lastly and most importantly, I would like to thank my family for their kindness, encouragement, and support. I would like to thank my parents Jim and Pat Tanner for encouraging and assisting me in pursuing my post-secondary studies. Finally, great thanks go to my amazing grandmother Joan Burns for always believing in me, as well as always making sure I had somewhere to eat dinner on Sunday nights.

Chapter 1: Introduction

As animals grow, they must develop from single cells into complex moving organisms. Of the many stages involved in this development, one integral aspect is nervous system formation. This is the process by which neurons are born, migrate to their final locations, send out axons and dendrites, and finally make synaptic connections. Once connected, nervous systems allow animals to sense and process information from their environments, and communicate various outputs to their muscles and other tissues. A properly connected nervous system is crucial for the survival of complex moving organisms. There are many cellular signaling pathways involved in choreographing the various facets of nervous system development, and one such pathway is the Planar Cell Polarity, or PCP, pathway (Fanto and McNeill, 2004), which is a non-canonical Wnt signaling pathway.

Discovered in *Drosophila* through forward genetic screens, the PCP pathway was originally identified to cause polarity defects in mutant fly ommatidia and wing hairs (Adler, 2002). Since this discovery, the PCP pathway has been linked to regulating cell intercalations during vertebrate convergent extension (Jones and Chen, 2007), as well as axon guidance (Shafer et al., 2011) and neuronal polarity (Sanchez-Alvarez et al., 2011). In humans, the PCP pathway and its core components have been identified as playing roles in spina bifida (Juriloff and Harris, 2012) and seizures (Tao et al., 2011). As time goes on, it is becoming more apparent that this pathway plays several diverse and important roles during nervous system development. Understanding how this pathway functions at the molecular level will help develop future treatments for human diseases associated with the PCP pathway.

1.1 The canonical Wnt-Frizzled pathway

The PCP pathway is termed "non-canonical" because is it a derivative of the canonical Wnt-Frizzled pathway. This canonical pathway features the core proteins Wnt, Frizzled, Dishevelled, and β-catenin (Wang and Malbon, 2004). The hallmark of this pathway is the activation of Frizzled by Wnt, leading to the stabilization of β-catenin via Dishevelled (Liu et al., 2002). β-catenin is normally ubiquitinated and degraded by a complex involving Axin and GSK (Liu et al., 2002). Dishevelled interacts with the Axin/GSK complex and stabilizes β-catenin by inhibiting its degradation; β-catenin then accumulates and translocates to the nucleus, where it activates gene transcription and canonical signaling (Liu et al., 2002). The canonical is well understood, and plays numerous crucial roles during development, including regulating neurogenesis (Gulasci and Anderson, 2008) and neuronal differentiation (Hirabayashi et al., 2004). A schematic diagram of the canonical Wnt-Frizzled pathway is shown in **Figure 1**.

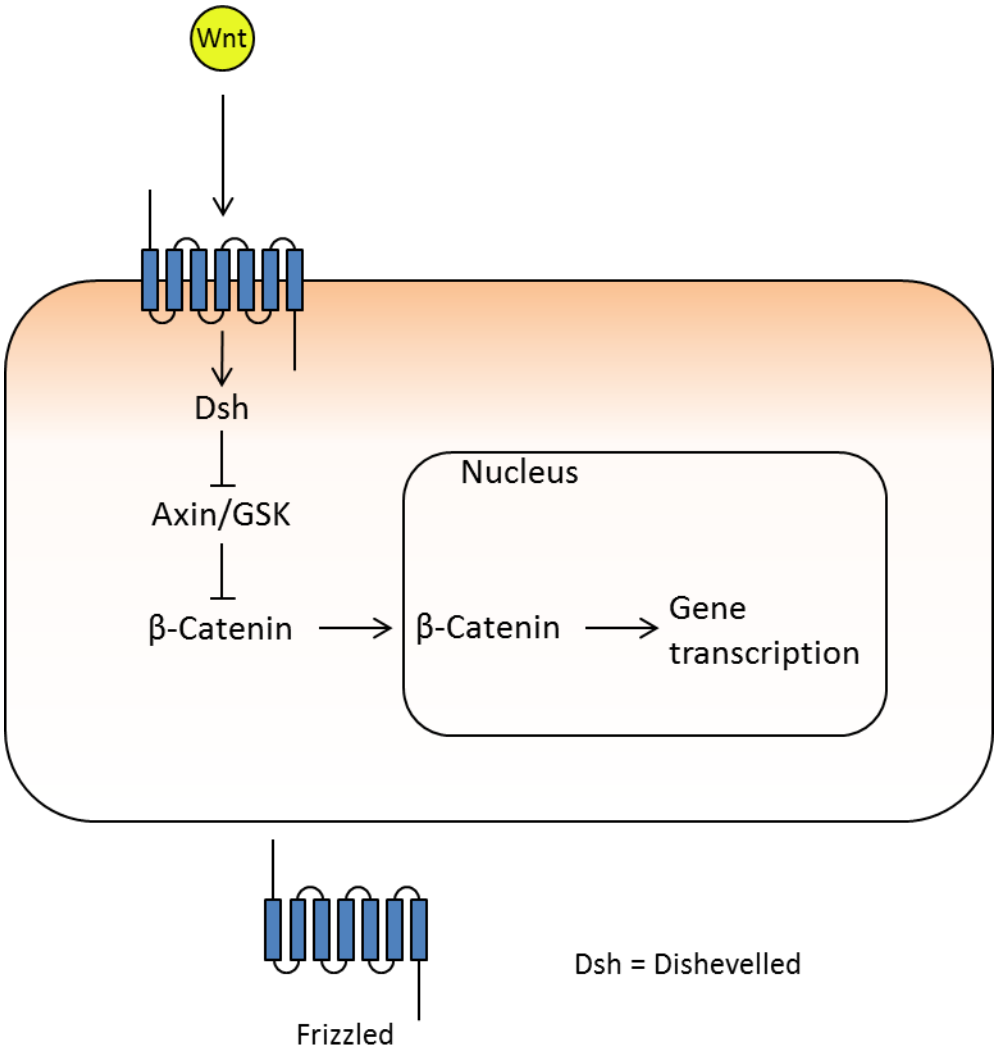

Figure 1. Schematic representation of the canonical Wnt-Frizzled pathway, signaling through β-catenin. The ligand Wnt activates the 7-TM GPCR Frizzled, which then activates Dishevelled. β-catenin is normally ubiquitinated and degraded by the Axin/GSK complex. Activated Dishevelled binds the Axin/GSK complex and relieves the degradation of β-catenin, allowing it to accumulate. Once this occurs, β-catenin is free to enter the nucleus and ultimately leads to gene transcription and canonical pathway signaling.

1.2 Non-canonical Wnt pathways

In addition to the canonical Wnt-Frizzled pathway, there are many non-canonical Wnt pathways, which lack the involvement of β-catenin (Kühl, 2002). For example, the Wnt-Ca^{2+} pathway (Calisto et al., 2005) features CamKII and PKC signaling (Kühl et al., 2000). There are also two Wnt pathways with receptor tyrosine kinases, Wnt-ROR (Receptor tyrosine kinase-like Orphan Receptor) pathway featuring downstream c-Jun N-terminal Kinase (JNK) signaling (Oishi et al., 2003), as well as the Receptor-like Tyrosine Kinase (RYK) Wnt pathway (Clark et al., 2014) which can act as a Wnt co-receptor. There is also the Planar Cell Polarity, or PCP, pathway. Interestingly, the RYK pathway has been shown to interact with the PCP pathway component Van Gogh (Andre et al., 2012), indicating that these pathways may not necessarily be mutually exclusive.

1.3 The Planar Cell Polarity pathway

The PCP pathway features the canonical proteins Wnt, Frizzled, and Dishevelled, and is distinguished by the addition of the core PCP components Prickle, Van Gogh, and Flamingo (Gao, 2012). Wnt is a secreted glycoprotein capable of forming morphogen gradients (Bovolenta, 2005), which binds to and activates Frizzled, a seven transmembrane G-Protein coupled receptor (Ingham, 1996). Frizzled complexes with the scaffolding protein Dishevelled (Formstone and Mason, 2005), which leads to the activation of the small GTPases Rho or Rac (Saburi and McNeill, 2005). Rho signals through Rho activated kinase, or ROCK (Strutt, 2001), and both Rho and Rac ultimately cause cytoskeletal rearrangement (Tahincia and Symesa, 2003).

PCP signaling is thought to be regulated by the core PCP components Van Gogh (Vang) and Prickle (PK/prkl). Vang is a four transmembrane protein, and is known to recruit Prickle to the cell membrane (Jenny et al., 2003). Prickle is an inhibitory cytosolic protein, and has been shown to antagonize Frizzled-Dishevelled complexes by preventing the recruitment of Dishevelled to the membrane (Tree et al., 2002). Lastly, the core PCP component Flamingo is a seven transmembrane G-protein coupled receptor with a large extracellular cadherin domain (Usui et al., 1999). Flamingo may also be required for the proper asymmetric localization of PCP complexes (Strutt, 2002).

1.3.1 Wnt and Frizzled

As previously mentioned, the glycoprotein Wnt is an extra-cellular ligand that can be secreted from specific cells, creating morphogen gradients that guide development (Bovolenta, 2005). The primary receptor for Wnt is the 7-TM GPCR Frizzled (Ingham, 1996). In fact, work in *C. elegans* first confirmed the link between Wnt and Frizzled: Herman et al. (1995) discovered that *lin-44* (Wnt) mutations caused asymmetric cell division defects in the *C. elegans* male B and T cells of the tail, while Sawa et al. (1996) discovered the same defects for *lin-17* (Frizzled). These respective papers determined *lin-44* acted cell non-autonomously and *lin-17* acted cell autonomously within the B and T cells, ultimately confirming that *lin-44* (Wnt) binds *lin-17* (Frizzled) to produce the same phenotype. Subsequent studies confirmed that Wnt physically binds to Frizzled, requiring a cysteine rich extracellular domain of Frizzled (Bhanot et al., 1996; Lin et al., 1997).

From a mechanistic point of view, the binding of Wnt to Frizzled leads to heterotrimeric G-protein signaling via the Gα subunit of Frizzled; the Gα subunit is activated by exchanging bound GDP for GTP, and either $G\alpha_q$ or $G\alpha_o$ subunits can be activated (Wang, Liu, and Malbon, 2006). Activation of Frizzled by Wnt can also lead to complex formation with Dishevelled, which ultimately signals either canonical or non-canonical Wnt-Frizzled signaling (Li, Chong, and Maiese, 2005; Gao and Chen, 2010). Interestingly, the type of Frizzled Gα subunit activated may determine whether canonical or non-canonical signaling occurs: Bikkavilli et al. (2008) note that canonical β-catenin mediated signaling involves Frizzled $G\alpha_{q/o}$ subunits, whereas PCP signaling only involved $G\alpha_o$ subunit activation.

1.3.2 Dishevelled

Dishevelled is a scaffolding protein involved in both the canonical and PCP pathways, and acts dynamically to localize and catalyze the reactions of many signaling molecules (Formstone and Mason, 2005). The protein itself has three domains: a PDZ domain, a DIX domain, and a DEP domain, of which the DEP domain may be responsible for translocating Dishevelled to the membrane (Pan et al., 2004), where it is known to interact with Vang (Bastock et al., 2003). Dishevelled has been shown to interact with formins (Tanegashima et al., 2008), and leads to downstream PCP signaling via the small GTPases Rho (Strutt et al., 1997) and Rac (Habas et al., 2003); WGEF may connect Dishevelled signaling to Rho activation (Tangeshima et al., 2008).

1.3.3 Prickle and Van Gogh

Prickle is a cytosolic protein with one PET domain and three LIM domains; this structure is evolutionarily conserved from *C. elegans* to humans (Katoh and Katoh, 2003). Structurally, Prickle is farnesylated at its C-terminus; this farnesyl helps anchor Prickle to the membrane and also promotes strong interactions with Vang (Strutt et al., 2013). In zebrafish null mutants for Vang, Prickle is not recruited to the membrane, whereas Prickle was recruited to the membrane in a "web-like fashion" in wild type animals (Jenny et al., 2003). Additional evidence shows that Prickle may translocate to the nucleus to establish cell polarity (Tao et al., 2012), but this has not shown to be a consistent aspect of PCP signaling.

One consistent function of Prickle appears to be inhibiting Dishevelled in a cell autonomous manner (James et al., 2008). Indeed, Prickle competes for Dishevelled binding (Jenny et al., 2005) and causes its degradation (Fujimura et al., 2009). However, the interaction between Dishevelled and Prickle is not strictly inhibitory, as Prickle has been shown to amplify Dishevelled-Frizzled signaling in a cell non-autonomous fashion within the *Drosophila* wing system (Tree et al., 2002). Therefore, Prickle may simultaneously inhibit Dishevelled within a cell and activate it in neighboring cells (Tree et al., 2002).

Vang is a 4-TM protein with cytoplasmic N- and C-termini, and with a C-terminal PDZ binding motif (Jenny et al., 2003). Vang binds Prickle and recruits it to the membrane (Bastock, 2005), where Prickle and Vang form a functional complex (Jenny et al., 2003).

Vang also has other functions. For example, Vang binds to Dishevelled (Bastock et al., 2005), and thus may be capable of activating Dishevelled signaling itself. In addition, Vang regulates adherens junctions through the small GTPase Rac (Lindqvist et al., 2010). Mouse Vangl2 (Vang-like protein 2) was found to physically bind Rac1 and alter its localization; both Vangl2 and Rac1 loss-of-function mice displayed impaired adherens junctions and reduced cell-cell adhesion (Lindqvist et al., 2010). Lastly, evidence suggests that the extracellular domain of Frizzled may interact with Vang across cells (Wu and Mlodzik, 2008). This helps explain how the cytosolic protein Prickle would be capable of upregulating Frizzled-Dishevelled signaling in neighboring cells (Tree et al., 2002), which could occur through Vang.

1.3.4 Flamingo

The core PCP component Flamingo is a 7-GM GPCR with an extracellular cadherin domain (Usui et al., 1999). The cadherin domain is capable of cross-cell homophilic binding (Chen et al., 2008). These homophilic interactions may be important for cross-cell interactions, as Flamingo binds to Frizzled and Vang and may help mediate cross cell signaling between them (Chen et al., 2008). It is worth noting that although it is a core PCP component, Flamingo also has PCP-independent functions. For example, Najarro et al. (2013) showed that *fmi-1* (Flamingo) mutant worms displayed anterior/posterior axon guidance defects in the VD-type neurons of *C. elegans*. This function was independent of the PCP pathway.

1.4 The PCP pathway acts to establish polarity in *Drosophila* wings

The Planar Cell Polarity pathway was originally discovered in *Drosophila*, where it was determined to coordinate groups of cells within a plane to adopt a common polarity. In this paradigm, PCP components are able to communicate with each other across cell membranes; polarized cells will then communicate this polarity with further neighboring cells, presumably in a cascade effect. PCP components are polarized in the proximal-distal plane of wing cells (Shimada et al., 2001). There is also an apical-basal polarity in fly wings, in which PCP components are recruited to the apical membrane; this apical recruitment is a prerequisite for proximal-distal planar cell polarity (Strutt, 2002). When Flamingo is knocked out, none of the PCP components are asymmetrically recruited to the apical membranes (Strutt and Strutt, 2008), preventing proximal distal polarity.

After Flamingo recruits Frizzled to the apical membrane, Frizzled then causes Flamingo to localize to the proximal and distal sides of cells, called the adherens junction zone (Strutt, 2002). This subsequently causes Dishevelled to localize to the distal membrane of wing cells (Strut, 2002). A loss of Prickle, Vang, or Dishevelled results in the failure of proximal-distal polarity formation, indicating that these proteins work together with Flamingo and Frizzled to establish proximal-distal polarity (Strut, 2002). Once this polarity is established, Flamingo, Frizzled, and Dishevelled form a functional complex at the distal edge of wing cells, which promotes cytoskeletal remodeling and ultimately causing hair formation in the wing cells (Shimada et al., 2001).

Until recently no firm evidence of a role for Wnt in *Drosophila* wing polarity had been identified. However, Wu et al. (2013) found a redundant role for the *Drosophila* Wnts Wingless and dWnt4, as double mutant flies for Wingless and dWnt4 displayed PCP type defects in the fly wing. The over-expression of either Wingless or dWnt4 was sufficient to significantly impair the recruitment of Vang to the membrane by Frizzled (Wu et al., 2013). This implies that the selective inhibition of Frizzled-Vang interactions by Wnt is important in the initial establishment of PCP polarity within the fly wing, and provides further insights into the nuances of the PCP pathway.

1.5 The PCP regulates axon guidance, growth cones, and neurite polarity

The PCP pathway is involved in growth cone dynamics. Mouse Vangl2 was shown to be localized to the tips of filopodia in the growth cones of commissural axons (Shafer et al., 2011). Vang was found to antagonize Dishevelled in these growth cones and promoted the internalization of Frizzled (Shafer et al., 2011), although a role for Prickle was not investigated. These Vangl2 -/- mice displayed significantly impaired anterior axon turning of commissural neurons (Shafer et al., 2011), indicating a role for Vang in growth cone guidance. In fact, Wnt, Frizzled, Flamingo, and Vang were all shown to guide monaminergic axons in the mouse brain stem (Fenstermaker et al., 2010). Evidence from our lab indicated that *C. elegans prkl-1/Prickle* and *vang-1/Van Gogh* cooperated to negatively regulate VC4/VC5 neurite formation (Sanchez-Alvarez et al., 2011). As neurite formation is known to depend on growth cone dynamics, this implies a further role for the PCP pathway in both promoting and inhibiting growth cone formation.

1.6 PCP signaling during convergence and extension in vertebrates

Another major process the PCP helps regulate is the convergent extension, or CE, of chordate embryos (Roszko et al., 2009). CE involves mediolateral cell movements and intercalations, which ultimately drive embryo extension (Roszko et al., 2009). These dynamic cells are polarized by the PCP pathway (Roszko et al., 2009) and are in physical contact with one and other, which differs from the *Drosophila* wing system and its static polarized cells. One example of the PCP pathway regulating CE is neurulation (Ybot-Gonzalez et al., 2007). Mutations in PCP genes cause neural tube closure defects (Jones and Chen, 2007). These neural tube closure defects can result in open spinal cords in mammals, and include the condition *spina bifida* in humans (Simons and Mlodzik, 2008).

The neural tube is an embryonic structure in chordate development, which ultimately gives rise to the brain and spinal cord (Karfunkel, 1974). Neural tube formation involves primary and secondary neurulation (Lawson, 2009), with neural tube closure occurring during primary neurulation. Primary neurulation consists of neural plate formation, thickening of the plate edges to create neural folds and the neural groove, and lastly convergence and fusion of these folds to close the neural tube (Nievelstein et al., 1993). This process takes place on top of the notochord, and involves mediolateral convergence and fusion of the neural folds (Nievelstein et al., 1993).

Most of the core PCP components appear to have roles in regulating chordate neural tube closure. In mouse neural tube development Wnt5a was necessary for proper Vangl2 localization, and Wnt5a knockout mice enhanced Vangl2 neural tube closure defects (Qian et

al., 2007). Mutations in the Flamingo homologue Celsr1 were also found to cause neural tube defects in mice (Curtin et al., 2003; Robinson et al., 2012). In fact, homologues for Dishevelled, Frizzled, and Vang have also been found to cause neural tube closure defects when knocked out in vertebrate animals (Simons and Mlodzik, 2008). Additionally, human patient data indicates that Prickle2 mutations may be a pre-disposing factor for open spinal cord diseases, indicating a role for Prickle in human neural tube closure (Bosoi et al., 2011). Thus, the PCP pathway plays crucial roles in guiding neural tube closure in vertebrates.

The molecular mechanisms for the PCP pathway in mediolateral cells during CE are not fully understood, however some insights exist. For example, Wnt11 functions to regulate CE in the anterior of the zebrafish embryos (Heisenberg et al., 2000), whereas Wnt5 guides CE in the posterior (Kiliana et al., 2003). This data supports the idea that Wnt ligands may be giving these dynamic cells spatial clues prior to or during their mediolateral movements. Also discovered in zebrafish, Prickle protein localizes to the anterior cell membrane of intercalating neural keel cells in wild type animals (Ciruna et al., 2006). This membrane localization of Prickle was abolished in Vang and Wnt morpholino knockdown animals (Ciruna et al., 2006), which also displayed notable cell polarity defects in the left-right axis. Cell intercalations were also impaired in these same knockdown animals (Ciruna et al., 2006). Taken together, this evidence suggests a general role for the PCP pathway in guiding mediolateral cell movements and intercalation during CE, and also implies that physical cell polarity established by the asymmetric localization of PCP pathway components is important for guiding proper cell intercalations.

1.7 Summary of PCP signaling

Thus, literature evidence suggests numerous and varied roles for PCP signaling. This pathway regulates hair polarity in sheets of static cells within the *Drosophila* wing, growth cone formation and guidance, and dynamic mediolateral cell movements and intercalations during convergent extension. A generalized schematic representation of PCP signaling is shown (**Figure 2**), which incorporates elements of static and dynamic cell signaling, and is also quite similar to a recent review (Lapebie et al., 2011).

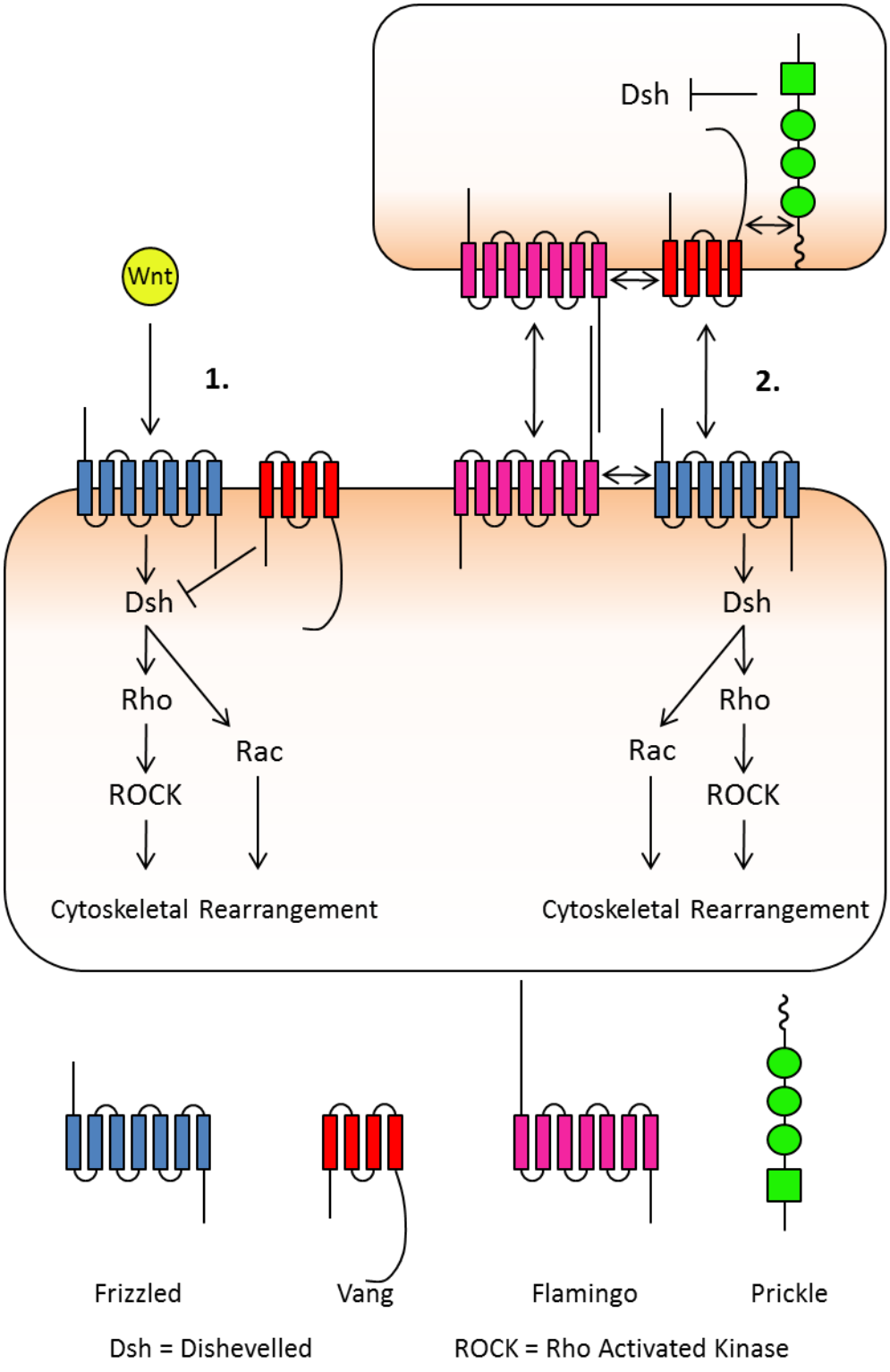
Dsh
Wnt
1.
2.
Dsh
Dsh
Rho
Rac
ROCK
Rac
Rho
ROCK
Cytoskeletal Rearrangement
Cytoskeletal Rearrangement
Frizzled
Vang
Flamingo
Prickle
Dsh = Dishevelled
ROCK = Rho Activated Kinase

Figure 2. Schematic model of PCP signaling. **1.** The PCP pathway is capable of responding directly to Wnt gradients, a process that is regulated by Vang. **2.** PCP components form complexes at the membrane interfaces of two cells, which can be either static or dynamic moving cells. This generally involves the asymmetric localization of Vang and Prickle to one side of cells, and Frizzled and Dishevelled the opposite side of a neighboring cell. PCP signaling ultimately results in cytoskeletal rearrangement via signaling from the small GTPases Rho and Rac.

1.8 *C. elegans* as a model organism

Caenorhabditis elegans is a microscopic nematode, and is an important model organism for developmental biology. *C. elegans* offers many advantages as a model organism: It is transparent, allowing for simple *in vivo* microscopy; it has a 3-day life cycle, which permits a rapid timetable for experiments and genetic crosses; and it has detailed cell lineages (Sulston et al., 1983) with maps of nervous system connectivity (White et al., 1986).

Studies of nervous system development are often complicated by the staggering number of neurons present in most animals, as even the simple fruit fly, *Drosophila melanogaster*, has upwards of 100,000 neurons (Kohl and Jefferis, 2011). At only 302 neurons out of 959 total cells in the adult hermaphrodite, *C. elegans* is a very simple, elegant organism, which is highly amenable to studying individual neurons as they develop (White et al., 1986a).

The six DD-type motor neurons (named DD1-DD6) are a set of GABAergic inhibitory motor neurons born during embryogenesis (White et al., 1986). These neurons have stereotyped positions (**Figure 3**), and are evenly spaced within the ventral cord of wild type animals. They have axonal commissures that branch out of the ventral cord and cross over to the dorsal side of the worm; there, the DD neurons function to inhibit the dorsal muscles during sinusoidal worm locomotion (White et al., 1986). We hypothesize that the PCP pathway plays a role in the development of *C. elegans* embryonic motor neurons. We will therefore use the DD neurons as our model for studying the role of the PCP pathway in neuronal positioning.

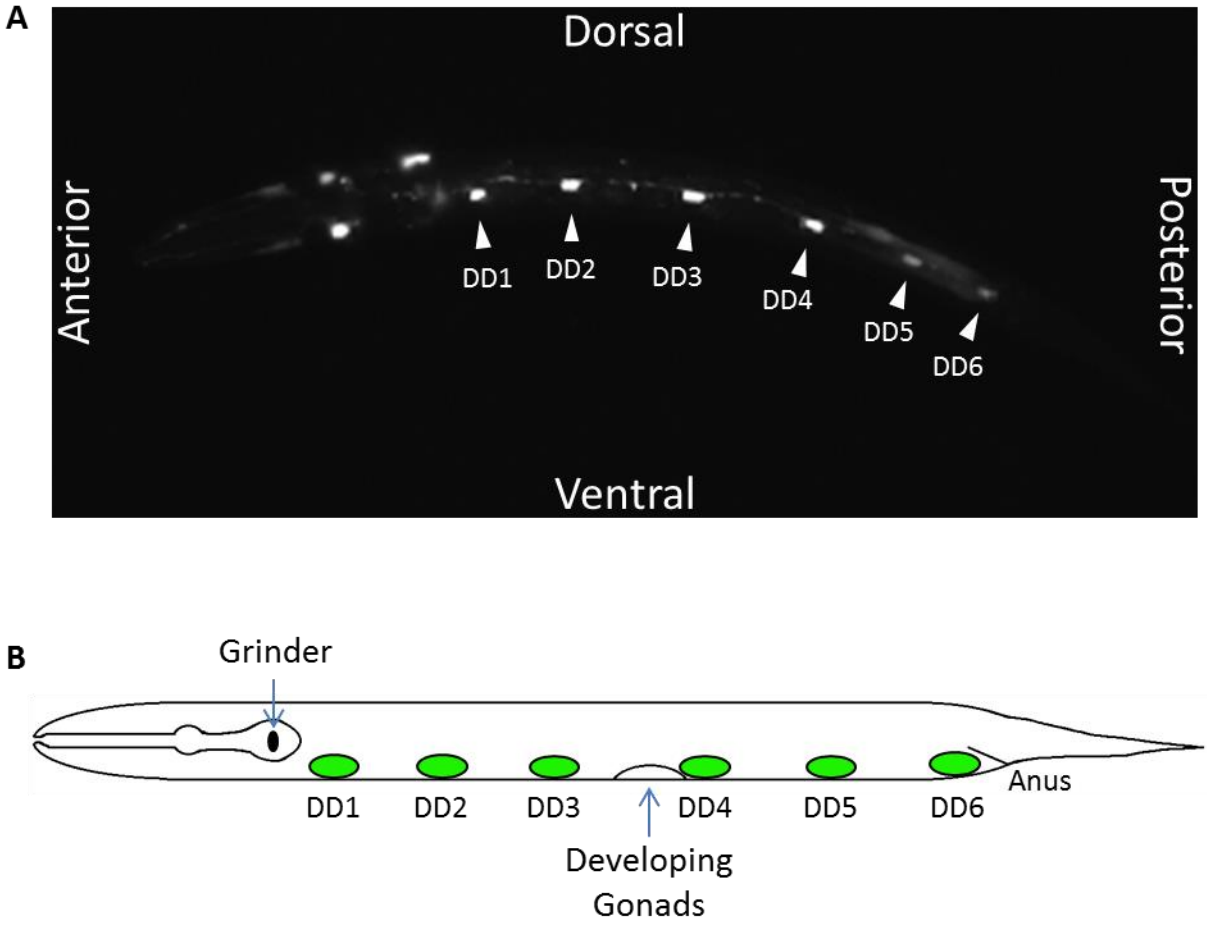

Figure 3. GFP image and schematic diagram of the DD neurons during the L1 larval stage. The DD neurons (DD1-DD6) are shown by (**A**) GFP and (**B**) schematic diagrams, in the same orientation. The DD neurons are located in in the ventral nerve cord of the worm, with DD1 being located at the anterior end of the worm, just posterior to the grinder of wild type animals. The DD neurons are numbered in an anterior to posterior order, ending with the DD6 neuron, which is just anterior of the anus. Arrowheads mark the DD neurons in the GFP image.

In addition to the DD neurons, there are two other sets of embryonic motor neurons, which are the cholinergic DA and DB type motor neurons (White et al., 1986a). The nine DA and seven DB neurons are also located in the ventral cord of *C. elegans,* and act to innervate muscles during sinusoidal movement (White et al., 1986). The DA, DB, and DD neurons are born just after the 300 minute mark of embryogenesis (Sulston et al., 1983). The DD neurons are born in the left (DD1, DD3, and DD5) and right (DD2, DD4, and DD6) sides of the embryo, and must migrate towards the midline during the bean stage embryo (Sulston et al., 1983). By the 1.5 fold embryo stage, the DD neurons have entered the ventral cord and begun to migrate apart in wild type animals (Sulston et al., 1983). It is not clear how the DD neurons transition from bean stage DD neuron positioning to the 1.5 fold DD neuron positioning. However, we speculate that the DD neurons must converge at the midline of the comma stage embryo and intercalate as they enter the ventral cord. Therefore, one of our goals is to establish that the DD neurons do in fact converge at the midline and intercalate between the comma and 1.5 fold embryo stages. The embryo stages and timelines can be seen, along with a brief embryonic lineage of the DD neurons is shown (**Figure 4**). The embryonic lineages depict the DD neurons arising from the left and right embryo, three on each side. Lastly, schematic diagrams of the DD neurons during the comma and 1.5 fold stages are shown (**Figure 5**), which are based on literature observations (Sulston et al., 1983).

A

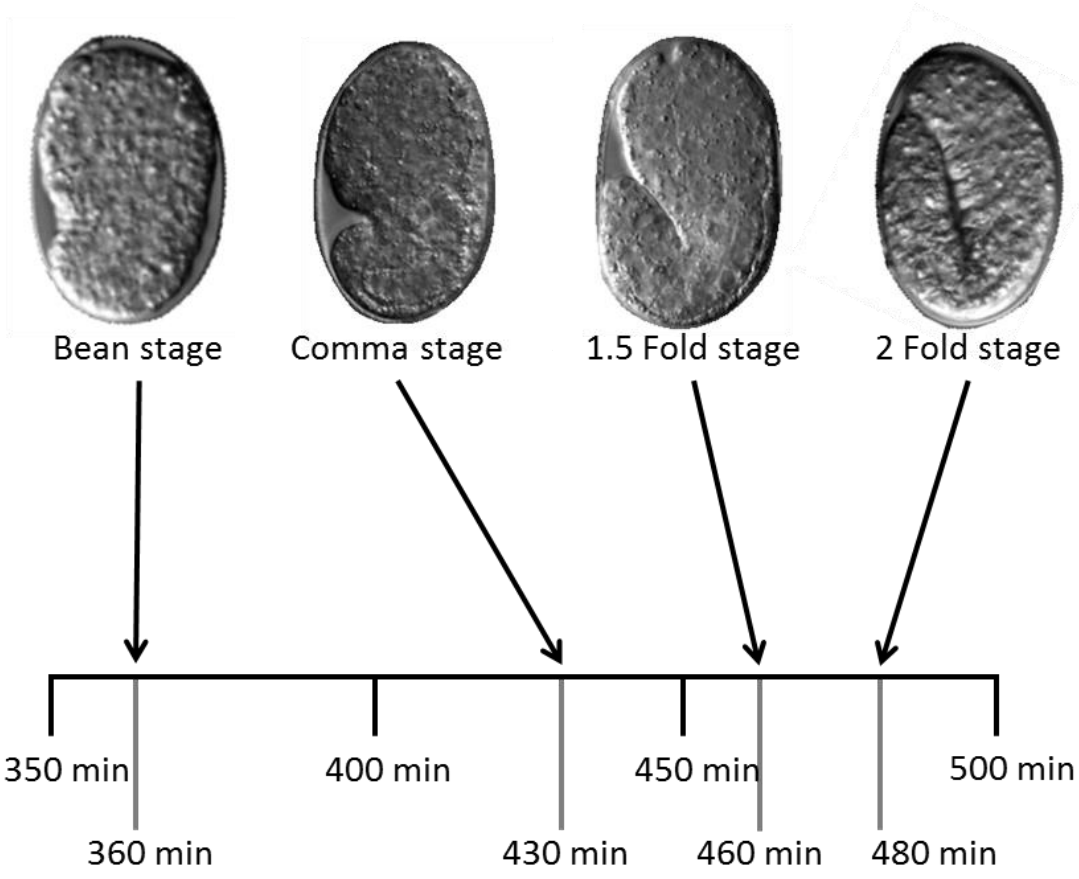
Bean stage
Comma stage
1.5 Fold stage
2 Fold stage
350 min
360 min
400 min
430 min
450 min
460 min
480 min
500 min

B

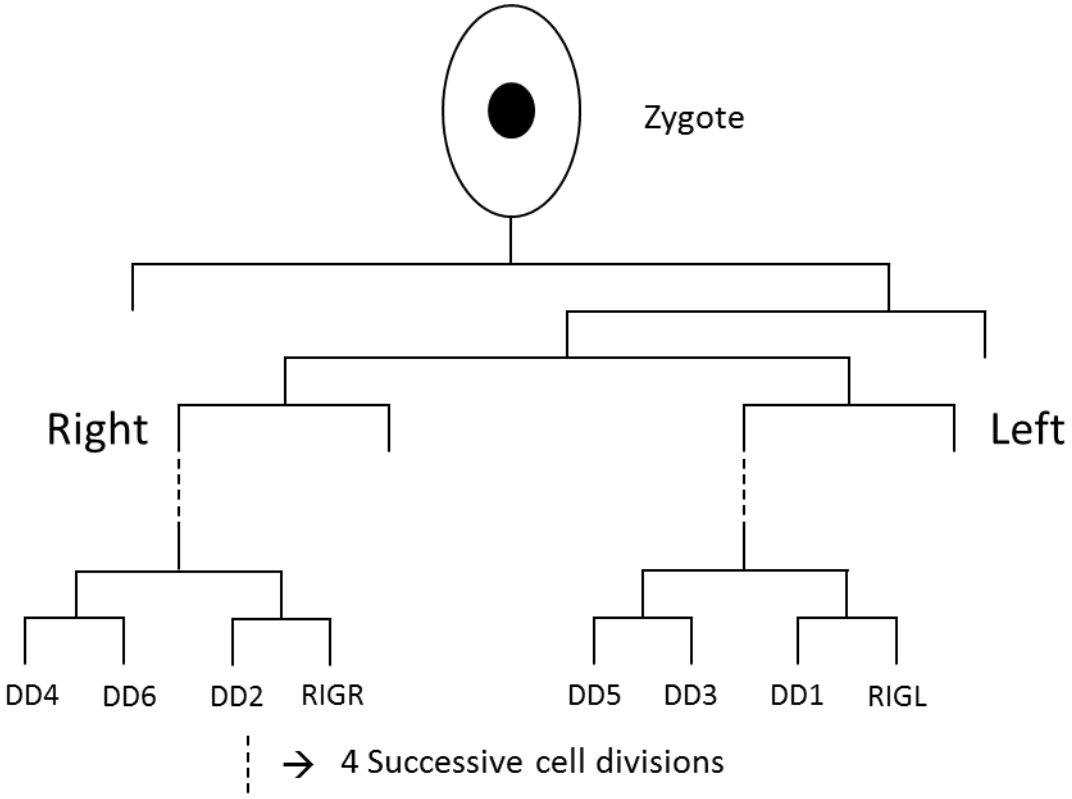
Zygote
Right
Left
DD4
DD6
DD2
RIGR
DD5
DD3
DD1
RIGL
→ 4 Successive cell divisions

Figure 4. *C. elegans* embryonic development timeline from the bean stage to the 2-fold stage and developmental lineage of the DD neurons. **(A)** The bean stage is marked by embryos shaped like lima beans, and begins at approximately the 360 minute mark of embryonic development, with the fertilization of the zygote marking the 0 minute. The comma stage arises at approximately the 430 minute of embryonic development, with rapid changes beginning thereafter. The 1.5 fold stage arises 30 minutes after the comma stage, and the 2-fold stage arises only another 20 minutes after that. This change to a quicker pace of embryonic development marks the beginning of embryonic elongation. (**B)** A lineage schematic diagram of DD neuron cell fate during *C. elegans* embryogenesis, in which the DD neurons arise from the left (DD1, DD3, and DD5) and right (DD2, DD4, and DD6) embryo. Information in images obtained from Sulston et al. (1983) and White et al. (1986).

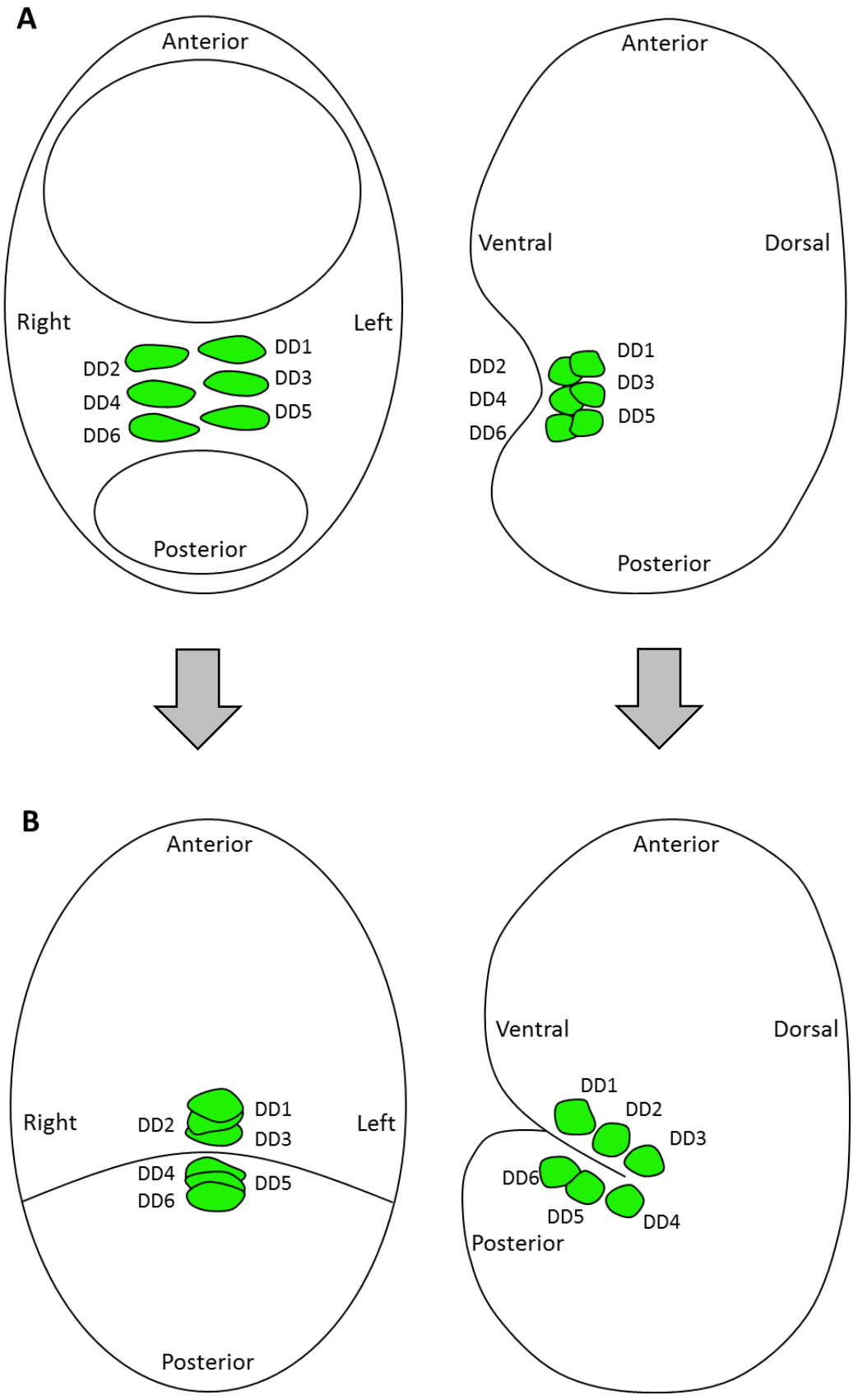
A
Anterior
Right
Left
Posterior
DD1
DD2
DD3
DD4
DD5
DD6
Anterior
Ventral
Dorsal
Posterior
DD1
DD2
DD3
DD4
DD5
DD6
B
Anterior
Right
Left
Posterior
DD1
DD2
DD3
DD4
DD5
DD6
Anterior
Ventral
Dorsal
Posterior
DD1
DD2
DD3
DD4
DD5
DD6

Figure 5. Embryonic schematic diagram of the left-right DD origins before and after hypothetical intercalation. (**A**) Bean stage embryos are shown from ventral and left side views, with DD neurons migrating towards the midline as described in the literature. From there, the DD neurons hypothetically line up and intercalate, as the literature describes (**B**) 1.5 fold embryos as having the DD neurons DD1-DD6 already in proper order, lined up within the ventral cord. These images describe the extent of literature descriptions of DD neuron embryonic origins, and are based on Sulston et al. (1983) and White et al. (1986).

1.9 Objectives

I. Characterize DD neuron defects in *prkl-1*, *vang-1*, and *fmi-1* mutants, and determine whether or not there are any genetic interactions between these genes.

II. Conduct a candidate screen of both canonical and non-canonical Wnt-Frizzled pathway components with respect to regulation of DD neuron AP positioning.

III. Attempt cell tissue specific rescues of *prkl-1* and *vang-1*, and confirm cell specific rescues with genetic mosaic rescue.

IV. Determine the origins of *prkl-1* DD neuronal positioning defects by examining three dimensional deconvoluted images of the embryonic DD neurons.

1.10 Hypotheses

I. *prkl-1* and *vang-1* will show DD neuron positioning defects and genetic interactions between phenotypes.

II. Multiple canonical and non-canonical Wnt-Frizzled pathway components will be found to regulate DD neuron positioning along the AP axis.

III. Both *prkl-1* and *vang-1* will function within the nervous system, and may function cell-autonomously within the DD neurons.

IV. The embryonic origin of DD neuron positioning defects will be either defective neuronal migration or defective DD neuron intercalation.

Chapter 2: Materials and Methods

2.1 Solutions and reagents:

M9 Buffer:

30mM KH_2PO_4, 40mM Na_2HPO_4, 85 mM NaCl, and 1mM $MgSO_4$ dissolved in ddH_2O (solution is then autoclaved). "M9" is an isotonic solution used for washing and collection of *C. elegans*, and can also be used to rescue desiccated worms.

Bleaching Solution:

20% bleach by volume, 1M NaOH. Bleaching solution should be made on a regular basis to maintain effectiveness. For 1mL of bleaching solution, add 100µL 10M NaOH and 200µL pure bleach to 700µL ddH_2O. Bleaching solution is used to either clean up contaminated worm plates, or to synchronize worms (*C. elegans* eggs will survive bleaching and hatch).

Lysis Buffer:

85µL ddH_2O, 10µL 10X PCR buffer (100mM Tris, 500mM KCl, 15mM $MgCl_2$), 5µL 20mg/mL proteinase K (stock held at 4°C). Lysis buffer is used to isolate genomic DNA from *C. elegans*. ~10µL of lysis buffer is placed in a PCR tube, and approximately 20-50 worms are then placed in the lysis buffer. Worms are then placed at -80°C for 5 minutes to freeze crack their cuticles. Lastly, lysis tubes are placed at 65°C for 90 minutes to dissolve the worms, ending with a 20 minute 95°C denaturation.

Growth and maintenance of *C. elegans*:

Worms are grown on 10mm diameter polystyrene, sterile plates (Fisher Scientific) on Nematode Growth Media (NGM), seeded with OP50 bacteria. NGM is made in large flasks, 5 liters at a time: Mix 4.8L ddH_2O, 85g bacto-agar, 12.5g bacto-peptone, and 15g NaCl, then autoclave. Once autoclaved, add 5mL Cholesterol (5mg/mL dissolved in ethanol), 5mL 1M $MgSO_4$, 5mL 1M $CaCl_2$, and 125mL phosphate buffer (KH_2PO_4/K_2HPO_4 50/50 mix) to the 5 Liter NGM mix – mix. OP50 bacteria are cultured and seeded onto these plates once dried, and ready to use once the OP50 dries.

Tetramisole (20mM):

(-)-Tetramisole hydrochloride (Sigma-Aldrich) is used to paralyze larval and adult *C. elegans* for *in vivo* microscopy. 20mM solutions are prepared by dissolving tetramisole in M9 isotonic solution, which prevents lysis in the paralyzed worms. 20mM tetramisole is dropped onto 4% agarose padded microscope slides with cover slips on top.

2.2 Microscopy:

Immobilized worms were imaged using either a Zeiss AxioImager M2 epifluorescent microscope (with Zeiss AxioVision release 4.8 image acquisition software) or a Zeiss LSM510 confocal microscope (with Zeiss Zen software for image acquisition). In order to image the DD neurons in 3D during embryogenesis, Zeiss Axiovision 4.8 deconvolution software was used on Z-stacks embryos taken at 40X magnification. The resulting images could be rotated in 3D to give a view of DD neurons lining up in the embryo, prior to and during intercalation.

2.3 Genetics:

All animals were crossed into an N2 background as described in Brenner (1974) and grown at 20°C, unless otherwise specified. *C. elegans* loss of function alleles used were: *bar-1(ga80), dsh-1(ok1445), dsh-2(or302), mig-5(tm2639), fmi-1(tm306), cfz-2(ok1201), lin-17(n677), mig-1(n687), prkl-1(ok3182), prkl-1(zy11), let-502(sb118), cam-1(gm122), vang-1(tm1422), vang-1(ok1142), cwn-1(ok546), cwn-2(ok895), egl-20(n585), lin44(n1792),* and *mom-2(ne874).* All alleles are presumed to be strong loss of function, unless otherwise stated. *mom-2(ne874)* and *let-502(sb118)* are temperature sensitive alleles, which are healthy at 20°C and lethal at 25°C; they were grown at 24°C, where they were marginally viable. Unless otherwise stated, all mutant alleles were received from the *C. elegans* Genomic Center at the University of Minnesota. **Table 1** lists these genes and alleles, and names their corresponding component as well as the nature of allelic mutations.

Component	Gene name	Allele name	Mutation
β-Catenin	*bar-1*	*ga80*	Nonsense
Dishevelled	*dsh-1*	*ok1445*	Deletion
Dishevelled	*dsh-2*	*or302*	Deletion
Dishevelled	*mig-5*	*tm2639*	Deletion
Flamingo	*fmi-1*	*tm306*	Deletion
Frizzled	*cfz-2*	*ok1201*	Deletion
Frizzled	*lin-17*	*n677*	Nonsense
Frizzled	*mig-1*	*n687*	Nonsense
Prickle	*prkl-1*	*ok3182*	Deletion
Prickle	*prkl-1*	*zy11**	Nonsense
ROCK	*let-502*	*sb118*	Substitution
ROR	*cam-1*	*gm122*	Nonsense
Vang	*vang-1*	*ok1142*	Deletion
Vang	*vang-1*	*tm1422*	Deletion
Wnt	*cwn-1*	*ok546*	Deletion
Wnt	*cwn-2*	*ok895*	Deletion
Wnt	*egl-20*	*n585*	Nonsense
Wnt	*lin-44*	*n1792*	Nonsense
Wnt	*mom-2*	*ne874*	Substitution

Table 1. *C. elegans* loss of function alleles used. Unless otherwise stated, all loss of function alleles were received from the *C. elegans* Genomic Center at the University of Minnesota. *The *zy11* allele was obtained from Sanchez-Alvarez et al. (2011).

2.4 Transgenic Arrays:

Inserted sequences (*Is)* are concatemers of transgenic DNA (usually several plasmids), which have been integrated into *C. elegans* chromosomes via treatment with UV light. As such, these arrays are stable and inherited in a Mendelian fashion.

Inserted Sequences: *ynIs37 (flp-13p::GFP); zyIs7(prkl-1p::GFP); zyIs22 (vang-1p::GFP::vang-1); zyIs24 (unc-30p::GFP; unc-119p::tagRFP).*

Extra-chromosomal Arrays are large concatemers of plasmids resulting from DNA micro-injection into the gonads of gravid young adult worms. These arrays are not stable and not inherited in a Mendelian fashion. DNA concentrations of these extra-chromosomal arrays is approximated from the DNA concentration in the injection mix (*ng/μL*). It is worth noting that actual DNA copy number for different transgenic lines from the same injection mix will vary.

Extra-chromosomal Arrays: *Ex[unc-30p::tagRFP 5ng/μL];Ex[unc30p::tagRFP 40ng/μL]; Ex[prkl-1p::prkl-1 fosmid 1ng/μL; rgef-1p::tagRFP 25ng/μL]; Ex[mom-2p::tagRFP 20ng/μL; unc-30p::GFP 10ng/μL]; Ex[cwn-1p::mom-2 20ng/μL] Ex[unc-119p::tagRFP 25ng/μL];Ex[unc-119p::GFP::prkl-1 10ng/μL]; Ex[unc-119p::GFP::vang-1 15ng/μL]; Ex[unc-30p::GFP::prkl-1 4ng/μL]; Ex[ajm-1p::GFP::prkl-1 10ng/μL];*

2.5 Molecular Biology

Standard restriction-enzyme based cloning techniques were used to generate plasmids. *prkl-1* and *vang-1* rescue constructs were created by cloning various promoters into pre-existing plasmids, containing either *GFP::prkl-1* or *GFP::vang-1* genomic constructs (Sanchez-Alvarez et al., 2011). These genomic constructs were in pPD95.77 background vectors (gift from Andrew Fire, Stanford University). 3.4kb of the *unc-119* promoter was amplified, digested, and ligated into plasmids containing genomic constructs to yield *unc-119p::GFP::prkl-1* (PstI/SalI) and *unc-119p::GFP::vang-1* (PstI/XbaI). 2.5kb of the *unc-30* promoter was amplified, digested, and inserted into digested genomic vectors to produce *unc-30p::GFP::prkl-1* (PstI/SalI) and *unc-30p::GFP::vang-1* (PstI/XbaI). The *ajm-1p::GFP::prkl-1* plasmid was made by amplifying and digesting a 1.6kb *ajm-1* promoter into a digested *unc-30p::GFP::prkl-1* plasmid (PstI/SalI).

All RFP vectors used were made by cloning promoters into a shuttle vector containing *tagRFP* cDNA. 2.5kb *unc-30,* 3.4kb *unc-119,* 2.4kb *rgef-1,* and 2kb *mom-2* promoters were amplified and stitched into the SL2 tagRFP vector, which made: *unc-30p::tagRFP*, *unc-119p::tagRFP, rgef-1p::tagRFP,* and *mom-2p::tagRFP*, respectively. Additionally, *mom-2* cDNA was inserted into PSK bluescript vector. This *mom-2* cDNA was then cloned into a pPD95.77 vector, along with the amplified *cwn-1* promoter, to produce the *cwn-1p::mom-2* plasmid. In all cases, the Gibson Assembly method (Gibson et al., 2009) was used to stitch promoters into the tagRFP shuttle vector.

2.6 C. elegans Strains Used:

ynIs37

cam-1(gm122); ynIs37

prkl-1(ok3182); ynIs37

vang-1(ok1142); ynIs37

prkl-1(zy11); ynIs37

fmi-1(tm306); ynIs37

vang-1(tm1422); ynIs37

bar-1(ga80); ynIs37

prkl-1(ok3182); vang-1(ok1142); ynIs37

prkl-1(ok3182); vang-1(tm1422); ynIs37

prkl-1(ok3182); fmi-1(tm306); ynIs37

vang-1(ok1142); fmi-1(tm306); ynIs37

cfz-2(ok1201); ynIs37

lin-17(n677); ynIs37

mig-1(n687); ynIs37

dsh-1(ok1445); ynIs37

dsh-2(or302); ynIs37

mig-5(tm2639); ynIs37

cwn-1(ok546); cwn-2(ok895); ynIs37

egl-20(n585); ynIs37

lin44(n1792); ynIs37

cwn-1(ok546); cwn-2(ok895); egl-20(n585); lin44(n1792); ynIs37

mom-2(ne874); ynIs37

let-502(sb118); ynIs37

prkl-1(ok3182); ynIs37; Ex[unc119p::GFP::prkl-1 10ng; odr-1p::dsRED 40ng]

prkl-1(ok3182); ynIs37; Ex[unc119p::tagRFP 25ng]

ynIs37; Ex[unc119p::tagRFP 25ng]

prkl-1(ok3182); vang-1 tm1422; ynIs37;

Ex[unc119p::GFP::vang-1 15ng; myo-2p::tagRFP 20ng]

prkl-1(ok3182); vang-1(tm1422); ynIs37; Ex[unc119p::tagRFP 25ng]

prkl-1(ok3182); ynIs37; Ex[unc30p::GFP::prkl-1 4ng; odr-1p::dsRED 40ng]

prkl-1(ok3182); ynIs37; Ex[unc30p::tagRFP 4ng]

Ex[mom-2p::tagRFP 20ng; unc-30p::GFP 10ng]

ynIs37; Ex[cwn-1p::mom-2 20ng]

zyIs7; Ex[unc-30p::tagRFP 40ng]

zyIs22; Ex[unc-30p::tagRFP 40ng]

prkl-1(ok3182); ynIs37;

Ex[prkl-1p::prkl-1 fosmid 1ng; rgef-1p::tagRFP 25ng]

ynIs37; Ex[unc119p::GFP::prkl-1 10ng; odr-1p::dsRED 40ng]

zyIs24

prkl-1(ok3182); zyIs24

2.7 DNA Micro-injection:

Our method for expressing cDNA of interest in *C. elegans* is by creating "extra-chromosomal arrays", via the DNA micro-injection technique (Stinchcomb et al., 1985). This technique works because the developing haploid germ cells are permeable to DNA. Plasmids injected into the worm gonads enter germ line cells and concatemerize, forming large extra-chromosomal arrays (Evans, 2006). Arrays contain multiple copies of each plasmid injected, and will eventually be expressed by the injected worm's offspring. These arrays are inherited in a non-Mendelian fashion, and can be selected for by fluorescent co-injection markers. These transgenic arrays are not always inherited by every cell lineage during mitotic developmental divisions, resulting in mosaic animals that lack transgenic arrays in some of their cells but not others.

Plasmids and co-injection markers were mixed to final concentrations between 1ng/mL and 40 ng/mL. DNA solution was then loaded into micro-injection needles, pressurized by an Eppendorf Femtojet^{TM} injection machine. Gravid young adult animals are placed on long cover slips in halocarbon oil on top of dried 2% agarose pads (so they stick to the pad), and DNA solution is injected directly into the worms' gonads. Worms are then rescued with M9 solution and placed onto a recovery plate, and screened three days later under a fluorescent dissecting microscope for the co-marker. These animals positive for the co-marker are F1 animals; they are cloned out onto fresh plates and screened 3 days later for F2 (fluorescent positive) worms. F2 worms represent stable transgenic "lines", which contain a stable extra-chromosomal array that can be replicated by cell machinery and passed onto the worms' offspring.

2.8 Quantification of DD Neuron Positioning and Spacing defects:

The DD neurons of each worm strain were measured from the grinder to the anus, calculating the location of each DD neuron as a percentage position along this axis; percentage positions were also calculated from DD1 to the anus for each DD neuron in each worm strain. These neuron locations were then used to generate scatter plots, means, and standard deviations for each DD neuron in each worm strain. Worms were imaged with a Zeiss AxioImager M2 and measured with AxioVision release 4.8 Software. Worms were measured from DD1, DD1 to DD2, DD2 to DD3, etc., ending with the DD6 to the anus measurement. These measurements were then summed in Microsoft Excel and the positions of the DD neurons calculated as a percentage of the worm's length. These scatter plots were created in MatLab using a code written by Dr. Theodore Perkins (OHRI).

Before choosing DD1 as a 0% start location for our percentage position plots, three start locations were considered: The tip of the worm head, the grinder at the posterior end of the pharynx, and DD1. We eliminated the tip of the head as an option, as this introduced great variability in the location of DD1 and ultimately all of the DD neurons. This may have been due to variability in head length, which in theory could introduce significant variability to the location of DD1. To confirm this, we used regression analysis on worm length data from the three start points: The tip of the head, the grinder, and DD1 (all measured to the anus). We graphed these worm lengths against the locations of each DD neuron in wild type animals. This regression can be seen in **Figures 6A-C**.

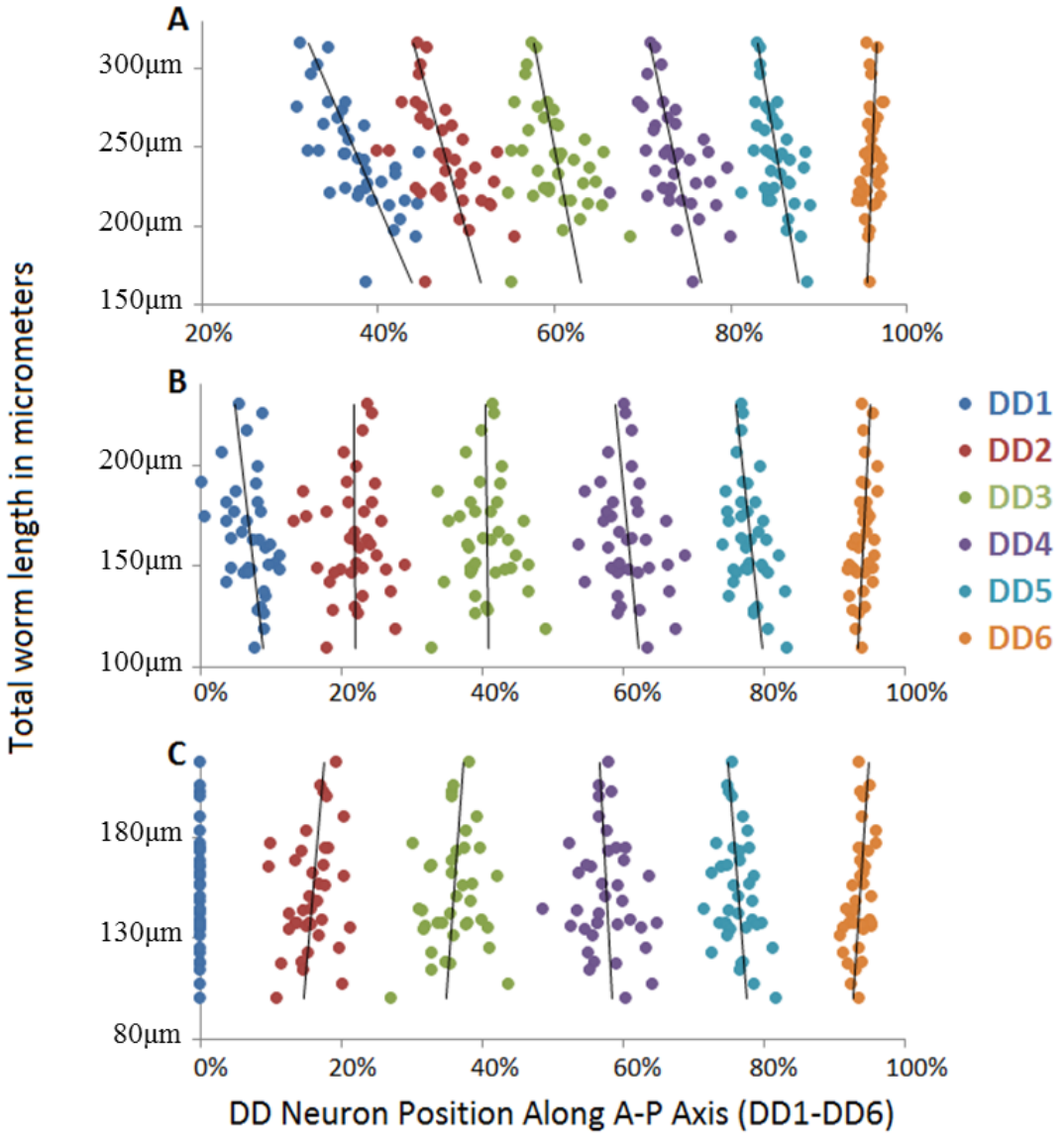

Figure 6. Regression analysis to determine start location for DD neuron position measurements. Total worm length for each worm measured from (**A**) the tip of the head, (**B**) the grinder and (**C**) DD1 to the anus, with their DD neurons plotted as a percentage of total worm length. Regression lines are shown for each DD neuron in each measurement paradigm. A completely vertical line indicates no correlation (good) and lines closer to 45 degrees indicate stronger correlations (bad). Measurements beginning at the tip of the head showed greater correlation between body length and DD neuron location, which would increase variability in the measurement data. This made it an unsuitable choice for our plots. The grinder and DD1 showed essentially the same amount of correlation overall, making them both viable choices as start points for our measurement plots.

Neurons measured from the grinder (**Figure 6B**) and DD1 (**Figure 6C**) to the anus showed lesser correlation between DD neuron percentage location along the A-P axis, and worm length than those measured from the tip of the head (**Figure 6A**). An ideal measurement scheme would see completely vertical correlational lines for all of the DD neurons, which would indicate little variability in DD neuron mean locations between worms of varying lengths. We ultimately chose to use DD1 as a start point for the majority of cases. The DD neurons seem to have the ability space themselves equidistant from each other through an unknown mechanism. As a result, if DD1 is shifted forward (for example in *cam-1* mutants, as well as others), the other DD neurons tend to shift forward as well. **Figures 7A** and **7B** display how an anteriorly localized DD1 neuron can influence the location of all DD neurons, while still maintaining a mostly wild type-like DD neuron spacing.

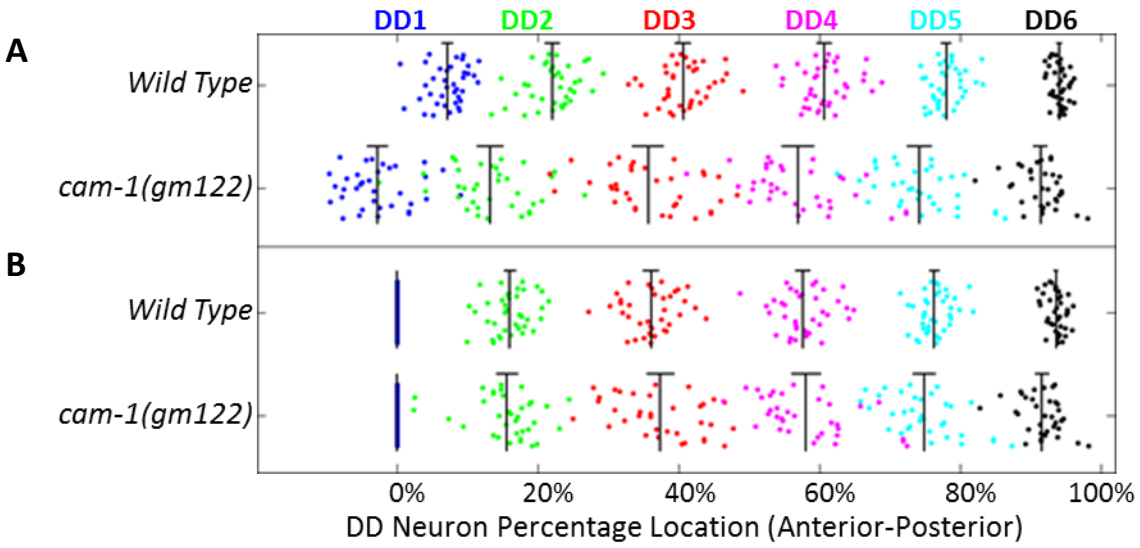

Figure 7. Comparison of DD neuron measurement systems. (**A**)Wild type worms versus *cam-1* mutant worms, measured from the grinder to the anus. (B) Wild type worms versus *cam-1* mutant worms, measured from DD1 to the anus. The *cam-1(gm122)* worm strain appeared to have a general anterior shift of the DD neurons, when worm length was measured from the grinder to the anus. However, normalizing the data by plotting neuron position as a percentage of animal length from DD1 to the anus resulted in almost identical DD neuron distributions for wild type and *cam-1(gm122)* worms. Because we wanted to investigate the role of the PCP pathway on neuronal positioning relative to DD1, we chose to normalize all of our DD neuron plots with DD1 as a start point, to avoid potential caveats from worm strains such as *cam-1*.

When using measurements beginning at the grinder, it was clear that *cam-1* mutants had anteriorly positioned DD neurons (**Figure 7A**). Conversely, the *cam-1(gm122)* worms appeared mostly normal when plotted as a percentage of animal length from a DD1 start point to the anus (**Figure 7B**). As we were interested in mutant worms whose DD neurons showed spacing defects, we chose to use DD1 as a starting point for all of our graphs. It is worth noting that PCP mutants such as *vang-1* and *prkl-1* did not display significant DD1 location shifts, and thus were not affected by this measurement system.

2.9 Alternative DD neuron data presentation as 95% confidence interval bar graphs

Although the DD neuron scatter plots are highly encompassing, displaying all pertinent information, they suffer from the potential weakness of simply presenting too much data at once. For this reason, bar graphs were created which plot the percentage of anteriorly and posteriorly positioned neurons for each DD neuron of each worm strain. Neurons were considered anterior or posterior if they are outside of a 95% confidence interval for the corresponding wild type DD neuron percentage position. These bar graphs more clearly highlighted DD neuron positioning defects. We also generated tables that correspond to each Anterior-Posterior bar graph, which give exact numbers for each defect in each worm strain. These are shown in the **Appendix A**.

2.10 Mosaic Analysis:

As previously mentioned, extra-chromosomal arrays are not inherited in a Mendelian fashion, and are not necessarily passed onto both daughter cells of mitotic divisions. When cells in transgenic animals fail to receive an array after mitotic divisions, that array will be lost to all subsequent daughter cells as well. Should this occur during *C. elegans* embryonic development, any cell that loses an array will result in that cell's downstream lineage also lacking the array. This mosaicism can be harnessed to conduct genetic mosaic rescue experiments.

For example, *prkl-1* mutant defects in the DD neurons could be rescued by an extra chromosomal array containing a *prkl-1p::prkl-1 fosmid*. Mosaic animals lacking the array within the DD neurons may not rescue the phenotype, indicating a requirement for *prkl-1* within the DD neurons. This could be confirmed by searching for mosaic worms expressing *prkl-1* in just the DD neurons, and looking for rescue of the *prkl-1* mutant phenotype. This method has the advantage of rescuing phenotypes in a cell specific manner, but from a wild type copy of the *prkl-1* gene with full introns and a full promoter. This avoids any pitfalls of rescuing phenotypes with cDNA's from unnatural promoters. In our experiments, we marked *prkl-1p::prkl-1 fosmid* arrays with a pan-neuronal *rgef-1p::tagRFP* co-marker. The presence of RFP within a cell marked the presence of the *prkl-1 fosmid*; those RFP expressing cells were said to be "*prkl-1+*". We looked for various types of *prkl-1+* mosaic worms with respect to the DD neurons in a *prkl-1* mutant background, and looked for rescue of DD neuron positioning defects.

Chapter 3: Results

3.1 The DD neurons of *prkl-1* and *vang-1* mutant worms showed cell body spacing and positioning defects

We wanted to investigate the role of the Planar Cell Polarity (PCP) pathway in guiding *C. elegans* neuronal cell body positioning and spacing, and chose the worms' DD-type motor neurons as a model. The six DD neurons of wild type worms are born during embryogenesis, and must space themselves in stereotyped positions within the ventral nerve cord of the worm (White et al., 1986). We used the *ynIs37 (pflp-13::GFP)* reporter to visualize the DD neurons, which showed this stereotypical spacing in wild type animals (**Figure 8A**). In contrast, worms homozygous for the *prkl-1(ok3182)* deletion mutation displayed distinct DD neuron cell body spacing and positioning defects (**Figure 8B**). These *prkl-1* mutants had their DD1 and DD2 & DD3 and DD4 neurons spaced more closely together than did wild type animals, and also showed a general anterior shift of the DD neurons relative to DD1. Similar DD neuron spacing and positioning defects were observed in *vang-1(ok1142)* mutant worms (**Figure 8C**). Taken together, this evidence suggested to us a role for the PCP pathway in guiding DD neuron spacing and positioning.

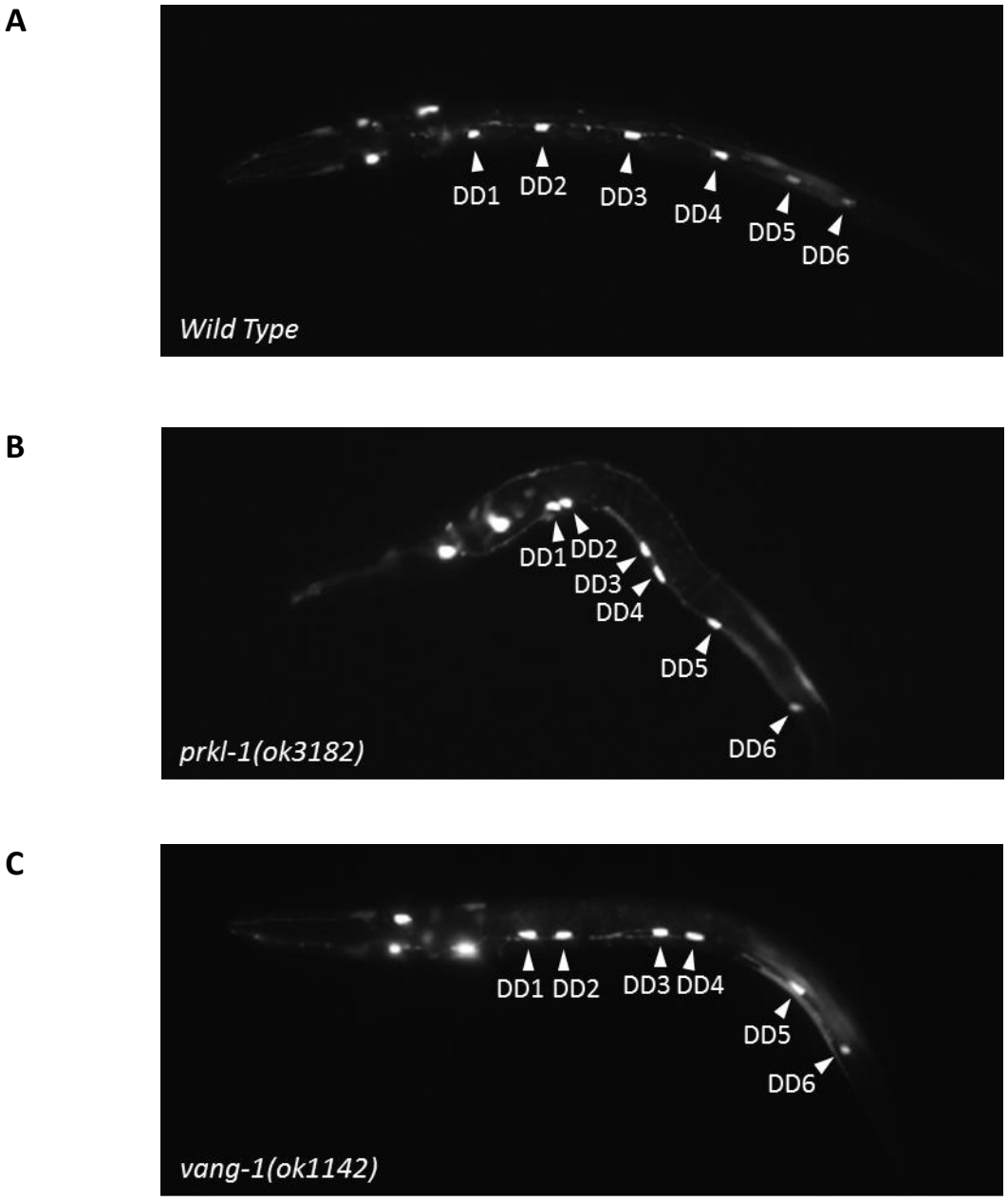

Figure 8. L1 stage *prkl-1* and *vang-1* mutant worms display DD neuron spacing and positioning defects. (**A**) Wild type, (**B**) *prkl-1(ok3182),* (**C**) *vang-1(ok1142)* L1 stage worms, with six DD neurons (DD1-DD6, Anterior-Posterior) marked. *prkl-1* and *vang-1* mutant worms showed anteriorly positioned DD neurons, as well as DD1-DD2 and DD3-DD4 spacing defects, whereas wild type animals displayed evenly spaced DD neurons. There also appeared to be a general anterior shift of the DD neurons relative to DD1 in the *prkl-1* and *vang-1* mutants. All animals carry the *ynIs37* (*flp13p::GFP*) DD neuron GFP reporter.

3.2 *prkl-1* and *vang-1* single mutant worms display significant DD neuron positioning defects

We next sought to quantify DD neuron positioning defects in core PCP mutant worm strains for *prkl-1/Prickle*, *vang-1/Vang*, and *fmi-1/Flamingo*. We also investigated a *bar-1/β-catenin* mutant to determine whether or not the canonical pathway also guides DD neuron positioning. The *prkl-1(ok3182)* worms had the most penetrant DD neuron defects, with DD1 and DD2 & DD3 and DD4 mean locations spaced closely together, as well as a general shift of the DD neurons relative to DD1 (**Figure 9A**). The most severe *prkl-1(ok3182)* DD neuron anterior positioning defects were DD2 (70%), DD4 (80%), and DD5 (86%). *prkl-1(zy11)* had similar defects to *prkl-1(ok3182)* (**Figure 9B**).

The *vang-1(tm1422)* and *vang-1(ok1142)* mutant worms also displayed DD1 and DD2 spacing and positioning defects, with DD2 being anteriorly positioned in 44% of *vang-1(tm1422)* and 41% of *vang-1(ok1142)* mutants. However, DD3 and DD4 and DD5 spacing and positioning defects were weaker in *vang-1* mutants compared to *prkl-1*. For example, DD4 was anteriorly positioned in only 21% of *vang-1(tm1422)* and 39% of *vang-1(ok1142)* mutants versus 80% in *prkl-1(ok3182)*. *fmi-1(tm306)* showed no significant DD neuron defects. The *β-catenin bar-1(ga80)* did display significant DD neuron positioning defects, with DD2 being anteriorly positioned in 95% of worms, as well as weaker but significant DD4, DD5. Although these *bar-1* defects are qualitatively different than *prkl-1* and *vang-1* defects, these results suggest roles for both the PCP and canonical pathways in guiding the positioning of the DD neurons.

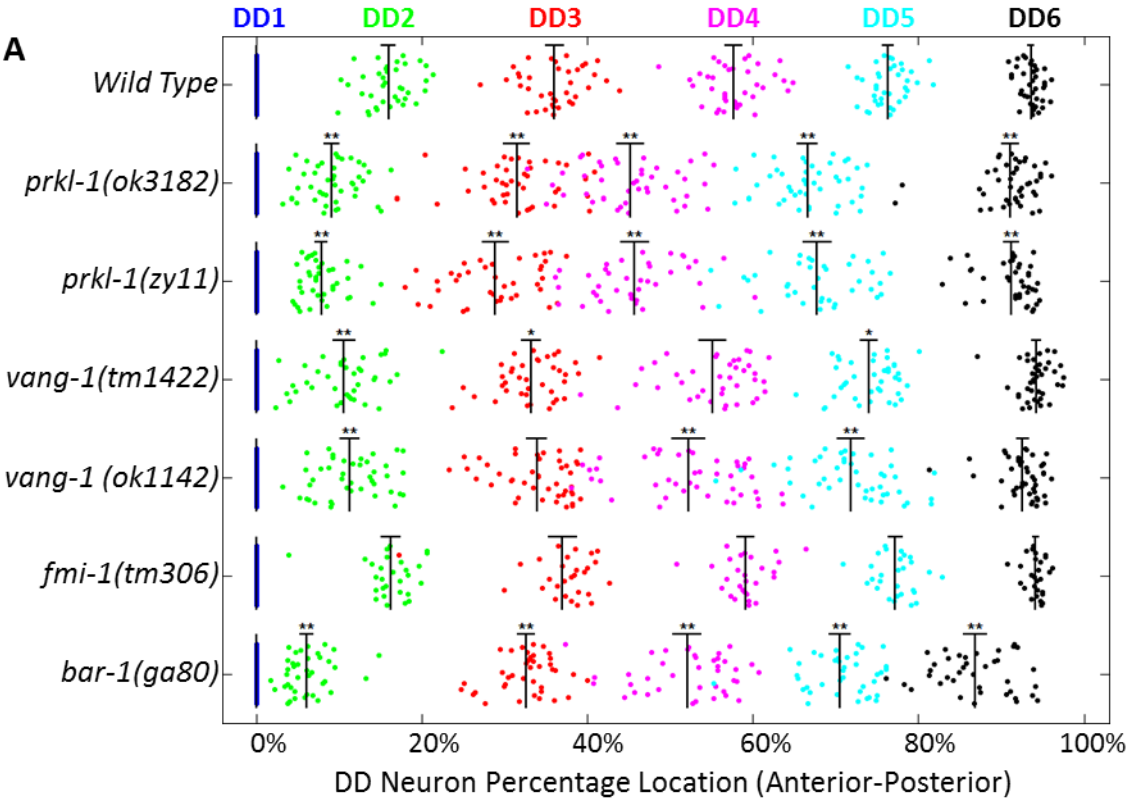
A
DD1
DD2
DD3
DD4
DD5
DD6
Wild Type
prkl-1(ok3182)
prkl-1(zy11)
vang-1(tm1422)
vang-1 (ok1142)
fmi-1(tm306)
bar-1(ga80)
0%
20%
40%
60%
80%
100%
DD Neuron Percentage Location (Anterior-Posterior)

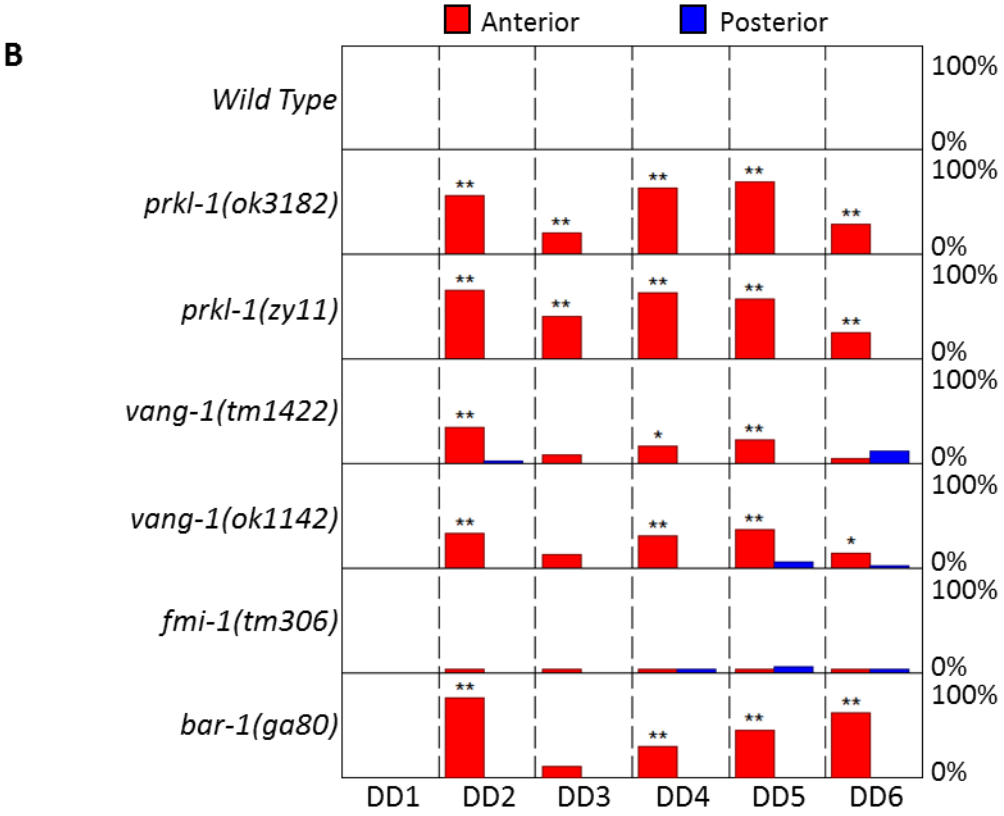
B
Anterior
Posterior
Wild Type
prkl-1(ok3182)
prkl-1(zy11)
vang-1(tm1422)
vang-1(ok1142)
fmi-1(tm306)
bar-1(ga80)
100%
0%
DD1
DD2
DD3
DD4
DD5
DD6

Figure 9. ***prkl-1*** **and** ***vang-1*** **single mutant worms display significant DD neuron spacing and positioning defects.** The DD neurons of *prkl-1*, *vang-1*, *fmi-1*, and *bar-1* single mutant worms are compared to wild type animals. (**A**) Each DD neuron (DD1-DD6) in each worm strain was plotted as a percentage of animal length (measured DD1 to the anus). Vertical lines represent mean DD neuron locations; error bars represent standard error of the mean. (**B**) Bar graphs for each DD neuron of each worm strain represent the percentage of neurons anterior to (red) and posterior to (blue) a wild type 95% confidence interval. Exact % values for bar graphs available in **Appendix A1.** Significance was calculated by comparing each mutant DD neuron data set to the corresponding wild type DD neuron control, using two-tailed t-tests for scatter plots and Chi-squared tests for bar graphs. * P-value ≤ 0.01. ** P-value ≤ 0.001. All animals carry the *ynIs37 (flp-13p::GFP)* inserted sequence.

3.3 The more severe *prkl-1(ok3182)* DD neuron positioning defects are suppressed in double mutant combinations with *vang-1* and *fmi-1*.

We next asked if the core PCP components *prkl-1* and *vang-1* act in the same genetic pathway by creating double mutant combinations. If these genes function within the same pathway, there should be no additive phenotypic penetrance of DD neuron defects. Surprisingly, *prkl-1; vang-1* double mutants displayed defects that were less severe than those of the *prkl-1(ok3182)* mutant (**Figure 10**). For instance, the *prkl-1(ok3182); vang-1(tm1422)* double mutant had DD2 / DD4 / DD5 anterior positioning defects of 33% / 28% / 25% versus 70% / 80% / 86% in the *prkl-1(ok3182)* single mutant. The *prkl-1(ok3182); vang-1(ok1142)* double mutant worms also showed significant phenotypic suppression. These results prompted us to look at *prkl-1* and *vang-1* double mutant combinations with *fmi-1*. As was the case with *vang-1*, the *prkl-1(ok3182); fmi-1(tm306)* double mutants showed significant DD neuron phenotypic suppression versus *prkl-1(ok3182)* single mutants, with double mutants having anterior positioning defect penetrance of 43% (DD2) and 46% (DD4) versus *prkl-1(ok3182)*, at 70% and 80% respectively. *vang-1(ok1142); fmi-1(tm306)* double mutant worms were not significantly different from the *vang-1(ok1142)* single mutants, with the exception of DD6.

The double mutant data indicates that *prkl-1* may interact genetically with *vang-1* and *fmi-1*, and this genetic interaction suggests that PRKL-1 may act to negatively regulate VANG-1 and FMI-1.

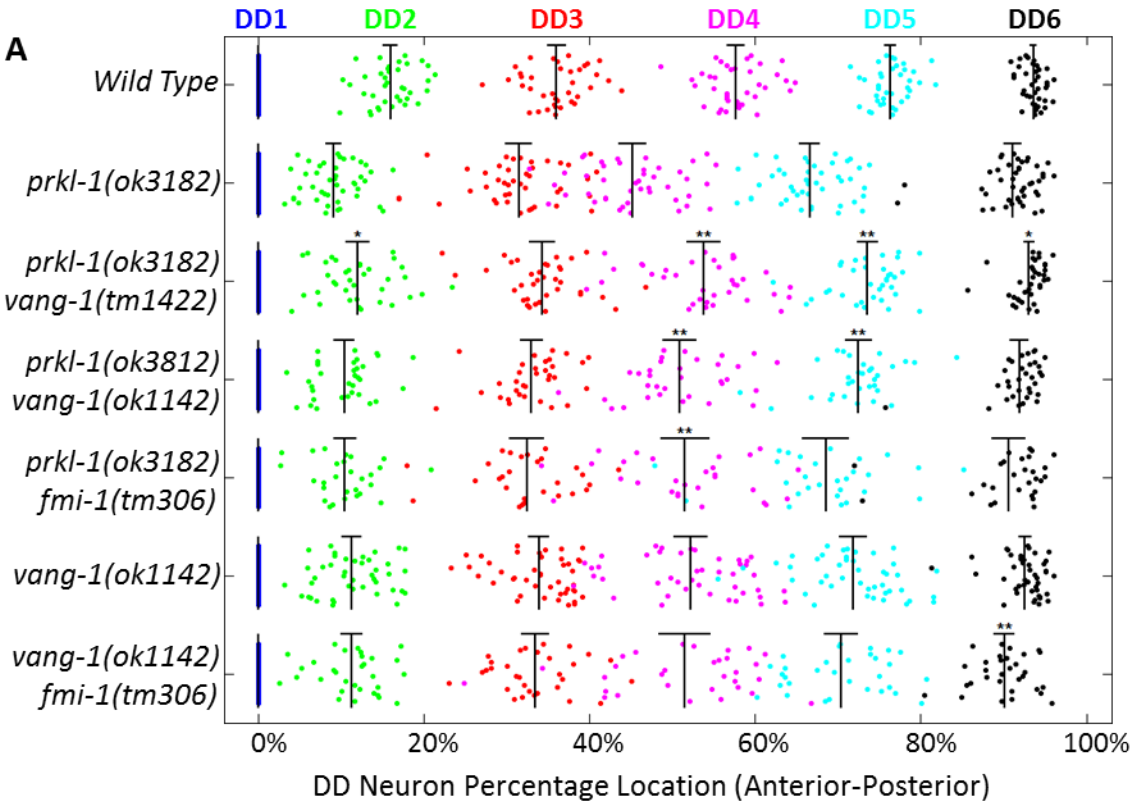
A
DD1
DD2
DD3
DD4
DD5
DD6
Wild Type
prkl-1(ok3182)
prkl-1(ok3182)
vang-1(tm1422)
prkl-1(ok3812)
vang-1(ok1142)
prkl-1(ok3182)
fmi-1(tm306)
vang-1(ok1142)
vang-1(ok1142)
fmi-1(tm306)
0%
20%
40%
60%
80%
100%
DD Neuron Percentage Location (Anterior-Posterior)

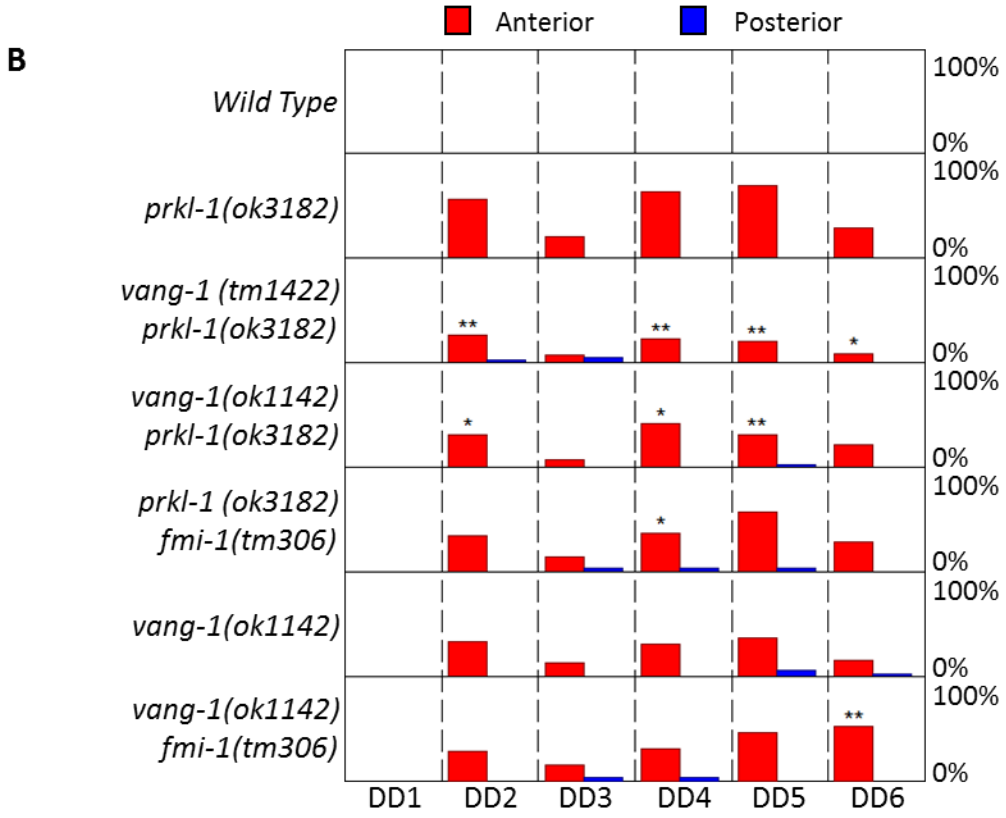
B
Anterior
Posterior
Wild Type
prkl-1(ok3182)
vang-1 (tm1422)
prkl-1(ok3182)
vang-1(ok1142)
prkl-1(ok3182)
prkl-1 (ok3182)
fmi-1(tm306)
vang-1(ok1142)
vang-1(ok1142)
fmi-1(tm306)
100%
0%
DD1
DD2
DD3
DD4
DD5
DD6

Figure 10. ***vang-1* and *fmi-1* suppress the *prkl-1(ok3182)* phenotype in double mutant animals.** (**A**) Scatter plots and (**B**) Anterior/Posterior bar graphs are shown for each DD neuron in p*rkl-1* double mutants with *vang-1(tm1422)*, *vang-1(ok1142)*, and *fmi-1(tm306)*, respectively; these are compared to the *prkl-1(ok3182)* mutant. Also shown is the *vang-1(ok1142); fmi-1(tm306)* double mutant strain, which is compared to the *vang-1(ok1142)* single mutant strain. *ynIs37* wild type worms are shown for comparison. P-values for the *prkl-1* double mutant worms were calculated relative to the *prkl-1(ok3182)* single mutant animal. Significance for the *vang-1(ok1142); fmi-1(tm306)* double mutant was calculated relative to the *vang-1(ok1142)* single mutant. Exact % values for bar graphs available in **Appendix A2.** P-values were generated using two-tailed t-tests for scatter plots and Chi-squared tests for bar graphs. * P-value ≤ 0.01. ** P-value ≤ 0.001. All animals carry the *ynIs37 (flp-13p::GFP)* inserted sequence.

3.4 Conserved Wnt-Frizzled signaling regulates DD neuron positioning

In addition to Prickle, Vang, and Flamingo, PCP signaling also involves the secreted Wnt glycoproteins, their Frizzled receptors, and cytoplasmic components such as Dishevelled and Rho/ROCK. To determine if these other PCP genes are involved in DD neuron positioning, we investigated mutant worm strains for their genes in *C. elegans*. Single knockout mutant worms for four of the five Wnts, three of the four Frizzled genes, and all three Dishevelled genes in *C. elegans* were investigated for DD neuron defects, as was the *C. elegans* ROCK homologue *let-502* (**Figure 11**). As both *vang-1* and *fmi-1* previously suppressed the DD2 and DD4 anterior positioning defects of *prkl-1(ok3182)*, any other gene with mutants showing anterior positioning defects of DD2 and DD4 could be considered to have PCP-type defects.

We found that none of the three *C. elegans* Frizzled genes investigated (*cfz-2, lin-17, mig-1*) display any significant DD neuron defects with respect to DD3- DD4 spacing or anterior positioning of DD4; a similar situation is observed with the dishevelled genes (**Figure 11A-B**). A fourth Frizzled gene in *C. elegans*, *mom-5*, is embryonically lethal (Rocheleau et al., 1997), and was therefore not characterized. Despite single Frizzled and Dishevelled mutants not having PCP-type defects, they may still act redundantly to regulate DD neuron positioning. *cfz-2/Frizzled* displayed mild anterior shifts of DD2 and DD3, and *mig-5/Dishevelled* displayed a 53% strong anterior shift of DD2 with a milder 25% shift of DD3. Interestingly, *dsh-1/Dishevelled* showed mild but significant posterior shifts of the DD neurons relative to DD1, which is opposite to the phenotypes observed in *prkl-1* and *vang-1* mutants. Complication aside, this data is consistent with Frizzled and Dishevelled having

roles in Wnt-Frizzled pathways that guide DD neuron positioning. As for the Wnt ligand itself, only *C. elegans mom-2/Wnt* mutants result in significant defects that could be said to resemble those of *prkl-1* and *vang-1* mutants (**Figure 11C-D)**. However, the Wnt genes in *C. elegans* may also be capable of acting redundantly, and thus we created a quadruple *cwn1-;cwn-2;lin-44;egl-20* mutant to confirm that these Wnts did not play a role in PCP-type defects. This quadruple Wnt mutant did display significant anterior shifts of DD2 (23%), DD5 (23%) and DD6 (77%), but lacked significant DD4 defects. *mom-2/Wnt* was the only gene to display a significant anterior shift of DD4 (35%), but lacked significant DD1 defects. As for the Rho Activated Kinase *let-502/ROCK*, it too displayed a significant DD4 anterior shift (46%) but lacked significant DD1 defects.

These *mom-2* and *let-502* alleles displayed full embryonic lethality at 25-26°C, and were marginally viable when grown at 24°C. As such, *mom-2* and *let-502* L1 animals measured were hypomorphs, and only represented mild losses of function at 24°C. It is reasonable to assume stronger defects would be seen in hypothetical full knockout animals for these genes. Regardless, ROCK is known to signal downstream of Rho (Strutt, 2001), a PCP pathway effector; as similar phenotypes were seen between *mom-2/Wnt and let-502/ROCK*, the data indicates these genes may regulate DD neuron positioning as part of the PCP pathway.

In general, Wnt, Frizzled, Dishevelled, and ROCK mutants showed various DD neuron positioning defects, indicating that conserved Wnt-Frizzled signaling acts to guide DD neuron positioning.

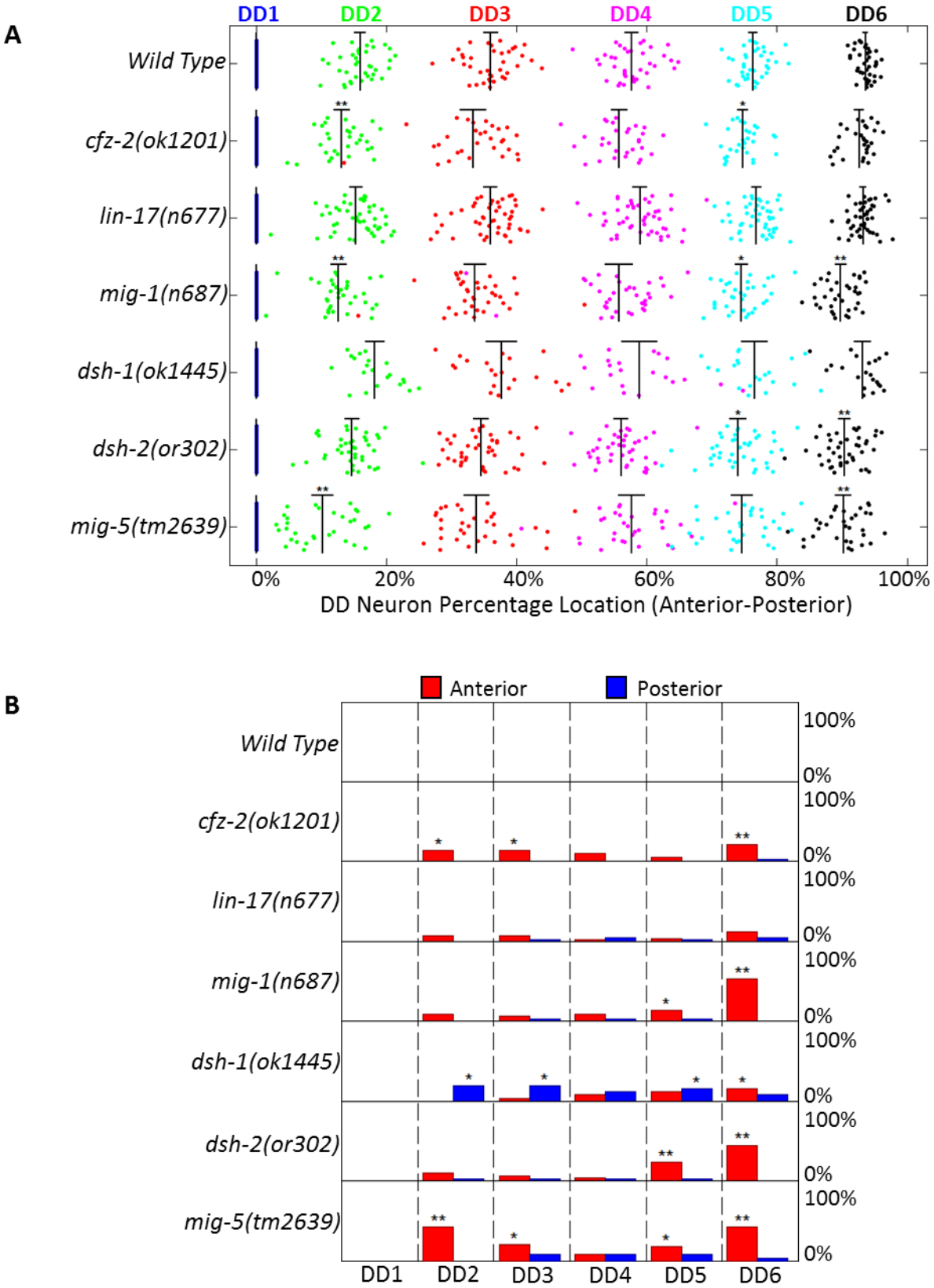
A
DD1
DD2
DD3
DD4
DD5
DD6
Wild Type
cfz-2(ok1201)
lin-17(n677)
mig-1(n687)
dsh-1(ok1445)
dsh-2(or302)
mig-5(tm2639)
0%
20%
40%
60%
80%
100%
DD Neuron Percentage Location (Anterior-Posterior)
B
Anterior
Posterior
Wild Type
cfz-2(ok1201)
lin-17(n677)
mig-1(n687)
dsh-1(ok1445)
dsh-2(or302)
mig-5(tm2639)
100%
0%
DD1
DD2
DD3
DD4
DD5
DD6

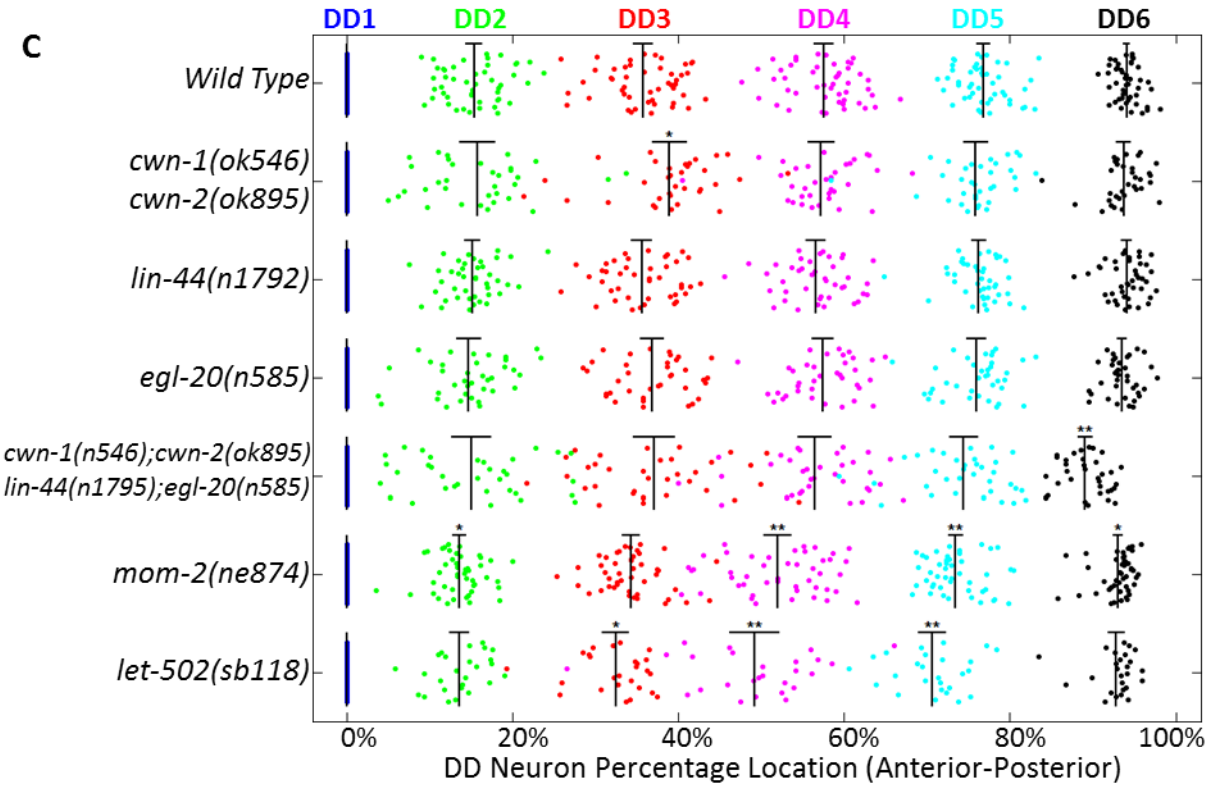
C
DD1
DD2
DD3
DD4
DD5
DD6
Wild Type
cwn-1(ok546)
cwn-2(ok895)
lin-44(n1792)
egl-20(n585)
cwn-1(n546);cwn-2(ok895)
lin-44(n1795);egl-20(n585)
mom-2(ne874)
let-502(sb118)
0%
20%
40%
60%
80%
100%
DD Neuron Percentage Location (Anterior-Posterior)

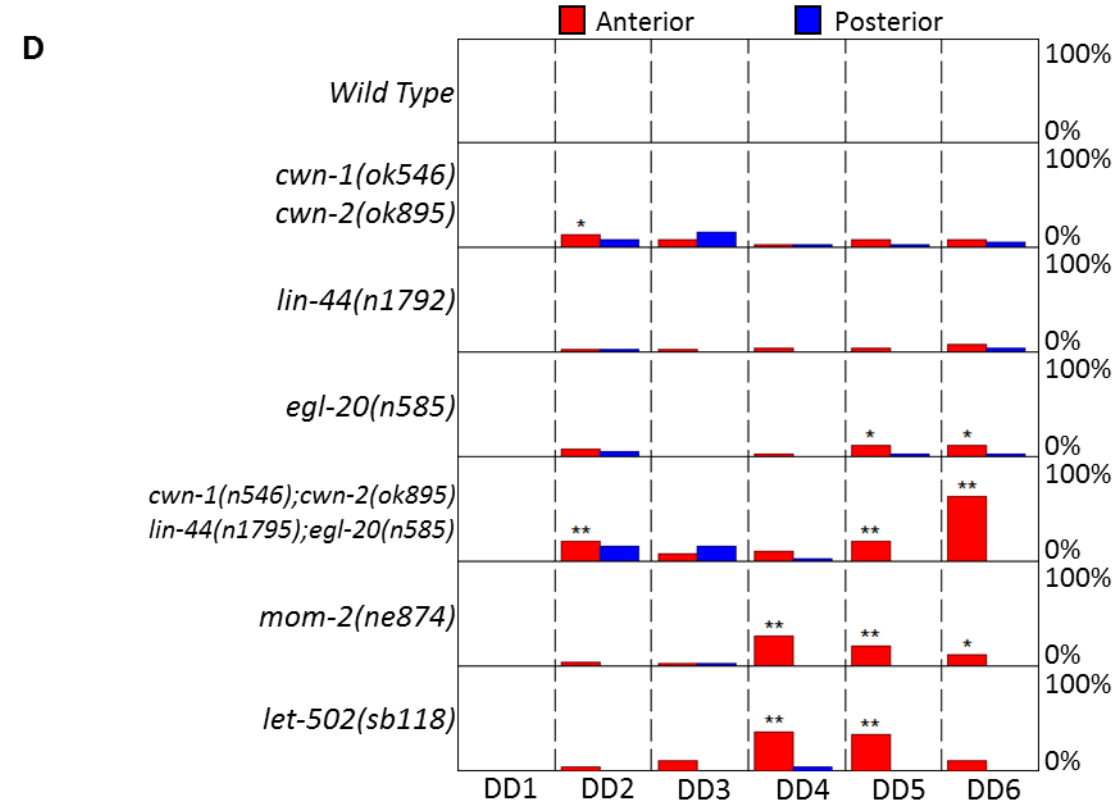
D
Anterior
Posterior
Wild Type
cwn-1(ok546)
cwn-2(ok895)
lin-44(n1792)
egl-20(n585)
cwn-1(n546);cwn-2(ok895)
lin-44(n1795);egl-20(n585)
mom-2(ne874)
let-502(sb118)
100%
0%
DD1
DD2
DD3
DD4
DD5
DD6

Figure 11. **Conserved Wnt-Frizzled signaling regulates DD neuron positioning.** (**A**) Scatter plots and (**B**) Anterior/Posterior bar graphs are shown for each DD neuron in Frizzled and Dishevelled mutant worms. (**C**) Scatter plots and (**D**) Anterior/Posterior bar graphs for the Wnt mutants, as well as the ROCK mutant *let-502*. Exact % values for bar graphs available in **Appendix A3-4.** Significance was calculated by comparing each mutant DD neuron data set to the corresponding wild type DD neuron control, using two-tailed t-tests for scatter plots and Chi-squared tests for bar graphs. * P-value ≤ 0.01.
** P-value ≤ 0.001. All animals carry the *ynIs37 (flp-13p::GFP)* inserted sequence.

3.5 MOM-2/WNT may function instructively to guide DD neuron positioning

With a potential role identified for *mom-2/Wnt* in a PCP pathway guiding DD neuronal positioning, we asked whether *mom-2* could be acting instructively. We hypothesized that any instructive role from Wnts would occur during embryogenesis, where the DD neurons are born and develop (White et al., 1986). Thus, we first sought to visualize cells expressing *mom-2* in comma stage embryos. We created a *mom-2p::tagRFP* plasmid and co-injected this plasmid with *unc-30p::GFP* into wild type animals*;* the transgenic animal generated expressed RFP in *mom-2* producing cells and GFP in the embryonic DD neurons. As can be seen from a left point of view confocal slice, *mom-2* secreting cells were positioned posterior of the DD neurons during the comma stage (**Figure 12A**). A ventral point of view from collated confocal slices indicated that cells expressing *mom-2* were also positioned asymmetrically left of the DD neurons in the same embryo (**Figure 12B**). This asymmetric distribution suggested that *mom-2* may be acting instructively. To confirm this we cloned the *cwn-1/Wnt* promoter into a plasmid with *mom-2* cDNA and injected into wild type *ynIs37* animals, which then expressed *MOM-2* from the *cwn-1* promoter roughly anterior of the DD neurons (Harterink et al., 2011). These worms showed significant anterior shifts of the DD neurons relative to DD1 (**Figure 12C-D**), and resembled *mom-2(ne874).* This evidence suggested that an endogenous MOM-2 gradient may be disrupted in *cwn-1p::mom-2* worms, and that MOM-2 may act instructively to guide DD neuron positioning.

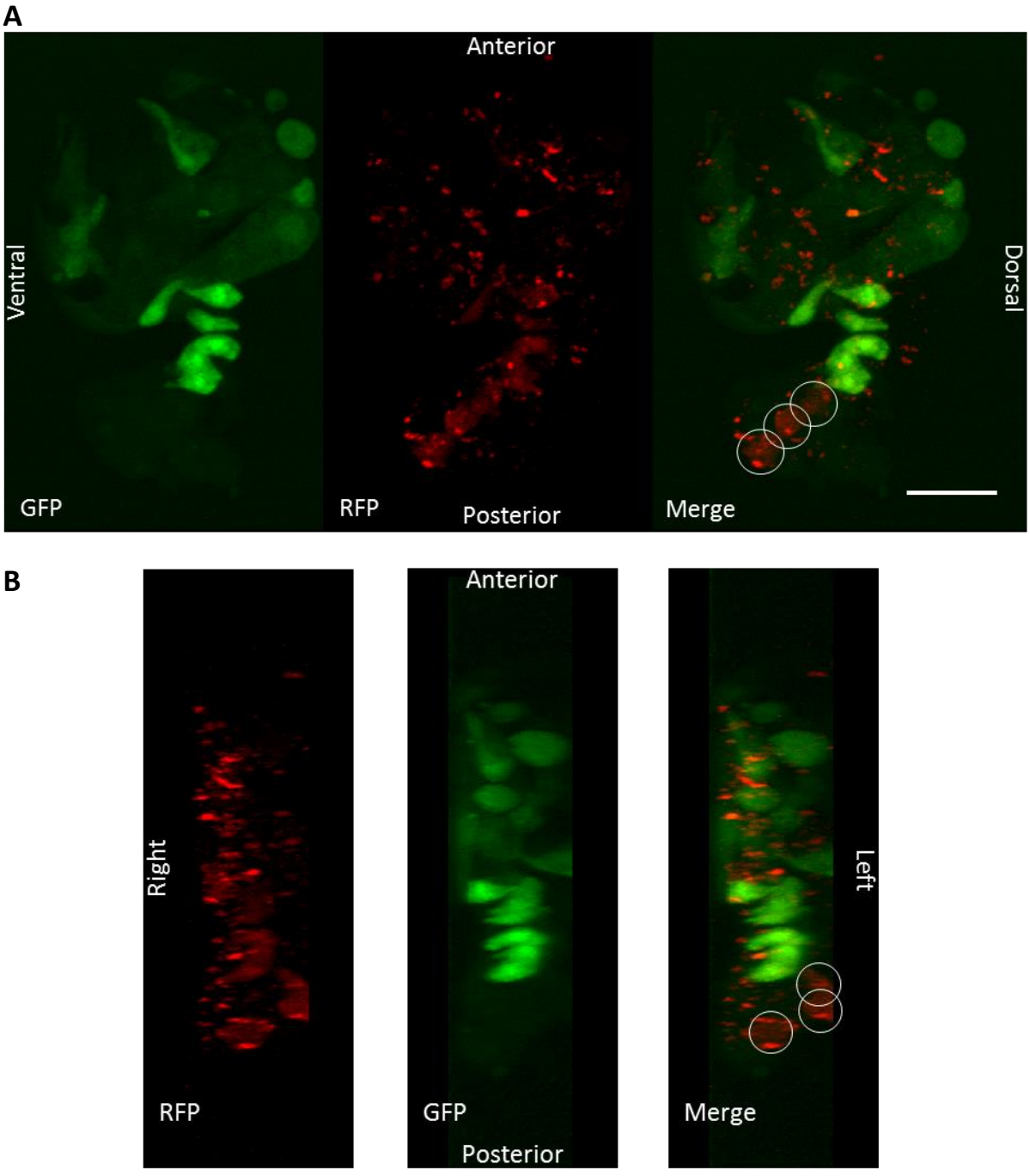
A
Anterior
Ventral
Dorsal
GFP
RFP
Posterior
Merge
B
Right
Anterior
Left
RFP
GFP
Posterior
Merge

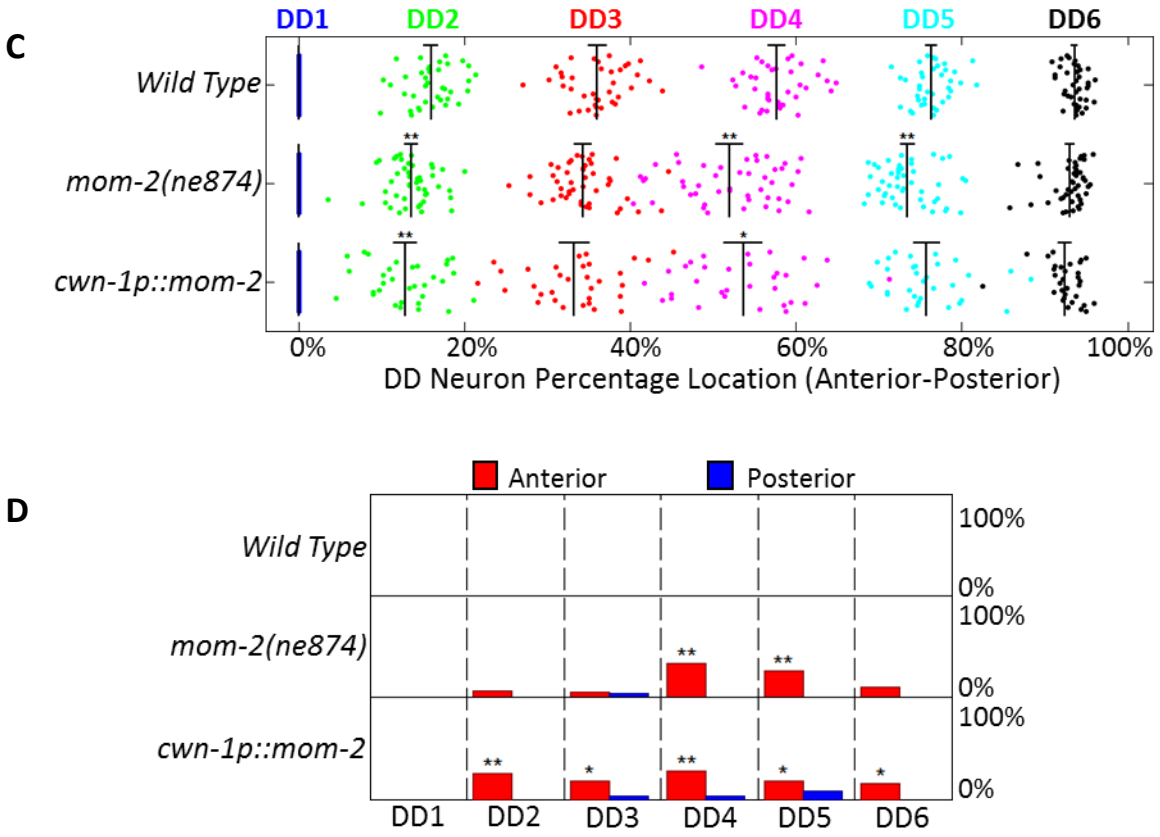

Figure 12. *mom-2* exploratory experiments investigating *mom-2* promoter expression and *mom-2* cDNA ectopic expression. (**A**) Left side and (**B**) ventral views of a comma stage embryo expressing *unc-30p::GFP* in the DD neurons and *mom-2p::tagRFP* in *mom-2* expressing cells, with GFP, RFP, and merge channels shown. The *mom-2* promoter is expressed posteriorly and to the left of the developing DD neurons. (**C**) Scatter plots and (**D**) Anterior/Posterior bar graphs of *cwn-1p::mom-2* worms expressing MOM-2 from the more anterior embryonic *cwn-1* promoter. This transgenic animal is compared to wild type and *mom-2(ne874)* worms, and shows similar defects to the *mom-2* mutant. Scatter plot vertical lines represent mean DD neuron and error bars represent standard error. Exact % values for bar graphs available in **Appendix A5.** Significance was calculated by comparing each mutant DD neuron data set to the corresponding wild type DD neuron control, using two-tailed t-tests for scatter plots and Chi-squared tests for bar graphs. * P-value ≤ 0.01. ** P-value ≤ 0.001. All animals carry the *ynIs37 (flp-13p::GFP)* inserted sequence. Scale bar represents 10μm.

3.6 *prkl-1* and *vang-1* are expressed in the embryonic DD neurons

We wanted to determine whether or not *prkl-1* and *vang-1* might act cell autonomously to guide DD neuron positioning. Our first step was to confirm that they were expressed in the DD neurons during embryogenesis, as the DD neurons develop. We cloned the early DD neuron promoter *unc-30p* into a tagRFP shuttle vector to create *unc-30p::tagRFP*, with which we produced a transgenic reporter line expressing RFP in the DD neurons. This allowed us to visualize the embryonic DD neurons.

Next, we crossed this *unc-30p::tagRFP* reporter into a *prkl-1p::GFP* transcriptional reporter. A 2-fold stage embryo from this double reporter strain is shown, with cytoplasmic RFP expressed in the DD neurons and GFP expressed under the *prkl-1* promoter (**Figure 13**). It can be seen that GFP is co-localized with RFP in the DD neurons, implying that *prkl-1* is expressed in the embryonic DD neurons of *C. elegans*. Additionally, GFP from the *prkl-1* promoter was expressed in cells around the DD neurons, which appear to be the DA and DB neurons of the embryonic ventral cord.

We crossed the *unc-30p::tagRFP* line into a *vang-1p::GFP::vang-1* transcriptional reporter background, which resulted in a worm strain that expressed RFP in the DD neurons and GFP::VANG-1 under the *vang-1* promoter. In general, VANG-1 is widely expressed throughout the nervous system and is mostly membrane localized at the 1.5 fold embryo stage (**Figure 14**). Specifically, GFP::VANG-1 protein seemed to localize to the cell membranes of the DD neurons, confirming that VANG-1 may be expressed in and localize to the cell membrane of the embryonic DD neurons.

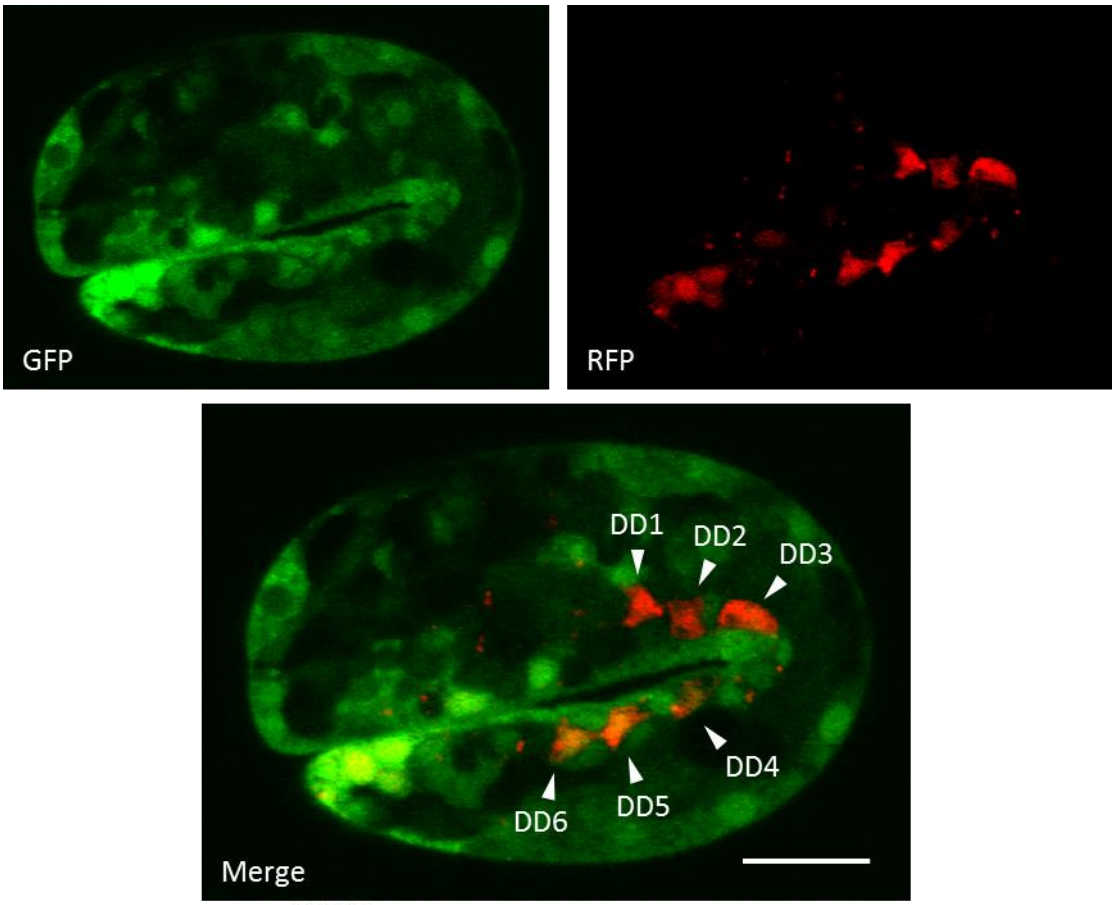

Figure 13. The *prkl-1* promoter is expressed in *C. elegans* embryonic DD neurons.
A 2-fold *C. elegans* embryo is shown with *unc-30p::tagRFP* expressing RFP in the DD neurons and *prkl-1p::GFP* expressing GFP under the *prkl-1* promoter. Confocal GFP, RFP, and merge images are shown. RFP-GFP co-localization indicates that the *prkl-1* promoter is expressed in DD3, DD4, DD5, and DD6. GFP expression in DD1 and DD2 was too weak to be conclusive. Arrow heads indicate the DD neurons in the merged image. Scale bar represents 10μm.

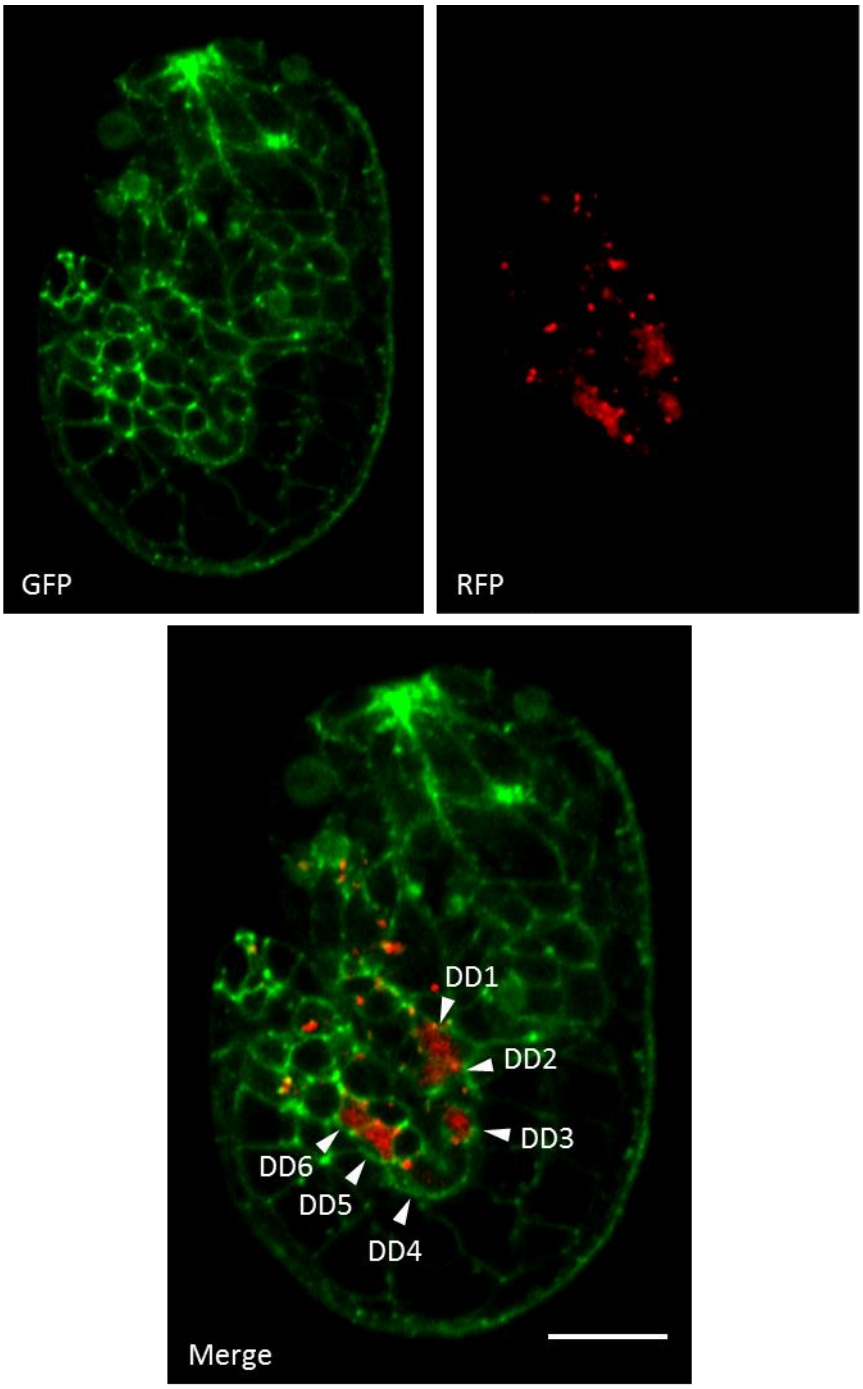

Figure 14. VANG-1 protein is expressed in the DD neurons of *C. elegans* embryos, and localizes to cell membranes. A 1.5-fold *C. elegans* embryo is shown with *unc-30p::tagRFP* expressing RFP in the DD neurons and *vang-1p::GFP::vang-1* expressing GFP::VANG-1 under the *vang-1* promoter. Confocal GFP, RFP, and merge images are shown. RFP-GFP co-localization indicates that that GFP::VANG-1 is expressed in all of the embryonic DD neurons, where it localizes to the cell membranes. Arrow heads indicate the DD neurons in the merged image. Scale bar represents 10μm.

3.7 *prkl-1* and *vang-1* function autonomously in the *C. elegans* nervous system to guide DD neuron positioning, and *prkl-1* functions cell autonomously within the DD neurons

With evidence that *prkl-1* and *vang-1* are widely expressed in the *C. elegans* embryonic neurons, we sought to determine if these genes were acting within the nervous system to regulate DD cell positioning along the A-P axis. Cell specific rescue lines with *prkl-1* or *vang-1* cDNA expressed under either a pan-neuronal promoter (*unc-119*) were assessed for rescue of the appropriate mutant phenotype.

Expressing *prkl-1* cDNA throughout the *C. elegans* nervous system from the *unc-119* promoter yielded a successful and statistically significant rescue in the *prkl-1(ok3182);unc-119p:prkl-1* worms, compared to the *prkl-1(ok3182); unc-119::tagRFP* control mutants (**Figure 15A-B**). An *unc-119p::tagRFP* wild type control is shown without DD neuron positioning defects for reference.

Because the *vang-1* single mutant defects were quantitatively weak, statistically significant rescue may have been difficult to attain. Thus, we decided to express *vang-1* cDNA under the *unc-119* promoter in *prkl-1(ok3182); vang-1(tm1422)* double mutant worms. In theory, this would rescue *vang-1* and in effect create a *prkl-1(ok3182)* single mutant, restoring the more severe *prkl-1(ok3182)* single mutant phenotype. Indeed, this *prkl-1(ok3182);vang-1(tm1422); unc-119p::vang-1* rescue strain showed the more severe *prkl-1(ok3182)* type defects (**Figure 15A-B**), compared to the double mutant *prkl-1(ok3182); vang-1(tm1422)* control strain expressing *unc-119p::tagRFP.*

Lastly, we conducted a cell autonomous rescue experiment for *prkl-1* within the DD neurons. We used the early DD neuron promoter *unc-30* to drive *prkl-1* cDNA expression in a *prkl-1(ok3182)* mutant background. This *prkl-1(ok3182); unc-30p::prkl-1* rescue strain shows a clear restoration of wild type DD neuron positioning, with the exception of DD2. This raises the possibility that DD1-DD2 spacing is regulated, at least in part, cell non-autonomously. The *unc-30p::prkl-1* rescue strain was compared to *prkl-1(ok3182)* mutant worms expressing the control *unc-30p::tagRFP* construct.

Thus, both *prkl-1* and *vang-1* rescued autonomously within the *C. elegans* nervous system, from the *unc-119* promoter. Additionally, *prkl-1* rescued cell autonomously within the DD neurons from the *unc-30* promoter. Unfortunately, we were unable to successfully generate a rescue line for *vang-1* cDNA driven under the *unc-30* promoter. An *unc-30p::vang-1* rescue plasmid was generated and injected at various concentrations into *prkl-1(ok3182); vang-1(tm1422)* double mutant worms, but no rescue was observed. Nonetheless, this evidence suggests that *vang-1* functions within the nervous system to specify DD neuron positioning, and that *prkl-1* functions cell autonomously within the DD neurons themselves to help regulate their locations relative to DD1.

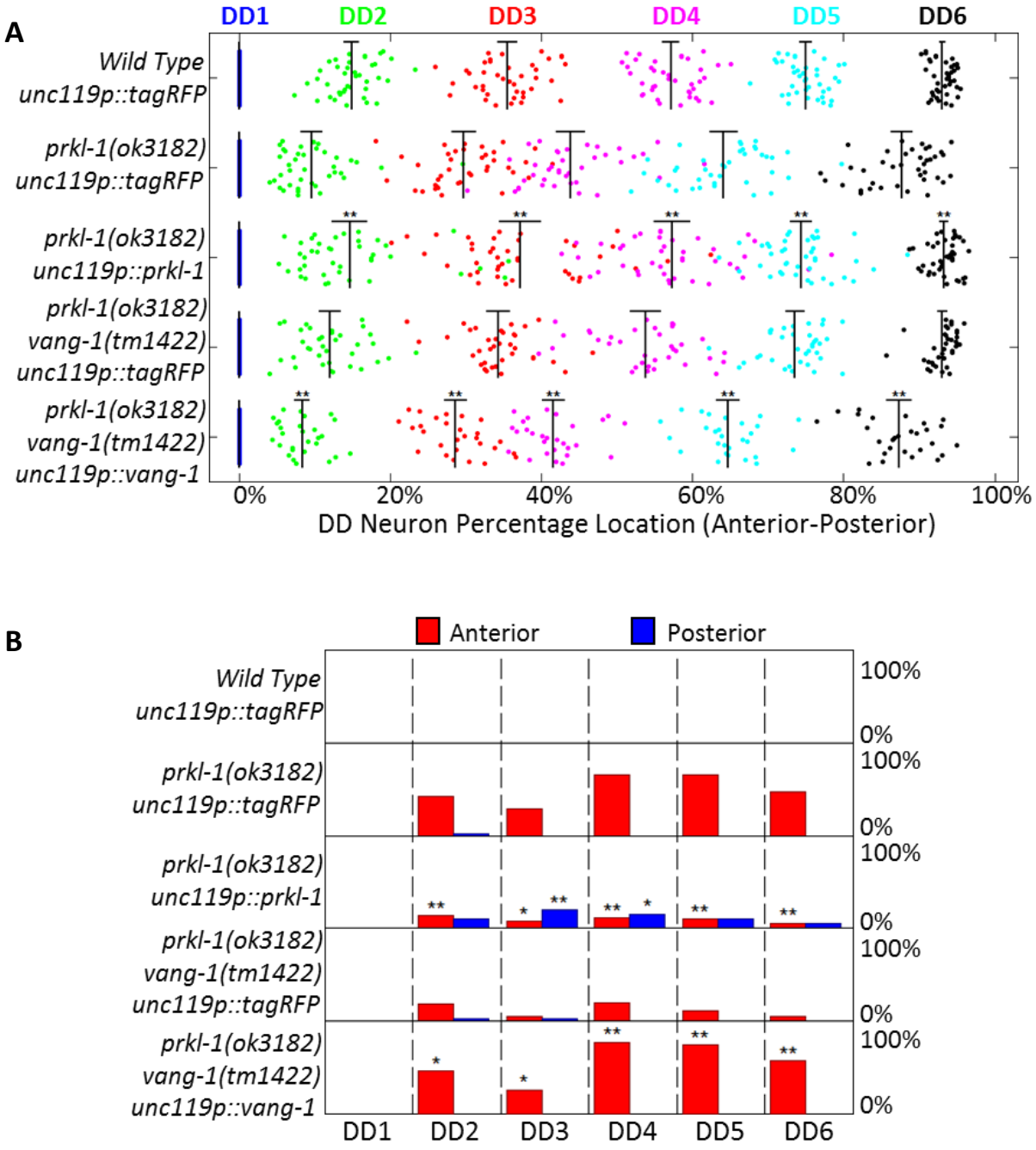
A
DD1
DD2
DD3
DD4
DD5
DD6
Wild Type
unc119p::tagRFP
prkl-1(ok3182)
unc119p::tagRFP
prkl-1(ok3182)
unc119p::prkl-1
prkl-1(ok3182)
vang-1(tm1422)
unc119p::tagRFP
prkl-1(ok3182)
vang-1(tm1422)
unc119p::vang-1
0%
20%
40%
60%
80%
100%
DD Neuron Percentage Location (Anterior-Posterior)
B
Anterior
Posterior
Wild Type
unc119p::tagRFP
prkl-1(ok3182)
unc119p::tagRFP
prkl-1(ok3182)
unc119p::prkl-1
prkl-1(ok3182)
vang-1(tm1422)
unc119p::tagRFP
prkl-1(ok3182)
vang-1(tm1422)
unc119p::vang-1
100%
0%
DD1
DD2
DD3
DD4
DD5
DD6

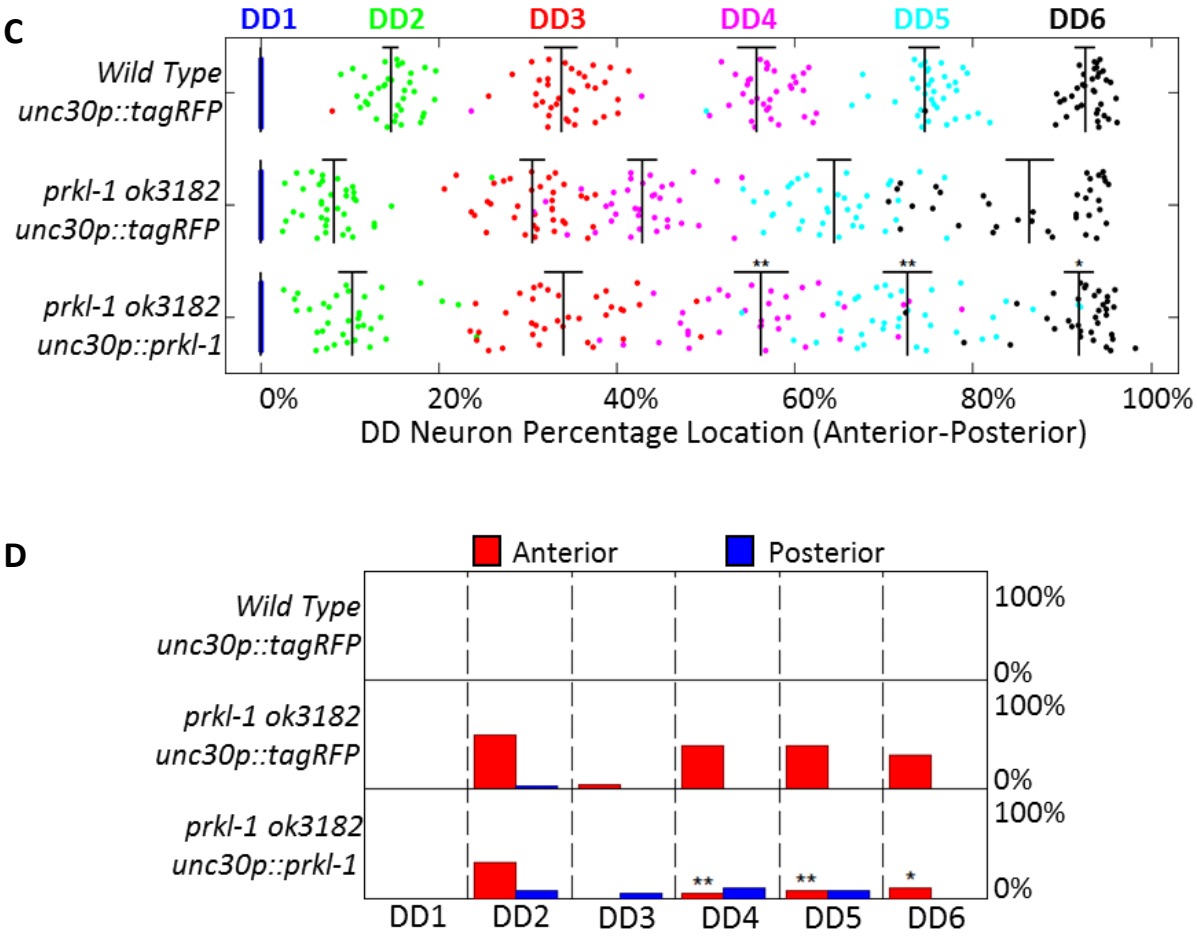

Figure 15. ***prkl-1* and *vang-1* act autonomously within the *C. elegans* nervous system, and *prkl-1(ok3182)* acts cell autonomously within the DD neurons.** (**A**) Scatter plots and (**B**) Anterior/Posterior bar graphs of *prkl-1* and *vang-1* pan-neuronal rescue. The *prkl-1(ok3182)* DD neuron defects were restored to a wild type distribution by *unc-119p::prkl-1*, and the *prkl-1(ok3182); vang-1(tm1422)* double mutant was successfully restored the more severe *prkl-1(ok3182)* single mutant phenotype. Taken together this evidence suggests a tissue specific role for *prkl-1* and *vang-1* within the *C. elegans* nervous system. Wild type, *prkl-1(ok3182)*, and *prkl-1(ok3182);vang-1(tm1422)* worms are shown, which express the *unc-119p::tagRFP* control construct. (**C**) Scatter plots and (**D**) Anterior/Posterior bar graphs of *prkl-1* cell specific rescue are shown, in which the *unc-30p::prkl-1* construct successfully rescued the *prkl-1(ok3182)* defects. Wild type and *prkl-1(ok3182)* control mutants are shown, expressing the *unc-30p::tagRFP* construct. Exact % values for bar graphs available in **Appendix A6.** Significance was calculated by comparing each rescue strain to the corresponding mutant control strain. Wild type *unc-119p::tagRFP* control strain shown for comparison. * P-value ≤ 0.01. ** P-value ≤ 0.001.
All animals carry the *ynIs37 (flp-13p::GFP)* inserted sequence.

3.8 Genetic mosaic rescue experiments confirm *prkl-1* acts cell autonomously.

Extra-chromosomal arrays expressing transgenic DNA in developing *C. elegans* embryos are not always inherited by every cell, which can leave entire embryonic cell lineages without any transgenic DNA. These transgenic animals with arrays in some cells, but not others, are referred to as genetic mosaic animals, or "mosaics". We used mosaic animals expressing a *prkl-1p::prkl-1 fosmid* to conduct cell autonomous rescue experiments for *prkl-1* within the DD neurons. A transgenic worm line was created with an array expressing both the *prkl-1 fosmid* and a pan-neuronal *rgef-1p::tagRFP* co-marker. The co-marker expressed RFP in all larval neurons; any cell expressing RFP was said to be "*prkl-1+"*, containing the *prkl-1 fosmid* transgenic DNA. This array was expressed in *prkl-1(ok3182)* mutant worms, looking for phenotypic rescue in various types of mosaic animals.

The DD neurons arise from the left (DD1/DD3/DD5) and the right (DD2/DD4/DD6) sides of the embryo (Sulston et al., 1983). If an array is lost after this left/right divergence of DD neuron lineage, then that set of DD neurons will lack transgenic arrays. If an array is lost before this left/right divergence, all larval DD neurons will lack transgenic arrays. Thus, we searched for four types of *prkl-1+* mosaics: All DD neurons *prkl-1+*, zero DD neurons *prkl-1+*, DD1/DD3/DD5 *prkl-1+*, and DD2/DD4/DD6 *prkl-1+*. We hypothesized that *prkl-1 fosmid* in all six DD neurons would rescue defects from the *prkl-1(ok3182)* mutant background. Furthermore, we speculated that these mutant defects would not be rescued in mosaics where none of the DD neurons were *prkl-1+*, and that mild phenotypic rescue would occur with *prkl-1 fosmid* in only DD1/DD3/DD5 or DD2/DD4/DD6.

When the *prkl-1 fosmid* array was present in all six DD neurons of mosaic animals, the positioning defects of the *prkl-1(ok3182)* mutant background were rescued (**Figure 16A-B**). Conversely, there was no rescue of the *prkl-1(ok3182)* defects for mosaics in which none of the DD neurons were *prkl-1+*. DD1/DD3/DD5 were *prkl-1+* mosaics still displayed DD neuron positioning defects, but nonetheless showed significant rescue. Lastly, mosaic animals that were *prkl-1+* for DD2/DD4/DD6 showed almost complete rescue of DD neuron defects in the *prkl-1(ok3182)* mutant background.

These results, combined with the previous *unc-30p::prkl-1* rescue, provide further evidence that *prkl-1* functions cell autonomously to regulate DD neuron positioning. Additionally, this experiment suggests that *prkl-1* acts both cell autonomously and non-autonomously within the DD neurons themselves, as the *prkl-1 fosmid* was able to rescue *prkl-1(ok3182)* positioning defects for all six DD neurons when expressed in only DD2, DD4, and DD6.

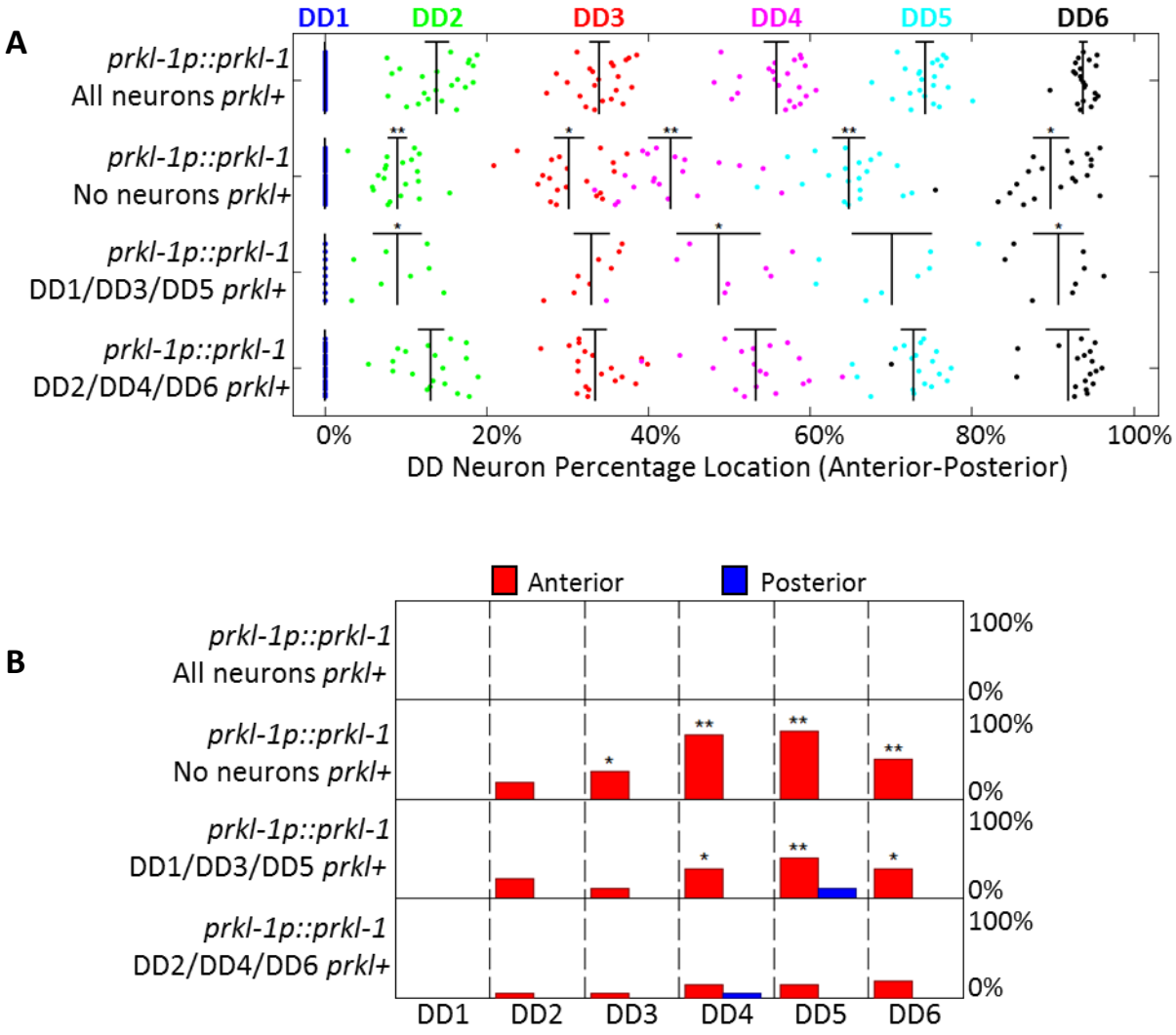

Figure 16. Genetic mosaic rescue experiments confirm *prkl-1* acts cell autonomously. (**A**) Scatter plots and (**B**) Anterior/Posterior bar graphs are shown for each of the four types of mosaic animals investigated. The *prkl-1p::prkl-1 fosmid* successfully rescued the *prkl-1(ok3182)* defects when all six DD neurons were *prkl-1+*. Animals with no DD neurons *prkl-1+* were not rescued, and displayed *prkl-1(ok3182)* defects. DD1/DD3/DD5 *prkl-1+* mosaics showed mild rescue, and DD2/DD4/DD6 *prkl-1+* mosaics showed strong rescue. These results indicate a cell autonomous role for *prkl-1* within the DD neurons. Exact % values for bar graphs available in **Appendix A7.** Significance was calculated by comparing each mutant DD neuron data set to the corresponding wild type DD neuron control, using two-tailed t-tests for scatter plots and Chi-squared tests for bar graphs. * P-value ≤ 0.01. ** P-value ≤ 0.001. All animals carry the *ynIs37 (flp-13p::GFP)* inserted sequence.

3.9 Over-expressing *prkl-1* pan-neuronally produces posteriorly positioned DD neurons

Loss of function in *prkl-1* and *vang-1* results in anteriorly shifted DD neurons. We therefore hypothesized that a gain of function for these genes may have the opposite effect, resulting in posteriorly shifted DD neurons. To test this hypothesis, we chose to over-express *prkl-1* from the pan-neuronal *unc-119* promoter. The *unc-119p::prkl-1* rescue line used earlier was crossed into a wild type background, over-expressing *prkl-1* cDNA on top of endogenous *prkl-1* within the *C. elegans* nervous system. Consistent with our hypothesis, these *prkl-1* over-expression worms displayed posteriorly positioned DD neurons, with DD3-DD6 in the posterior half of the worm (**Figure 17A**). Subsequent quantification of these *unc-119p::prkl-1* over-expression worms confirmed that there were significant posterior shifts in DD neuron positioning. These animals showed 41% of DD3 and 28% of DD4 neurons posteriorly positioned when compared to wild type (**Figure 17B-C**). This data suggests that PRKL-1 plays a key role in DD neuron positioning, as loss of *prkl-1* shifts the DD neurons anterior and gain of *prkl-1* shifts the DD neurons posteriorly.

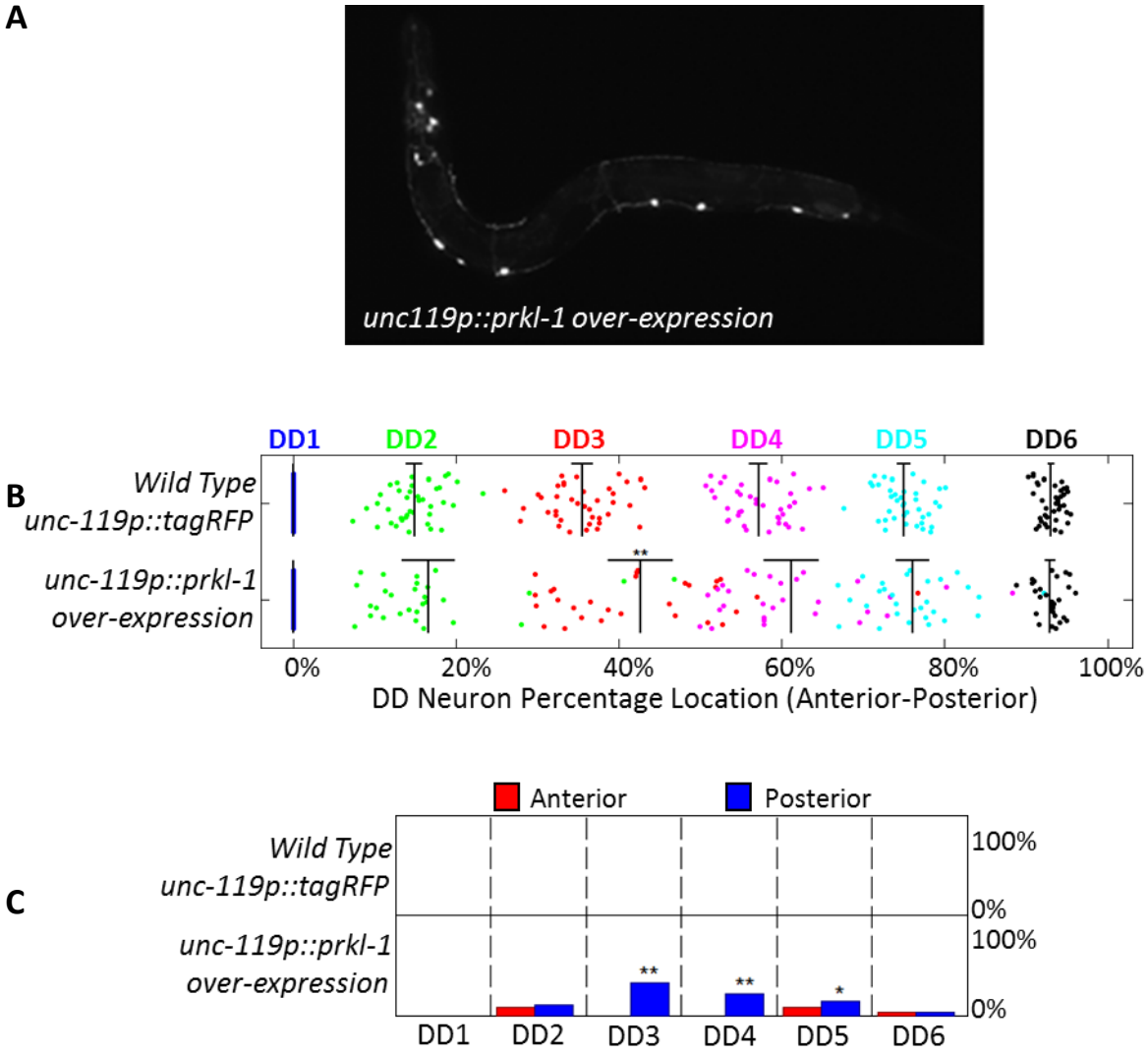

Figure 17. *prkl-1* over-expression animals have posterior DD neuron positioning phenotypes. (**A**) Scatter plots and (**B**) Anterior/Posterior bar graphs are shown for each DD neuron in each worm strain. The *unc-119p::prkl-1* over-expression worms display significant posterior shifts of DD3, DD4, and DD5 versus a wild type *unc-119p::tagRFP* control animal. Exact % values for bar graphs available in **Appendix A8.** Significance was calculated by comparing each mutant DD neuron data set to the wild type control, using two-tailed t-tests for scatter plots and Chi-squared tests for bar graphs. * P-value ≤ 0.01. ** P-value ≤ 0.001. All animals carry the *ynIs37 (flp-13p::GFP)* inserted sequence.

3.10 DD neuron positioning defects are likely caused by delayed DD neuron intercalation during embryogenesis.

Although we had characterized DD neuron positioning defects in PCP mutants, as well as identified a cell autonomous role for *prkl-1* in guiding DD neuron positioning, we still lacked the developmental mechanism regulated by the PCP pathway. Because *prkl-1(ok3182)* mutant worms hatch with DD neuron defects already present, we presumed the role of *prkl-1* lies in DD neuron development during embryogenesis. Another clue came from the fact that the DD neurons originate from the left and right sides of bean stage embryos (Sulston et al., 1983), which we hypothesized must stagger and intercalate as they meet in the midline of embryos. This interested us, as the PCP pathway is known to guide cell intercalations during vertebrate convergence and extension (Ciruna et al., 2006). Thus, we sought to visualize the DD neurons during embryogenesis as they intercalate around the comma stage, and again at the 1.5 fold stage when wild type DD neurons are known to have entered the ventral cord (White et al., 1986).

To image the embryonic DD neurons we used the *zyIs24 (unc-30p::GFP)* reporter and deconvoluted epifluorescent Z-stack images of comma and 1.5 fold stage embryos. This allowed us to generate three dimensional images of the embryonic DD neurons. Examination of comma stage embryos for both wild type (**Figure 18A**) and *prkl-1(ok3182)* (**Figure 18B**) showed the DD neurons lining up in a left-right fashion at the midline, and beginning to intercalate. At this point, there were no obvious differences between wild type and *prkl-1(ok3182)* embryos (although the *prkl-1* mutant embryo in **Figure 18B** has a gap between DD3 and DD4, gaps are also observed in some wild type embryos).

However, 1.5 fold stage images illustrated that the DD neurons had fully finished intercalation in wild type embryos (**Figure 18C**). We defined completion of intercalation as embryos showing all six DD neurons in the same plane, which was the case with 1.5 fold wild type embryos. In contrast, the DD neurons of 1.5 fold stage *prkl-1(ok3182)* embryos had not finished intercalation (**Figure 18D**). DD1 and DD2 & DD3 and DD4 were still staggered on top of each other, and thus not in the same plane at the midline. This was confirmed by rotating the three dimensional DD neuron images of wild type and *prkl-1(ok3182)* 1.5 fold stage embryos (**Figure 18E**). Taken together, these observations suggest that intercalation is delayed in *prkl-1(ok3182)* embryos.

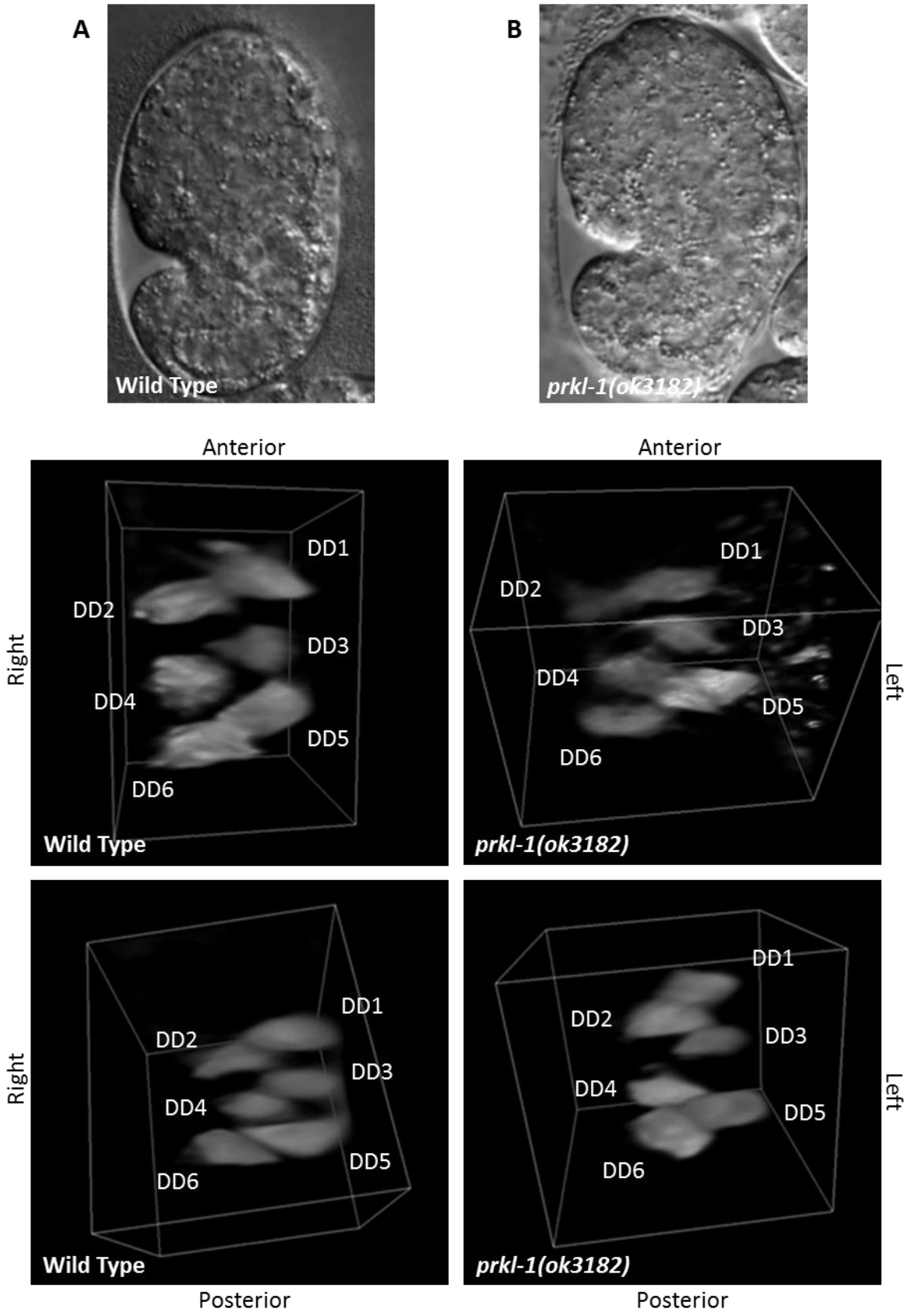
A
Wild Type
B
prkl-1(ok3182)
Anterior
Anterior
DD1
DD2
DD3
DD4
DD5
DD6
Right
Left
Wild Type
prkl-1(ok3182)
DD1
DD2
DD3
DD4
DD5
DD6
Right
Left
Wild Type
prkl-1(ok3182)
Posterior
Posterior

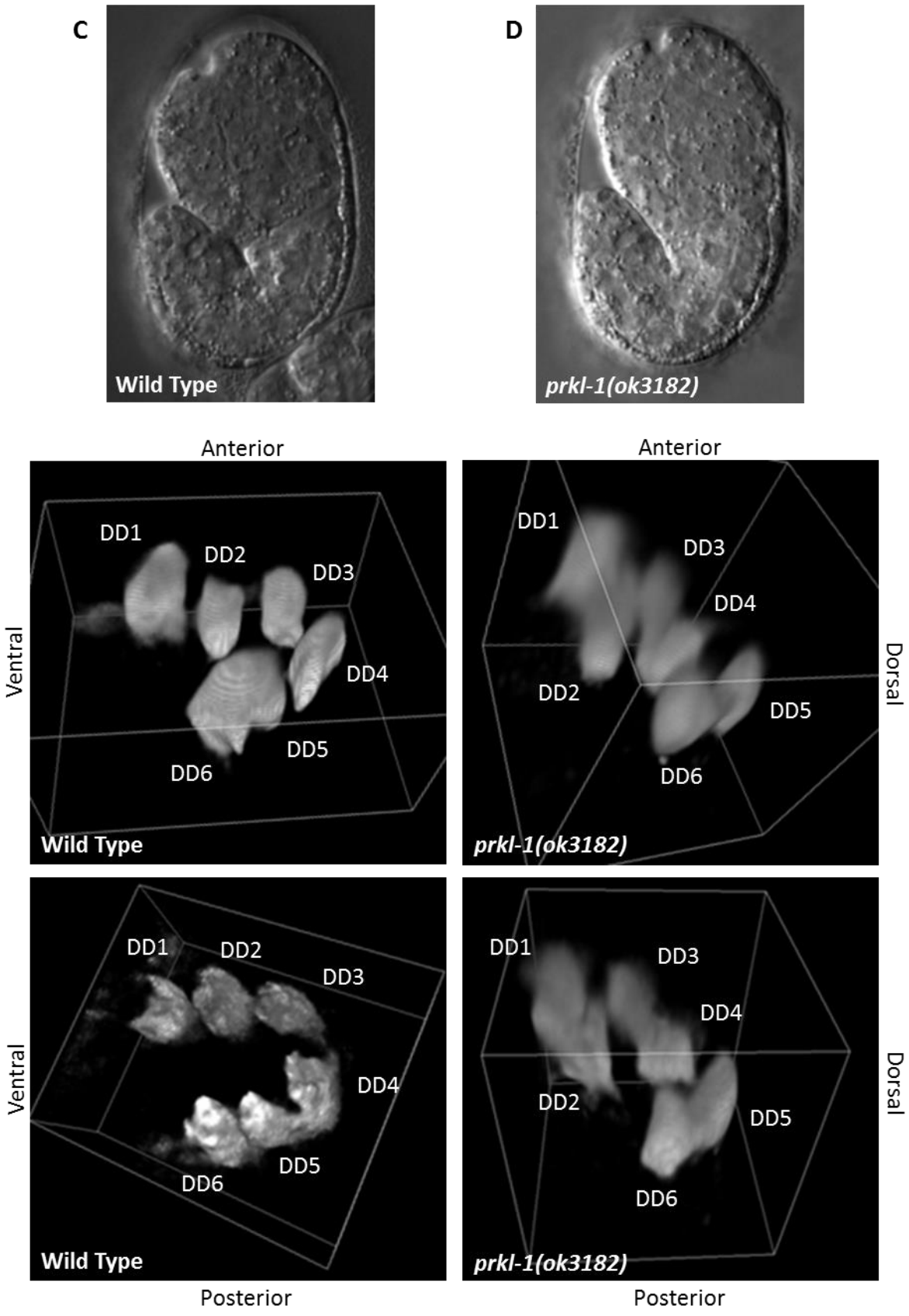
C
Wild Type
D
prkl-1(ok3182)
Anterior
Anterior
DD1
DD2
DD3
DD4
DD5
DD6
Ventral
Dorsal
Wild Type
prkl-1(ok3182)
DD1
DD2
DD3
DD4
DD5
DD6
Ventral
Dorsal
Wild Type
prkl-1(ok3182)
Posterior
Posterior

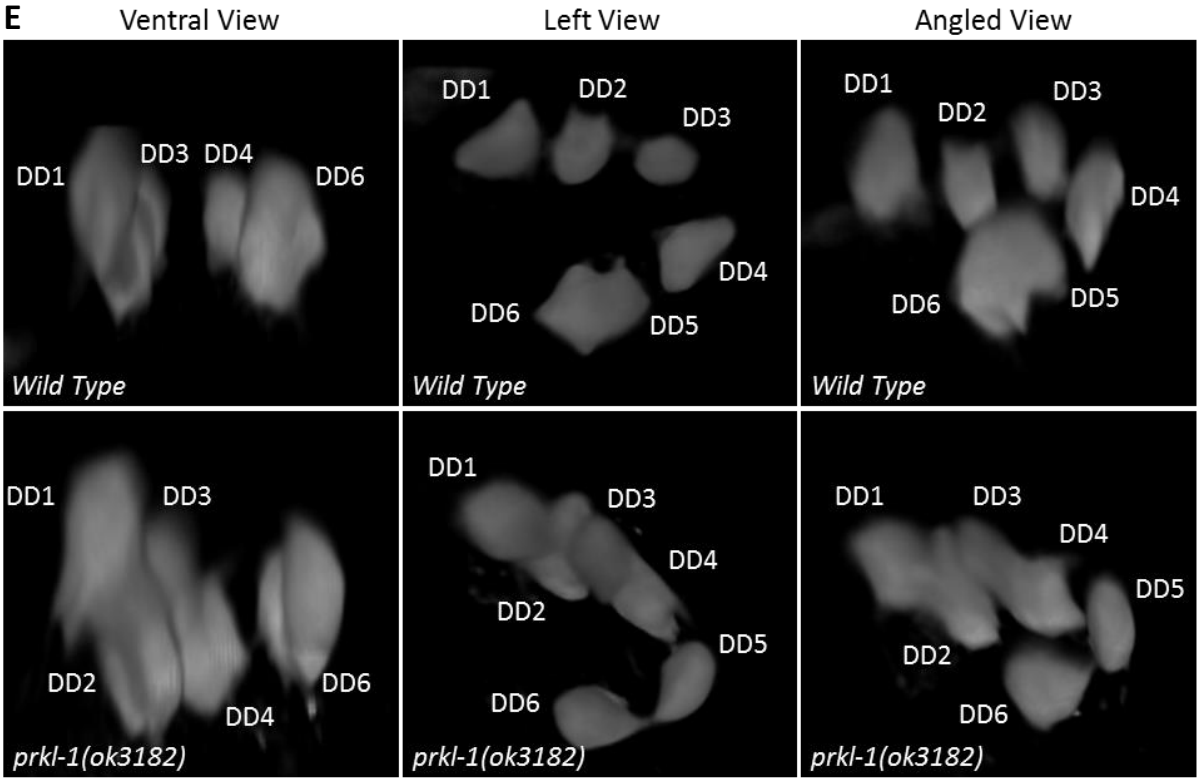

Figure 18. *Prkl-1(ok3182)* comma stage embryos are mostly normal, whereas *prkl-1(ok3182)* 1.5 fold embryos display delayed completion of intercalation. Deconvoluted epifluorescent images of the DD neurons in *C. elegans* embryos expressing *zyIs24 (unc-30p::GFP*) at the comma stage and the later 1.5 fold stage. The DD neurons of (**A**) wild type and (**B**) *prkl-1(ok3182)* comma stage embryos show the DD neurons lining up and beginning to intercalate normally. However, (**C**) wild type 1.5 fold embryos have finished intercalation, whereas the DD neurons of (**D**) *prkl-1(ok3182)* 1.5 fold embryos display delayed intercalation. A DIC image of each embryo stage is shown directly above it for staging purposes. (**E**) Three dimensional rotations to ventral views, left side views, and angled views were used to examine wild type and *prkl-1(ok3182)* 1.5 fold embryos in further detail. This analysis indicates that wild type 1.5 fold embryos have finished intercalation and begun to migrate apart, whereas *prkl-1(ok3182)* 1.5 fold embryos show delayed intercalation with DD1 and DD2 & DD3 and DD4 still staggered on top of each other.

Chapter 4: Discussion

4.1 DD neuron positioning defects may result from delayed intercalation

Our investigation into the role of the PCP pathway in *C. elegans* neuronal positioning concluded with the observation that *prkl-1(ok3182)* 1.5 fold stage embryos show delayed DD neuron intercalation. Specifically, *prkl-1(ok3182)* 1.5 fold stage embryos showed delayed intercalation of the DD1 and DD2 & DD3 and DD4 neuron pairs. The *prkl-1* and *vang-1* larval mutants also showed a pattern in which DD1 and DD2 & DD3 and DD4 were spaced more closely than in wild type. It may not be a coincidence that both embryonic and larval PCP mutant defects involved the same DD1-DD2 and DD3-DD4 neuron pairs. Thus, delayed DD neuron intercalation during embryogenesis may be the cause of the later observed DD neuron positioning defects in PCP mutant worms.

The planar cell polarity pathway has been shown to regulate mediolateral cell intercalations during both notochord formation and neural tube closure (Ciruna et al., 2006; Yin et al., 2008; Doudney and Stanier, 2005). Asymmetric distribution of PCP components seen in these models may apply to the DD neurons. For example, Prickle has been shown to form punctae on the anterior side (Ciruna et al., 2006) of these intercalating cells, requiring Vang for its localization. The PCP pathway in *C. elegans* may also require asymmetric localization of Prickle. Thus, *prkl-1* and *vang-1* mutant worms may have improperly polarized DD neurons, which may affect the abilities of these neurons to intercalate properly.

From a more speculative point of view, intercalating cells during notochord and neural tube closure were summarized to adhere to each other, providing traction for cellular migration as they pull themselves past each other (Walck-Shannon and Hardin, 2014). In this paradigm, delayed intercalation might result from either defective cell migration or excessive cell adhesion. We identified a role for *let-502/ROCK*, which is known to regulate cell migration and motility downstream of Rho signaling (LaMonica et al., 2009). A loss of function of *let-502/ROCK* could reduce motile force during DD neuron intercalation, resulting in a delay. We also found a role for *fmi-1/Flamingo*, which is known to form cross-cell homophilic interactions (Chen et al., 2008) and regulate cell adhesion (Halbleib and Nelson, 2006). Delayed DD neuron intercalation could therefore also result from over-active *fmi-1/Flamingo* causing excessive cell adhesion. Although highly speculative, these represent possible mechanisms by which these PCP genes regulate DD neuronal positioning.

4.2 Both canonical and non-canonical pathways regulate DD neuronal positioning

After we identified roles for core PCP components in *C. elegans* neuronal positioning, we conducted a candidate genetic screen to investigate other canonical and non-canonical genes. For example, the non-canonical ROR receptor tyrosine kinase *cam-1(gm122)* was shown to have anteriorly positioned DD neurons, including DD1, but did not seem to affect DD neuron spacing. *cam-1* has been shown to act with *cwn-2/Wnt* and *mig-1/Frizzled* to guide *C. elegans* nerve ring development, in which the nerve rings of mutant worms were anteriorly positioned (Kennerdell et al., 2009): As both the nerve ring and DD1 are located in the head portion of the worm, it is possible that *cam-1* may play a general role in marking anterior neuronal boundaries.

The *C. elegans* gene *bar-1* displayed DD neuron spacing defects in mutant worms, with a strong anterior positioning defect of DD2 leading to DD1 and DD2 spaced closely together. *BAR-1* is a β-catenin and a canonical Wnt-Frizzled pathway component (Eisenmann et al., 1998). Interestingly, β-catenins are known to have dual roles, acting both within the canonical pathway to promote gene transcription and interacting with Cadherins to regulate cell adhesion (Brembeck, Marta Rosario and Walter Birchmeier, 2006). Does *bar-1* regulate DD neuron adhesion during intercalation? Whatever the mechanism, *bar-1* was shown to have a general anterior shift of the DD neurons, a phenotype we might consider to be PCP-like. Thus, the question must be answered as to whether *bar-1* functions with the PCP pathway, or functions redundantly in a parallel pathway?

Lastly, our candidate screen identified mild DD neuron defects in Frizzled, Dishevelled, Wnt, and ROCK mutant worm strains. From this we concluded that conserved Wnt-Frizzled signaling acts to specify DD neuronal positioning. Three genes of interest that may function in a PCP pathway were identified from this candidate screen: *dsh-1/Dishevelled*, *mom-2/Wnt*, and *let-502/ROCK*. Firstly, the *dsh-1(ok1445)* DD neuron defects were not similar to *prkl-1* or *vang-1* loss of function DD neuron positioning defects. However, the posteriorly shifted DD neurons of *dsh-1(ok1445)* did resemble the *unc-119p::prkl-1* over-expression posterior positioning phenotypes. This data indicates that *prkl-1* may inhibit *dsh-1*, and that the *prkl-1* over-express phenotype occurs because of its suppression of *dsh-1*. This is consistent with literature observations that Prickle inhibits Dishevelled, possibly through causing its degradation (James et al., 2008).

As for *mom-2/Wnt*, there are two broad possibilities for its function: *mom-2* may act permissively, simply needing to be expressed at the right time, or *mom-2* may act instructively. *mom-2* acting instructively would mean it is expressed in asymmetric morphogen gradients, and that these gradients are important for DD neuron development. A *mom-2* morphogen gradient would be consistent with literature observations of Wnt gradients in both embryos and larval worms (Harterink et al., 2011). The observation that *cwn-1p::mom-2* ectopic MOM-2 expression caused defects similar to *mom-2(ne874)* tends to support the idea that MOM-2 acts instructively. Lastly, *let-502/ROCK* is a known effector of the PCP pathway downstream of Rho, leading to cytoskeletal rearrangement (Strutt. 2001). *let-502/ROCK* shows similar defects to *prkl-1* and *vang-1*, which indicates that Prickle and Vang may activate ROCK. Exactly how this might occur is unclear.

4.3 PCP signaling in DD neuronal intercalation

Our data for core PCP components yielded interesting genetic interactions, as both *vang-1* and *fmi-1* double mutants with *prkl-1* showed suppression of the more severe *prkl-1(ok3182)* single mutant defects. From a simple genetic perspective, this implied that *vang-1* and *fmi-1* are over-active in *prkl-1* loss of function animals, and thus *prkl-1* may inhibit *vang-1* and *fmi-1*. However, literature evidence points to the fact that Vang recruits Prickle to the membrane, where they form a functional complex (Jenny et al., 2003; Bastock et al., 2005; Strutt et al., 2013). Vang is also known to promote Flamingo's association with adherens junctions (Strutt and Strutt, 2008), indicating that *vang-1* may activate both *prkl-1* and *fmi-1*. *prkl-1* may then inhibit *fmi-1*, as *prkl-1* was previously hypothesized to inhibit *fmi-1* in *C. elegans* VC4/VC5 neurite polarity (Sanchez-Alvarez et al., 2011).

Combining this speculative interaction of *prkl-1*, *vang-1*, and *fmi-1* with data from *mom-2* and *let-502* yields a possible model for PCP signaling in DD neuron intercalation. *mom-2* may function instructively to establish DD neuron polarity, which may lead to *prkl-1* and *vang-1* asymmetric distribution at the membrane interfaces of neighboring DD neurons. This may cause a neuronal polarity required for proper intercalation, and any loss of *prkl-1* or *vang-1* would result in delayed intercalation. *prkl-1* and *vang-1* induced polarity may lead to downstream activation of ROCK, which would then facilitate the actin cytoskeletal rearrangements that physically cause intercalation. *fmi-1* could act as a non-essential regulator of intercalation, and is inhibited by *prkl-1*. This speculative model of PCP signaling in *C. elegans* neuronal intercalation is shown, with DD3-DD4 intercalation used as an example (**Figure 19**).

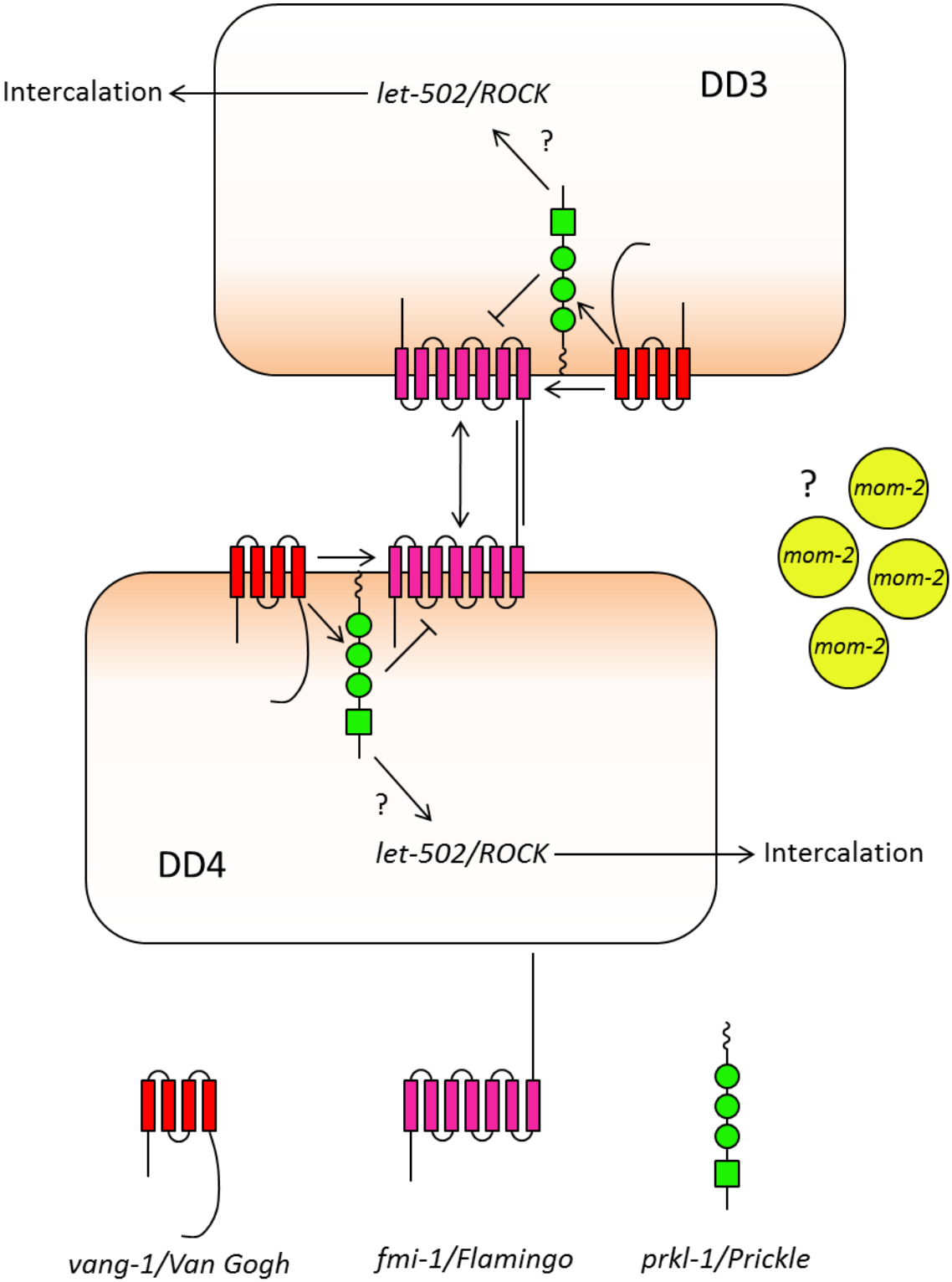
Intercalation
let-502/ROCK
DD3
?
?
mom-2
mom-2
mom-2
mom-2
?
DD4
let-502/ROCK
Intercalation
vang-1/Van Gogh
fmi-1/Flamingo
prkl-1/Prickle

Figure 19. A speculative model for the role of PCP signaling in DD neuronal intercalation. *prkl-1* and *vang-1* might act together to regulate DD3-DD4 neuronal intercalation, leading to downstream *let-502/ROCK* activation via and unknown mechanism. *fmi-1/Flamingo* mediates cell-cell homophilic interactions, playing a non-essential in DD neuron intercalation. *mom-2/Wnt* may give the DD neurons spatial cues, although a receptor for *mom-2* was not identified.

This speculative model, if proven correct, would help explain the various DD neuron defects in different PCP mutant backgrounds. For example, how do *prkl-1(ok3182)* worms have a stronger DD neuron positioning defects than *vang-1* mutants? And how do *vang-1* and *fmi-1* suppress *prkl-1(ok3182)* in the double mutant worms? According to this model, *vang-1* may upregulate both *prkl-1* and *fmi-1*. *prkl-1* would then inhibit *fmi-1* and possibly *vang-1*, in what resembles a feedback loop. In a *prkl-1(ok3182)* mutant, *fmi-1* could become overactive and lead to excessive cell adhesion through its homophilic cross cell binding, potentially delaying DD neuron intercalation. This would be ameliorated in either a *vang-1* or *fmi-1* double mutant with *prkl-1(ok3182)*, which would abolish the homophilic interactions of *fmi-1*. *vang-1* mutants would still have baseline DD neuron intercalation defects, as Vang/Prickle complexes be required for proper *let-502/ROCK* activation. It must be emphasized that, at this point, this model is purely speculative. Nonetheless, it does help explain how some of the genetic interactions seen between PCP components.

However, more detailed questions about the role of the PCP pathway in *C. elegans* neuronal positioning remain: Does *mom-2/Wnt* play a permissive or instructive role? What is the *mom-2* receptor? No role for Frizzled was found; could two or more *C. elegans* Frizzled genes be acting redundantly? And how does the over-expression of *unc-119p::prkl-1* or the loss of function of *dsh-1/Dishevelled* result in posterior positioning DD neuron defects? Does *fmi-1/Flamingo* mediate DD neuron adhesion during intercalation? And lastly, how does the *bar-1* mutant cause anteriorly positioned DD neurons? Does the canonical *bar-1* function with the PCP pathway to produce the same phenotypes? Or does *bar-1* regulate a similar process in a parallel pathway? All of these questions represent possible avenues of future research.

4.4 Future Directions

4.4.1 Answering key questions raised by our speculative model

Our findings of a PCP pathway regulating DD neuron intercalation and cell positioning, and subsequent speculative model, raised many questions about the molecular mechanisms involved. However, with limited time and resources, efforts must be focused on answering a few key questions. Two such key questions are: What is the role of *mom-2*? And what is the role of *fmi-1*?

Does *mom-2/Wnt* act instructively? *mom-2* may simply be permissive. Should this be true, then *cwn-1p::mom-2* expression should rescue the *mom-2(ne874)* defects. If *mom-2* does act instructively, conducting over-expression titrations of *mom-2* from the ectopic *cwn-1* promoter may give an answer. *cwn-1p::mom-2* may cause more severe DD neuron positioning defects with increasing dose, which would provide further evidence that *mom-2* acts instructively. In addition, *mom-2(ne874)* should be crossed into *zyIs24*, having its embryonic DD neurons imaged, deconvoluted, and examined for delayed intercalation.

Lastly, does *fmi-1* act to regulate DD neuron adhesion during intercalation? Although *fmi-1(tm306)* has no phenotype on its own, if *fmi-1* is truly over-active in *prkl-1* mutants then over-expressing *fmi-1* from its own promoter might produce anterior positioning defects. Should *fmi-1* over-expression result in these DD neuron positioning defects, the next step would be to examine *fmi-1* over-expression embryos for delayed intercalation.

4.4.2 Time lapse imaging of intercalation and actin dynamics

The identification of a role for *let-502/ROCK* in delayed DD neuron intercalation tells us that actin cytoskeletal rearrangement may play a role in our phenotypes, as ROCK is a known effector of the PCP pathway that leads to actin rearrangement (Strutt, 2001). One important experiment would be to co-image the embryonic DD neurons alongside a marker for F-actin, such as GFP tagged F-actin. The embryonic DD neuron marker would need to express a membrane bound protein tagged with CFP, YFP, or RFP to mark the DD neurons without interfering with any F-actin signal. Both wild type and PCP mutant embryos could then be imaged via time-lapse confocal microscopy from the bean to 1.5 fold embryo stages, as intercalation occurs. Differences in DD neuron F-actin dynamics between wild type and PCP mutants would give further evidence that a PCP pathway acts to regulate DD neuron intercalation, which may occur via the regulation of actin cytoskeletal dynamics. Embryos in PCP loss of function backgrounds could also be simultaneously assayed for delayed DD neuron intercalation, providing further power to this experiment.

4.4.3 Conducting a forward genetic screen for DD neuron positioning defects

prkl-1 and *vang-1* loss of function animals show anteriorly positioned DD neurons in larval worms, with a pattern that has DD1 and DD2 & DD3 and DD4 spaced closely together. This pattern is simple to identify, even under an epifluorescent dissecting microscope. Thus, a good experiment to follow up our results would be a forward genetic screen, looking for *prkl-1* and *vang-1* like defects in mutagenized worms. Worms with a *ynIs37* DD neuron reporter background could be mutagenized with EMS and screened for these PCP type defects. Screening of worm plates with an epifluorescent dissecting microscope would allow for thousands of genomes to be scanned in a reasonable amount of time. Any new mutants identified could represent new PCP pathway components with respect to regulation of DD neuronal positioning.

4.5 Conclusion and significance

In conclusion, we identified a role for the core PCP components in specifying DD neuron cell positioning and regulating DD neuronal intercalation. Our evidence indicated that *prkl-1* may function within the DD neurons to guide their positioning and intercalation. A candidate screen also identified *mom-2/Wnt* and *let-502/ROCK* as playing a role in DD neuronal positioning. Although the PCP pathway has been previously linked to cell intercalations during convergence and extension of embryos, our results represent a novel role for the PCP pathway in guiding the intercalation of neurons. Future studies should focus on time lapse confocal imaging of F-actin dynamics during DD neuronal intercalation in wild type and PCP mutant embryos. Lastly, forward genetic screens should be conducted, searching for *prkl-1* and *vang-1* like defects in new mutants.

References:

Ackley, B.D. (2013). *Wnt-signaling and planar cell polarity genes regulate axon guidance along the anteroposterior axis in C. elegans*. Developmental Neurobiology, 74(8): 781-796.

Adler, P.N. (2002). *Planar signaling and morphogenesis in Drosophila*. Developmental Cell, 2(5): 525-535.

Andre, P., Wang, Q., Wang, N., Gao, B., Schilit, A., Halford, M.M., Stacker, S.A., Zhang, X., and Yang, Y. (2012). *The wnt coreceptor ryk regulates wnt/planar cell polarity by modulating the degredation of the core planar cell polarity component vangl2.* J Biol Chem., 287(53): 44518-44525.

Bassuk, A.G. et al. (2008). *A Homozygous Mutation in Human PRICKLE1 Causes an Autosomal-Recessive Progressive Myoclonus Epilepsy-Ataxia Syndrome.* The American Journal of Human Genetics, 83(5):572-581.

Bastock, R., Strutt, H., and Strutt, D. (2003). *Strabismus is asymmetrically localized and binds to Prickle and Dishevelled during Drosophila planar polarity patterning.* Development, 130(13): 3007-3014.

Bikkavilli, R.K., Feigin, M.E., and Malbon, C.C. (2008). *G alpha o mediates wnt-JNK signalling through dishevelled 1 and 3, RhoA family members, and MEKK 1 and 4 in mammalian cells.* J Cell Sci., 121(2): 234-245.

Bosoi, C.M., Capra, V., Allache, R., Trinh, V., De Marco, P., Merello, E., Drapeau, P., Bassuk, A.G., and Kibar, Z. (2011). *Identification and characterization of novel rare mutations in the planar cell polarity gene PRICKLE1 in human neural tube defects.* Human Mutation, 32(12): 1371-1375.

Brown, M.D., Cornejo, B.J., Kuhn, T.B., and Bamburg, J.R. (2000). *Cdc42 stimulates neurite outgrowth and formation of growth cone filopodia and lamellipodia.* Journal of Neurobiology, 43(4): 352-364.

Brembeck, F.H., Rosario, M. and Birchmeier, W. (2006). *Balancing cell adhesion and Wnt Signaling, the key role of b-catenin.* Current Opinions in Genetics & Development, 16: 51-59.

Cadigan, K. M. and Liu, Y. I. (2006). *Wnt signalling: complexity at the surface.* Journal of Cell Science,119: 395-402.

Cadigan, K.M., and Nusse, R. (1997). *Wnt signalling: a common theme in animal development.* Genes and Development, 11: 3286-3305.

Calisto, J.D., Araya, C., Marchant, L., Riaz, C.F., and Mayor, R. (2005). *Essential role of non-canonical Wnt signalling in neural crest migration.* Development, 132(11): 2585-2597.
Chan, D.W., Chan, C.Y., Yam, J.W., Ching, Y.P., and Ng, I.O. (2006). *Prickle1- negatively*

regulates Wnt/beta-catenin pathway by promoting dishevelled ubiquitination/degradation in liver cancer. Gastroenterology, 131(4): 1218-1227.

Chen, W.S., Antic, D., Matis, M., Logan, C.Y., Povelones, M., Anderson, G., Nusse, R., and Axelrod, J.D. (2008). *Asymmetric homotypic interactions of the atypical cadherin flamingo mediate intercellular polarity signaling.* Cell, 133(6): 1093-1105.

Ciruna, B., Jenny, A., Lee, D., Mlodzik, M., and Schier, A. (2006). *Planar cell polarity signalling couples cell division and morphogenesis during neurulation.* Nature, 439: 220-224.

Clark, C.E., Richards, L.J., Stacker, S.A., and Cooper, H.M. (2014). *Wnt5a reduces Ryk-dependent and –independent effects on collosal axon and dendrite growth.* Growth Factors, 32(1): 11-17.

Curtin, J.A., Quint, E., Tsipouri, V., Arkell, R.M., Cattanach, B., Copp, A.J., Henderson, D.J., Spurr, N., Stanier, P., Fisher, E.M., Nolan, P.M., Steel, K.P., Brown, S., Gra, I.C. and (2003). *Mutation of celsr1 disrupts planar polarity of inner ear hair cells and causes severe neural tube defects in the mouse.* Current Biology, 13: 1129-1133.

Doudney, K., and Stanier, P. (2005). *Epithelial cell polarity genes are required for neural tube closure*. American Journal of Medical Genetics, 135C: 42-47.

Doyle, K., Hogan, J., Lester, M. and Collier, S. (2008). *The Frizzled planar cell polarity signaling pathway controls Drosophila wing topography*. Developmental Biology, 317(1): 354-367.

Eisenmann, D.M., Maloof, J.N., Simske, J.S., Kenyon, C., and Kim, S.K. (1998). *The β-catenin homolog BAR-1 and LET-60 Ras coordinately regulate the Hox gene lin-39 during Caenorhabditis elegans vulval development.* Development, 125: 3667-3680.

Fanto, M., and McNeill, H. (2002). *Planar polarity from flies to vertebrates*. J. Cell Sci., 117(4): 527-533.

Fanto, M., Weber, U., Strutt, D.I., and Mlodzik, M. (2000). *Nuclear signaling by rac and rho GTPases is required in the establishment of epithelial planar polarity in the Drosophila eye.* Current Biology, 10(16): 979-988.

Fenstermaker, A.G., Prasad, A.A., Bechara, A., Adolfs, Y., Tissir, F., Goffinet, A., Zou, Y., and Pasterkamp, R.J. (2010). *Wnt/planar cell polarity signaling controls the anterior-posterior organization of monoaminergic axons in the brainstem.* J. Neurosci., 30(47): 16053-16064.

Gao, B. (2012). *Wnt regulation of planar cell polarity (PCP)*. Current topics in Developmental Biology, 101(1): 263-295.

Gao, C., and Chen, Y.G. (2010). *Dishevelled: The hub of Wnt signaling*. Cellular Signaling, 22: 717-727.

Gibson, D.G., Young, L., Chuang, R.Y., Venter, J.C., Hutchison, C.A., and Smith, H.O. (2009). *Enzymatic assembly of DNA molecules up to several hundred kilobases.* Nature Methods, 6(5): 343-347.

Goodrich, L. V. (2008). *The plane facts of PCP in the CNS*. Neuron, 60: 9-27.

Goto, T., and Keller, R. (2002). *The planar cell polarity gene strabismus regulates convergence and extension and neural fold closure in Xenopus*. Developmental Biology, 247: 165-181.

Gulasci, A.A., and Anderson, S.A. (2008). *β-catenin-mediated wnt signaling regulates neurogenesis in the ventral telencephalon.* Nature Neuroscience, 11(1): 1383-1391.

Habas, R., Dawid, I.B., and He, X. (2003). *Coactivation of Rac and Rho by Wnt/Frizzled singaling is required for vertebrate gastrulation.* Genes and Development, 17(2): 295-309.

Halbleib, J.M., and Nelson, W.J. (2006). *Cadherins in development: cell adhesion, sorting, and tissue morphogenesis*. Genes and Development, 20(23): 3199-3214.

Harterink, M., Kim, D.H., Middelkoop, T.C., Doan, T.D., Oudenaarden, A.V., and Korswagen, H.C. (2011). *Neuroblast migration along the anteroposterior axis of C. elegans is controlled by opposing gradients of Wnts and a secreted Frizzled-related protein.* Development, 138(1):2915-2924.

Heisenberg, C.P., Tada, M., Rauch, G.J., Sauade, L., Concha, M.L., Geisler, R., Stemple, D.L., Smith, J.C., and Wilson, S.W., (2000). *Silberblick/Wnt11 mediates convergent extension movements during zebrafish gastrulation.* Nature, 405: 76-81.

Herman, M.A., Vassilieva, L.L, Horvitz, H.R., Shaw, J.E., and Herman, R.K. (1995). *The C. elegans* gene *lin-44, which controls the polarity of certain asymmetric cell divisions, encodes a Wnt protein and acts cell nonautonomously.* Cell, 83(1): 101-110.

Hilliard, M. A. and Bargmann, C. I. (2006). *Wnt signals and frizzled activity orient anterior-posterior axon outgrowth in C. elegans.* Developmental Cell, 10: 379-390.

Hirabayashi, Y., Itoh, Y., Tabata, H., Nakajmia, K., Akiyama, T., Masuyama, N., and Gotoh, Y. (2004). *The Wnt/β-catenin pathway directs neuronal differentiation of cortical neural precursor cells.* Development, 131 2791-2801.

Ingham, P.W. (1996). *Has the quest for a Wnt receptor finally frizzled out?* Trends in Genetics, 12(10): 382-384.

James, J.G., Conrad, W.H., and Moon, R.T. (2008). *β-Catenin-Independent Wnt Pathways: Signals, Core Proteins, and Effectors.* Methods in Molecular Biology™, 468: 131-144.

Jenny, A., Darken, R.S., Wilson, P.A., and Mlodzik, M. (2003). *Prickle and strabismus form a functional complex to generate a correct axis during planar cell polarity signaling.* EMBO J., 22(17): 4409-4420.

Jenny, A., Reynolds-Kenneally, J., Das, G., Burnett, M., Mlodzik, M. (2005). *Diego and prickle regulate frizzled planar cell polarity signaling by competing for dishevelled binding.* Nat. Cell Biol. 7(7): 691-697.

Jones, C., and Chen, P. (2007). *Planar cell polarity signaling in vertebrates.* BioEssays, 29(2): 120-132.

Juriloff, D.M., and Harris, M.J. (2012). *A consideration of the evidence that genetic defects in planar cell polarity contribute to the etiology of human neural tube defects.* Birth Defects Res A Clin Mol Teratol., 94(10): 824-840.

Karfunkel, P. (1974). *The mechanisms of neural tube formation.* Int Rev Cytol., 38(0): 245-271.

Katoh, M., and Katoh, M. (2003). *Identification and characterization of human PRICKLE1 and PRICKLE2 genes as well as mouse Prickle1 and Prickle2 genes homologous to Drosophila tissue polarity gene prickle.* Int J Mol Med., 11(2): 249-256.

Kennerdell, J.R., Fetter, R.D., and Bargmann, C.I. (2009). *Wnt-Ror signaling to SIA and SIB neurons directs anterior axon guidance and nerve ring placement in C. elegans.* Development, 136(22): 3801-3810.

Kohl, J., and Jefferis, G.S. (2011). *Neuroanatomy: decoding the fly brain.* Current Biology, 21(1): 19-20.

Komiyal, Y., and Habas, R. (2008). *Wnt signal transduction pathways.* Organogenesis 4(2): 68-75.

Korswagen, H.C., Herman, M.A., and Clevers, H.C. (2000). *Distinct b-catenins mediate adhesion and signalling functions in C. elegans.* Nature, 406: 527-532.

Kühl, M. (2002). *Non-canonical Wnt signaling in Xenopus: regulation of axis formation and gastrulation*. Seminars in Cell & Developmental Biology, 13(3): 243-249.

Kühl, M., Sheldahl, L.C., Park, M., Miller, J.R., and Moon, R.T. (2000). *The Wnt/Ca2+ pathway: a new vertebrate Wnt signaling pathway takes shape.* Trends in Genetics, 16(7): 279-283.

LaMonica, K., Bass, M., and Grabel, L. (2009). *The planar cell polarity pathway directs parietal endoderm migration.* Developmental Biology, 330(1): 44-53.

Lapebie, P., Borchiellini, C. and Houliston, E. (2011). *Dissecting the PCP pathway: One or more pathways?: Does a separate Wnt-Fz-Rho pathway drive morphogenesis?* Bioessays, 33(10): 759-768.

Lawson, A. *Neurulation.* Encyclopedia of Neurosience, Pages 1107-1113.

Li, F., Chong, Z.Z., and Maiese, K. (2005). *Vital elements of the Wnt-Frizzled signalling pathway in the nervous system.* Curr Neurovasc Res. 2(4): 331-340.

Liu, C., Li, Y., Semenov, M., Han, C., Baeg, G.H., Tan, Y., Zhang, Z., Lin, X., and He, X. (2002). *Control of β-catenin phosphorylation/degradation by a dual-kinase mechanism.* Cell, 108(1): 837-847.

Lindqvist, M., Horn, Z., Bryja, V., Schulte, G., Papachristou, P., Ajima, R., Dyberg, C., Arenas, E., Yamaguchi, T.P., Lagercrantz, H., and Ringstedt, T., (2010). *Vang-like protein2 and Rac1 interact to regulate adherenss junctions.* J. Cell. Sci., 123: 472-483.

Malbon, C.C., and Wang, H.Y., (2005). *Dishevelled: A mobile scaffold catalyzing development.* Current topics in developmental biology, 72(1): 153-166.

De Marco, P., Merello, E., Cama, A., Kibar, Z., and Capra, V. (2011). *Human neural tube defects: Genetic causes and prevention.* Biofactors, 37(4): 261-268.

Montcouquiol, M., Crenshaw, E. B. and Kelley, M. W. (2006). *Noncanonical wnt signaling and neural polarity*. Annual Rev. Neuroscience, 29: 363-386.

Najarro, E.H., and Ackley, D. (2013). *C. elegans fmi-1/flamingo and Wnt pathway components interact genetically to control the anteroposterior neurite growth of the VD GABAergic neurons.* Developmental Biology, 377(1): 224-235.

Nievelstein, R.A., Hartwig, N.G., Vermeij-Keers, C., and Valk, J. (1993). *Embryonic development of the mammalian caudal neural tube.* Teratology, 48(1): 21-31.

Oishi, I., Suzuki, H., Onishi, N., Takada, R., Kani, S., Ohkawara, B., Koshida, I., Suzuki, K., Yamada, G., Schwabe, G.C., Mundlos, S., Shibuya, H., Takada, S., and Minami, Y. (2003). *The receptor tyrosine kinase Ror2 is involved in non-canonical Wnt5a/JNK signalling pathway.* Genes to cells, 8: 645-654.

Okudaa, H., Miyataa, B., Moria, Y. and Tohyamaa, B. (2007). *Mouse Prickle1 and Prickle2 are expressed in postmitotic neurons and promote neurite outgrowth.* FEBS Letters, 581: 4754–4760.

Pan, C. L., Howell, J.E., Clark, S.G., Hilliard, M., Cordes, S., Bargmann, C.I. And Garriga, G. (2006). *Multiple wnts and frizzled receptors regulate anteriorly directed cell and growth cone migrations in Caenorhabditis elegans.* Developmental Cell, 10(3): 367-377.

Pan, W.J., Pang, S.Z., Huang, T., Guo, H.Y., Wu, D., and Li, L. (2004). *Characterization of function of three domains in dishevelled-1: DEP domain is responsible for membrane translocation of dishevelled-1.* Cell Res., 14(4): 324-330.

Panousopoulou, E., Tyson, R.A., Bretschneider, T., and Green, J.B.A. (2013). *The distribution of Dishevelled in convergently extending mesoderm.* Developmental Biology, 382(2): 496-503.

Phillips, H.M., Murdoch, J.N., Chaudhry, B., Copp, A.J., and Henderson, D.J. (2005). *Vangl2 acts via RhoA signaling to regulate polarized cell movements during development of the proximal outflow tract.* Circ Res., 96(3): 292-299.

Qian, D., Jones, C., Rzadzinska, A., Mark, S., Zhang, X., Steel, K.P., Dai, X., and Chen, P., (2007). *Wnt5a functions in planar cell polarity regulation in mice*. Developmental Biology, 306(1): 121-133.

Robinson, A., Escuin, S., Doudney, K., Vekemans, M., Stevenson, R.E., Greene, N., Copp, A.J., and Stanier, P. (2012). *Mutations in the planar cell polarity genes celsr1 and scrib are associated with the severe neural tube defect craniorachischisis.* Human Mutation, 33(2): 440-447.

Rocheleau, C.E., Downs, W.D., Lin, R., Wittmann, C., Bei, Y., Cha, Y.H., Ali, M., Priess, J.R., and Mello, C.C. (1997). *Wnt signalling and an APC-related gene specify endoderm in early C. elegans embryos*. Cell, 90(4): 707-716.

Roszkol, I., Sawada, A., and Solnica-Krezel, L.S. (2009). *Regulation of convergence and extension movements during vertebrate gastrulation by the Wnt/PCP pathway.* Semin Cell Dev Biol., 20(8): 986–997.

Saburi, S., and McNeill, H. (2005). *Organising cells into tissues: new roles for cell adhesion molecules in planar cell polarity.* Curr Opin Cell Biol., 17(5): 482-488.

Sanchez-Alvarez, L., Visanuvimol, J., McEwan, A., Su, A., Imai, J.H. and Colavita, A. (2011). *Vang-1 and Prkl-1 cooperate to negatively regulate neurite formation in Caenorhabditis elegans.* PLoS Genetics, 7(9): e1002257.

Sawa, H. (2012). *Chapter Three – Control of cell polarity and asymmetric division in C. elegans*. Planar cell polarity during development. Current topics in developmental biology, 101: 55-76.

Sawa, H., Lobel, L., and Horvitz, H.R. (1996). *The Caenorhabditis elegans gene lin-17, which is required for certain asymmetric cell divisions, encodes a putative seven-transmembrane protein similar to the Drosophila frizzled protein.* Genes and Development, 10(17): 2189-2197.

Schoenwolf, G.C. (1991). *Cell movements driving neurulation in avian embryos.* Development, 2: 157-168.

Shafer, B., Onishi, K., Lo, C., Colakoglu, G. and Zou, Y. (2011). *Signaling by antagonizing Dvl1-mediated feedback inhibition in growth cone guidance*. Developmental Cell, 20: 177-191.

Shimada, Y., Usui, T., Yanagawa, S., Takeichi, M., Uemura, T. (2001). *Asymmetric colocalization of flamingo, a seven-pass transmembrane cadherin, and dishevelled in planar cell polarization.* Current Biology, 11(11): 859-863.

Shimizu, K., Sato, M., and Tabata, T. (2011). *The Wnt5/planar cell polarity pathway regulates axonal development of the Drosophila mushroom body neuron.* J Neurosci., 31(13): 4944-4954.

Silhankova, M. and Korswagen, H. C. (2007). *Migration of neuronal cells along the anterior-posterior body axis of C. elegans: Wnts are in control*. Current Opinions in Genetics & Development, 17: 320-325.

Simons, M., and Mlodzik, M. (2008). *Planar cell polarity signaling: From fly development to human disease.* Annu Rev Genet. 42: 517-540.

Spencer, A.G., Orita, S., Malone, C.J., and Han, M. (2001). *A rho GTPase-mediated pathway is required during P cell migration in Caenorhabditis elegans.* Proc Natl Acad Sci U.S.A., 98(23): 13132-13137.

Stinchcomb, D.T., Shaw, J.E., Carr, S.H., and Hirsh, D. (1985). *Extrachromosomal DNA transformation of Caenorhabditis elegans.* Mol Cell Biol., 5(12): 3484-3496.

Strutt, D. (2001). *Planar polarity: Getting ready to ROCK.* Current Biology, 11(13): 506-509.

Strutt, D. (2002). *The asymmetric subcellular localization of components of the planar polarity pathway.* Semin Cell Dev Biol., 13(3): 225-231.

Strutt, H., and Strutt, D. (2002). *Nonautonomous planar polarity patterning in Drosophila: dishevelled-independent functions of frizzled.* Dev Cell., 3(6): 851-863.

Strutt, H., and Strutt, D. (2008). *Differential stability of flamingo protein complexes underlies the establishment of planar polarity.* Current Biology, 18(20-23): 1555-1564.

Strutt, H., Thomas-MacArthur, V., and Strutt, D. (2013). *Strabismus promotes recruitment and degredation of farnesylated prickle in Drosophila melanogaster planar polarity specification.* PLoS Genetics, 9(7). July 18, 2013. E-Publication.

Strutt, H., Warrington, S.J. And Strutt, D. (2011). *Dynamics of core planar polarity protein turnover and stable assembly into discrete membrane subdomains.* Dev. Cell., 20(4): 511-525.

Strutt, D.I., Weber, U., and Mlodzik, M. (1997). *The role of RhoA in tissue polarity and Frizzled signaling.* Nature, 387: 292-295.

Sulston, J.E., Schierenberg, E., White, J.G. and Thomson, J.N. (1983). *The embryonic cell lineage of the nematode Caenorhabditis elegans*. Developmental Biology, 100: 64-119.

Tahincia, E., and Symesa, K. (2003). *Distinct functions of Rho and Rac are required for convergent extension during Xenopus gastrulation.* Developmental Biology, 259(2): 318-335.

Takeuchi, M., Nakabayashi, J., Sakaguchi, T., Yamamoto, T.S., Takahashi, H., Takeda, H., and Ueno, N., (2003). *The prickle-related gene in vertebrates is essential for gastrulation cell movements.* Current Biology, 13: 674-679.

Tanegashima, K., Zhao, H., and Dawid I.B. (2008). *WGEF activates Rho in the Wnt-PCP pathway and controls convergent extension in Xenopus gastrulation.* EMBO J., 27(4): 606-617.

Tao, H. et al. (2011). *Mutations in Prickle Orthologs Cause Seizures in Flies, Mice, and Humans.* The American Journal of Human Genetics, 88: 138–149.

Tao, H., Inoue, K.I., Kiyonari, H., Bassuk, A.G., Axelrod, J.D., Sasaki, H., and Aizawa, S. (2012). *Nuclear localization of Prickle2 is required to establish cell polarity during early mouse embryogenesis.* Developmental Biology, 364(2): 138-148.

Timmons, L., Court, D.L., and Fire, A. (2001). *Ingestion of bacterially expressed dsRNAs can produce specific and potent genetic interference in Caenorhabditis elegans.* Gene, 263(1-2): 103-112.

Tree, D., Shulman, J.M., Rousset, R., Scott, M.P., Gubb, D., and Axelrod, J.D. (2002). *Prickle mediates feedback amplification to generate asymmetric planar cell polarity signaling.* Cell, 109: 371-381.

Usui, T., Shima, Y., Shimada, Y., Hirano, S., Burgess, R.W., Schwartz, T.L., Takeichi, M., and Uemura, T. (1999). *Flamingo, a seven-pass transmembrane cadherin, regulates planar cell polarity under the control of frizzled.* Cell, 95(5): 595-595.

Veeman, M.T., Slusarski, D.C., Kaykas, A., Louie, S.H., and Moon, R.T. (2003). *Zebrafish prickle, a modulator of noncanonical Wnt/Fz signalling, regulates gastrulation movements.* Curr. Biol., 13(8): 680-685.

Wada, H. and Okamoto, H. (2009). *Roles of planar cell polarity pathway genes for neuronal migration and differentiation.* Develop. Growth Differ., 51: 233-240.

Walck-Shannon, E., and Hardin, J. (2014). *Cell intercalation from top to bottom.* Nat. Rev. Mol. Cell Biol., 15(1): 34-48.

Wang, H.Y., Liu, T., and Malbon C.C. (2006). *Structure-function analysis of Frizzleds.* Cellular Signaling. 18(7): 934-941.

Wang, H.Y., and Malbon, C.C. (2004). *Wnt-Frizzled signalling to G-protein coupled effectors.* Cell Mol Life Sci., 61(1): 69-75.

Wen S., Zhu, H., Lu, W., Mitchell, L.F., Shaw, G.M., Lammer, E.J. and Finnell, R.H. (2010). *Planar cell polarity pathway genes and risk of spinal bifida*. American Journal of Medical Genetics A, 152(2): 299-304.

White, J. G. et al. (1986a). *The structure of the nervous system of the nematode C. elegans.* Philos. Trans. R. Soc. Lond. B. Biol. Sci., 314: 1-340.

White, J. G., Southgate, E., Thomson, J.N. and Brenner, S. (1986b). *The structure of the ventral nerve cord of Caenorhabditis elegans.* Phil. Trans. R. Soc. Lond. Biological Sciences, 275: 327-348.

Wu, J., and Mlodzik, M. (2008). *The frizzled extracellular domain is a ligand for Van Gogh/Stbm during nonautonomous planar cell polarity signaling.* Developmental Cell, 15(3): 462-469.

Wu, J., Roman, A.C., Carvajal-Gonzalez, J.M., Mlodzik, M. (2013). *Wg and Wnt4 provide long-range directional input to planar cell polarity orientation in Drosophila*. Nat Cell Biol. 15(9): 1045–1055.

Yin, C., Kiskowski, M., Pouille, P.A., Farge, E., and Solnica-Krezel, L. (2008). *Cooperation of polarized cell intercalations drives convergence and extension of presomitic mesoderm during zebrafish gastrulation.* Neuroscience Letters, 467(1): 6-10.

Ybot-Gonzalez, P., Savery, D., Gerrelli, D., Signore, M., Mitchell, C.E., Faux, C.H., Greene, N.D.E., and Copp, A.J. (2007). *Convergent extension, planar-cell-polarity signaling and initiation of mouse neural tube closure*. Development and disease, 134: 789-799.

Appendix A: Anterior-Posterior DD neuron bar graph numerical values

Bar graphs shown in the results section do not display exact percentage values for each bar. Thus, Appendix figures in this section display charts with the corresponding percentages for each bar graph.

		DD2	DD3	DD4	DD5	DD6
Wild Type	Ant	0%	0%	0%	0%	0%
	Post	0%	0%	0%	0%	0%
prkl-1(ok3182)	Ant	70%	25%	80%	86%	36%
	Post	0%	0%	0%	0%	0%
prkl-1(zy11)	Ant	82%	51%	79%	72%	31%
	Post	0%	0%	0%	0%	0%
vang-1(tm1422)	Ant	44%	10%	21%	28%	5%
	Post	3%	0%	0%	0%	15%
vang-1 (ok1142)	Ant	41%	16%	39%	45%	18%
	Post	0%	0%	0%	7%	2%
fmi-1(tm306)	Ant	4%	4%	4%	4%	4%
	Post	0%	0%	4%	7%	4%
bar-1(ga80)	Ant	95%	13%	36%	56%	77%
	Post	0%	0%	0%	0%	0%

Appendix A1. Anterior-Posterior bar graph numerical values for PCP single mutants.

Ant = Percentage of neurons anterior to 95% confidence interval.

Post = Percentage of neurons posterior to 95% confidence interval.

		DD2	DD3	DD4	DD5	DD6
Wild Type	Ant	0%	0%	0%	0%	0%
	Post	0%	0%	0%	0%	0%
prkl-1(ok3182)	Ant	70%	25%	80%	86%	36%
	Post	0%	0%	0%	0%	0%
prkl-1(ok3182) vang-1(tm1422)	Ant	33%	8%	28%	25%	11%
	Post	3%	6%	0%	0%	0%
prkl-1(ok3812) vang-1(ok1142)	Ant	39%	9%	52%	39%	27%
	Post	0%	0%	0%	3%	0%
prkl-1(ok3182) fmi-1(tm306)	Ant	43%	18%	46%	71%	36%
	Post	0%	4%	4%	4%	0%
vang-1(ok1142)	Ant	41%	16%	39%	45%	18%
	Post	0%	0%	0%	7%	2%
vang-1(ok1142) fmi-1(tm306)	Ant	35%	19%	39%	58%	65%
	Post	0%	3%	3%	0%	0%

Appendix A2. Anterior-Posterior bar graph numerical values for *prkl-1* and *vang-1* double mutant animals.

Ant = Percentage of neurons anterior to 95% confidence interval.

Post = Percentage of neurons posterior to 95% confidence interval.

		DD2	DD3	DD4	DD5	DD6
Wild Type	Ant	0%	0%	0%	0%	0%
	Post	0%	0%	0%	0%	0%
cfz-2(ok1201)	Ant	17%	17%	13%	7%	27%
	Post	0%	0%	0%	0%	3%
lin-17(n677)	Ant	9%	9%	2%	4%	15%
	Post	0%	2%	6%	2%	6%
mig-1(n687)	Ant	11%	9%	11%	17%	66%
	Post	0%	3%	3%	3%	0%
dsh-1(ok1445)	Ant	0%	5%	10%	14%	19%
	Post	24%	24%	14%	19%	10%
dsh-2(or302)	Ant	12%	7%	5%	29%	56%
	Post	2%	2%	2%	2%	0%
mig-5(tm2639)	Ant	53%	25%	9%	22%	53%
	Post	0%	9%	9%	9%	3%

Appendix A3. Anterior-Posterior bar graph numerical values for Frizzled and Dishevelled mutants.

Ant = Percentage of neurons anterior to 95% confidence interval.

Post = Percentage of neurons posterior to 95% confidence interval.

		DD2	DD3	DD4	DD5	DD6
Wild Type	Ant	0%	0%	0%	0%	0%
	Post	0%	0%	0%	0%	0%
cwn-1(ok546); cwn-2(ok895)	Ant	15%	9%	3%	9%	9%
	Post	9%	18%	3%	3%	6%
lin-44(n1792)	Ant	2%	2%	5%	5%	10%
	Post	2%	0%	0%	0%	5%
egl-20(n585)	Ant	8%	0%	3%	14%	14%
	Post	5%	0%	0%	3%	3%
cwn-1(n546);cwn-2(ok895); lin-44(n1795);egl-20(n585)	Ant	23%	9%	11%	23%	77%
	Post	17%	17%	3%	0%	0%
mom-2(ne874)	Ant	4%	2%	35%	24%	13%
	Post	0%	2%	0%	0%	0%
let-502(sb118)	Ant	4%	12%	46%	42%	12%
	Post	0%	0%	4%	0%	0%

Appendix A4. Anterior-Posterior bar graph numerical values for Wnts and ROCK.

Ant = Percentage of neurons anterior to 95% confidence interval.

Post = Percentage of neurons posterior to 95% confidence interval.

		DD2	DD3	DD4	DD5	DD6
Wild Type	Ant	0%	0%	0%	0%	0%
	Post	0%	0%	0%	0%	0%
mom-2(ne874)	Ant	9%	7%	41%	33%	13%
	Post	0%	4%	0%	0%	0%
cwn-1p::mom-2	Ant	31%	22%	34%	22%	19%
	Post	0%	3%	3%	9%	0%

Appendix A5. Anterior-Posterior bar graph numerical values for *cwn-1p::mom-2*.

Ant = Percentage of neurons anterior to 95% confidence interval.

Post = Percentage of neurons posterior to 95% confidence interval.

		DD2	DD3	DD4	DD5	DD6
Wild Type unc119p::tagRFP	Ant	0%	0%	0%	0%	0%
	Post	0%	0%	0%	0%	0%
prkl-1(ok3182) unc119p::tagRFP	Ant	54%	36%	82%	82%	59%
	Post	3%	0%	0%	0%	0%
prkl-1(ok3182) unc119p::prkl-1	Ant	17%	10%	15%	12%	7%
	Post	12%	24%	20%	12%	7%
prkl-1(ok3182) vang-1(tm1422) unc119p::tagRFP	Ant	22%	6%	25%	14%	6%
	Post	3%	3%	0%	0%	0%
prkl-1(ok3182) vang-1(tm1422) unc119p::vang-1	Ant	57%	32%	96%	93%	71%
	Post	0%	0%	0%	0%	0%
Wild Type unc30p::tagRFP	Ant	0%	0%	0%	0%	0%
	Post	0%	0%	0%	0%	0%
prkl-1 ok3182 unc30p::tagRFP	Ant	61%	6%	50%	50%	39%
	Post	3%	0%	0%	0%	0%
prkl-1 ok3182 unc30p::prkl-1	Ant	40%	0%	6%	9%	11%
	Post	9%	6%	11%	9%	0%

Appendix A6. Anterior-Posterior bar graph numerical values for *prkl-1* and *vang-1* tissue specific and cell autonomous rescue experiments.

Ant = Percentage of neurons anterior to 95% confidence interval.

Post = Percentage of neurons posterior to 95% confidence interval.

		DD2	DD3	DD4	DD5	DD6
prkl-1p::prkl-1 In all neurons	Ant	0%	0%	0%	0%	0%
	Post	0%	0%	0%	0%	0%
prkl-1p::prkl-1 In no neurons	Ant	20%	35%	80%	85%	50%
	Post	0%	0%	0%	0%	0%
prkl-1p::prkl-1 In DD1/DD3/DD5	Ant	25%	13%	38%	50%	38%
	Post	0%	0%	0%	13%	0%
prkl-1p::prkl-1 In DD2/DD4/DD6	Ant	5%	5%	16%	16%	21%
	Post	0%	0%	5%	0%	0%

Appendix A7. Anterior-Posterior bar graph numerical values for *prkl-1* genetic mosaic rescue experiments.

Ant = Percentage of neurons anterior to 95% confidence interval.

Post = Percentage of neurons posterior to 95% confidence interval.

		DD2	DD3	DD4	DD5	DD6
Wild Type unc-119p::tagRFP	Ant	0%	0%	0%	0%	0%
	Post	0%	0%	0%	0%	0%
unc-119p::prkl-1 over-expression	Ant	10%	0%	0%	10%	3%
	Post	14%	41%	28%	17%	3%

Appendix A7. Anterior-Posterior bar graph numerical values for *unc-119p::prkl-1* over-expression of *prkl-1*.

Ant = Percentage of neurons anterior to 95% confidence interval.

Post = Percentage of neurons posterior to 95% confidence interval.